~~Christopher~~ ~~Nicholas David Voltaire David F. Pollard~~

Synergetic use of IASI profile and TROPOMI ~~space borne sensors for generating a tropospheric~~ total column level 2 methane ~~profile product~~retrieval products

Matthias Schneider[1], Benjamin Ertl[1,2], Qiansi ~~J. Diekmann~~Tu[1,a], Christopher J. Diekmann[1,b], Farahnaz Khosrawi[1], Amelie N. Röhling[1], Frank Hase[1], Darko Dubravica[1], Omaira E. García[3], Eliezer Sepúlveda[3], Tobias Borsdorff[4], Jochen Landgraf[4], Alba Lorente[4], André Butz[5], Huilin Chen[6], Rigel Kivi[7], Thomas Laemmel[8,c], Michel Ramonet[8], Cyril Crevoisier[9], Jérome Pernin[9], Martin Steinbacher[10], Frank Meinhardt[11], Kimberly ~~M. Deutscher~~Strong[12], Debra ~~W. T. Griffith~~Wunch[12], Thorsten ~~A. Velazco~~Warneke[13], Coleen Roehl[14], Paul O. Wennberg[14], Isamu Morino[15], Laura T. Iraci[16], Kei Shiomi[17], Nicholas M. Deutscher[18], David W. T. Griffith[18], Voltaire A. Velazco[18,d], and David F. Pollard[19]

[1]Institute of Meteorology and Climate Research (IMK-ASF), Karlsruhe Institute of Technology, Karlsruhe, Germany
[2]Steinbuch Centre for Computing (SCC), Karlsruhe Institute of Technology, Karlsruhe, Germany
[3]Izaña Atmospheric Research Center, Agencia Estatal de Meteorología (AEMET), Santa Cruz de Tenerife, Spain
[4]Earth Science Group, SRON Netherlands Institute for Space Research, Utrecht, The Netherlands
[5]Institute of Environmental Physics, Heidelberg University, Heidelberg, Germany
[6]Center for Isotope Research, University of Groningen, Groningen, The Netherlands
[7]Space and Earth Observation Centre, Finnish Meteorological Institute, Sodankylä, Finland
[8]Laboratoire des Sciences du Climat et de l'Environnement (LSCE), CEA, 91191 Gif sur Yvette, France
[9]LMD/IPSL, CNRS, Ecole polytechnique, University Paris-Saclay, Palaiseau, France
[10]Swiss Federal Laboratories for Materials Science and Technology (EMPA), Dübendorf, Switzerland
[11]Air Monitoring Network, Federal Environment Agency (UBA), Langen, Germany
[12]Department of Physics, Universtity of Toronto, Toronto, Canada
[13]Institute of Environmental Physics, University of Bremen, Bremen, Germany
[14]California Institute of Technology, Pasadena, CA, USA
[15]Satellite Observation Center, National Institute for Environmental Studies (NIES), Tsukuba, Ibaraki, Japan
[16]Atmospheric Science Branch, NASA Ames Research Center, Moffett Field, CA, USA
[17]Japan Aerospace Exploration Agency (JAXA), Tsukuba, Japan
[18]Centre for Atmospheric Chemistry, School of Earth, Atmospheric and Life Sciences, Faculty of Science, Medicine and Health, University of Wollongong, Wollongong, Australia
[19]National Institute of Water and Atmospheric Research Ltd (NIWA), Lauder, New Zealand
[a]now at: School of Mechanical Engineering, Tongji University, Shanghai, China
[b]now at: Telespazio Germany GmbH, Darmstadt, Germany
[c]now at: Laboratory for the Analysis of Radiocarbon with AMS (LARA) Department of Chemistry, Biochemistry and Pharmaceutical Sciences (DCBP) & Oeschger Centre for Climate Change Research (OCCR), University of Bern, Switzerland
[d]now at: Deutscher Wetterdienst (DWD), Albin-Schwaiger-Weg 10, Hohenpeissenberg, Germany

Correspondence: M. Schneider
(matthias.schneider@kit.edu)

Abstract. The thermal infrared nadir spectra of IASI (Infrared Atmospheric Sounding Interferometer) are successfully used for retrievals of different atmospheric trace gas profiles. However, these retrievals offer generally reduced information about the lowermost tropospheric layer due to the lack of thermal contrast close to the surface. Spectra of scattered solar radiation observed in the near and/or short wave infrared, for instance by TROPOMI (TROPOspheric Monitoring Instrument) offer higher sensitivity near ground and are used for the retrieval of total column averaged mixing ratios of a variety of atmospheric trace gases. Here we present a method for the synergetic use of IASI profile and TROPOMI total column ~~data~~level 2 retrieval products. Our method uses the output of the individual retrievals and consists of linear algebra a posteriori calculations (i.e. calculation after the individual retrievals). We show that this approach ~~is largely equivalent~~ has strong theoretical similarities to applying the spectra of the different sensors together in a single retrieval procedure, but with the substantial advantage of being applicable to data generated with different individual retrieval processors, of being very time efficient, and of directly benefiting from the high quality and most recent improvements of the individual retrieval processors.

We demonstrate the method exemplarily for atmospheric methane (CH_4). We perform a theoretical evaluation and show that the a posteriori combination method yields a total column averaged CH_4 product (XCH_4) that conserves the good sensitivity of the corresponding TROPOMI product while merging it with the high quality upper tropospheric and lower stratospheric (UTLS) CH_4 partial column information of the corresponding IASI product. As consequence, the combined product offers ~~in addition~~ additional sensitivity for the tropospheric CH_4 partial column, which is not provided by the individual TROPOMI nor the individual IASI product. The theoretically predicted synergetic ~~effects are~~ effect is verified by comparisons to CH_4 reference data obtained from collocated XCH_4 measurements at ~~six~~ 14 globally distributed TCCON (Total Carbon Column Observing Network) stations, CH_4 profile measurements made by ~~24~~ 36 individual AirCore soundings, and ~~lower~~ tropospheric CH_4 data derived from continuous ground-based in-situ observations made at two nearby Global Atmospheric Watch (GAW) mountain stations. The comparisons clearly demonstrate that the combined product can reliably detect the actual variations of atmospheric XCH_4 ~~signals and allows to distinguish between tropospheric and UTLS~~ , CH_4 ~~partial column averaged mixing ratios, which is not possible~~ in the UTLS, and CH_4 in the troposphere. A similar good reliability for the latter is not achievable by the individual TROPOMI and IASI products. ~~We find indications of a weak positive bias of about +1% of the combined lower tropospheric data product with respect to the references. For the UTLS CH_4 partial columns we find no significant bias.~~

1 Introduction

Measurements from different ground- or satellite-based sensors target at the observations of the same atmospheric parameters (e.g. the same trace gases), but with different characteristics (e.g. sensitivities for different vertical regions). Often the different sensors use different observation geometries (limb scanning, nadir, solar light reflected at the Earth's surface) and/or different spectral regions (e.g. UV/vis, near infrared, thermal infrared, microwave). Dedicated experts and efforts are needed to develop retrieval techniques that are specifically optimized for an individual sensor. An algorithm that uses coincident measurements of all the different sensors for a multispectral approach (synergetic use of level 1 data) for the optimal estimation of the

atmospheric state would well exploit the synergies of the different observation geometries and spectral regions and thus allows for detecting the atmospheric state in more detail than achievable by individual optimal estimation retrievals.

~~Cuesta et al. (2013) present such 'super retrieval ', which performs an optimal estimation~~ There is a variety of studies investigating the multispectral synergism when retrieving atmospheric trace gases from space. Examples of theoretical studies using synthetic thermal infrared and UV spectra for a simulated synergistic retrieval of atmospheric ozone (O_3) ~~applying the spectra measured by the thermal nadir sensor IASI (Infrared Atmospheric Sounding Interferometer)and the UV /vis sensor GOME (~~are Landgraf and Hasekamp (2007); Worden et al. (2007); Cuesta et al. (2013); Costantino et al. (2017). These studies considered the thermal infrared spectra of TES (Tropospheric Emission Spectrometer) and IASI (as well as its succesor IASI - New Generation), and UV spectra of OMI (Ozone Monitoring Instrument) and GOME-2 (Global Ozone Monitoring Experiment ~~). Their publication shows that using the multispectral approach allows the detection of lower tropospheric O_3, which is not possible by an individual usage of the IASI and GOME spectra . Costantino et al. (2017) showed that the quality of this multispectral lower tropospheric O_3 product can be further improved with improved thermal nadir and UV/vis sensors.~~ - 2 as well as its succesor UVNS – Ultraviolet Visible Near-infrared Shortwave-infrared) and are complemented by studies with real spectra (e.g. Cuesta et al., 2013; Fu et al., 2013). Another example of a study with real spectra is Luo et al. (2013), who examine the combination of the TES thermal nadir spectra with the MLS (Microwave Limb Sounder) microwave limb spectra for a synergetic retrieval of atmospheric carbon monoxide (CO) profiles. All the different studies clearly show that the synergetic use of the measured spectra results in an inceased sensitivity with respect to the targeted trace gases.

~~The~~ However, the development of these ~~'super retrievals '~~ multispectral retrievals requires experts in different remote sensing techniques to work closely together. Furthermore, as soon as measurements from a new sensor become available (or as soon as sensors are modified/improved) such ~~super retrieval~~ multispectral processors have to be adapted accordingly, i.e. continuous collaborative retrieval developments are required. While this is certainly possible, it might be not the most efficient way, in particularly considering the steadily increasing amount of available satellite data products (level 2 retrieval products). The optimal synergetic exploitation of the already available ~~individual retrieval results~~ level 2 retrieval products would be much less computationally expensive than running dedicated ~~combined retrievals.~~ multispectral retrievals. Such synergetic combination of level 2 products is the topic of this paper.

~~Efficient a posteriori combination methods of individual retrieval products are currently of high interest, because the steadily increasing amount of available satellite data offers more and more possibilities for synergetic use. Worden et al. (2015) combines the~~ There are already several examples of a level 2 product fusion discussed in literature (the following list is not intented to be complete): Worden et al. (2015) combine the thermal and near infrared ~~observations~~ level 2 products of methane (CH_4) ~~made by TES (Thermal Emission Spectrometer)~~ of TES and GOSAT (Greenhouse gas mOnitoring SATellite), respectively, by performing approximative calculations and with a focus on monthly mean data. Data aggregation is necessary due to the reduced temporal and horizonal coverage of TES and GOSAT and their imperfect collocation. ~~The method of Ceccherini et al. (2009) focuses on avoiding uncertainties in the combined product due to constraints and vertical interpolation, which might be a problem when combining two vertically resolved profile products generated applying different constraints. However, this method needs the Jacobians (changes in the spectra caused by changes in the atmospheric state) of the retrieved~~

products, which are large matrices that are generally not stored in operational retrieval output files. Cortesi et al. (2016) applied this approach for combining the Cortesi et al. (2016) combine the thermal infrared MIPAS-STR (Michelson Interferometer for Passive Atmospheric Sounding - STRatospheric aircraft) and microwave MARSCHALS (Millimetre-wave Airborne Receivers for Spectroscopic Characterisation in Atmospheric Limb Sounding) aircraft-based remote sensing products of O_3, nitric acid (HNO_3), water vapour (H_2O), and atmospheric temperature . (applying the so-called Measurement-Space-Solution data fusion method of C . Another example is Warner et al. (2014), who use a Kalman filter for combining the CO data products of AIRS (Atmospheric Infrared Sounder) – available for a large horizontal area, but with weak vertical details – and TES (and MLS) – available with detailed vertical information, but only for very localised areas.

Here, we propose to generate a multi-sensor optimal estimation present a method for fusing the available level 2 CH_4 profile product by simple a posteriori calculations using available outputs of IASI and the XCH_4 (total column averaged methane) product of TROPOMI (Tropospheric Monitoring Instrument) retrievals. by means of a Kalman filter approach. Our objective is a data product with improved vertical profile information (determine tropospheric CH_4 independently from CH_4 at higher altitudes, which is not possible by IASI or TROPOMI data alone) by synergetically exploiting the different vertical sensitivities of the two products. The method allows a computationally very efficient generation of global daily maps of the combined data product and only needs the individually retrieved states, averaging kernels and noise covariances provided by the respective remote sensing experts in the context of their standard retrieval work. The proposed method can be used flexibly for combining measurement information of different satellite sensors . For most cases the method approximates closely and is in particularly interesting for combining a profile product with a total column product. The method has strong theoretical similarities to a dedicated combined optimal estimation retrieval that uses the combined IASI and TROPOMI spectra as input (synergetic use of level 1 data).

The reliable and global detection of tropospheric CH_4 independently from CH_4 at higher altitudes can lead to an improved understanding of the CH_4 cycle. Respective data allow a more direct investigation of the CH_4 boundary layer source and sink signals than total column averaged mixing ratios (XCH_4) provided globally for instance by GOSAT (e.g. Parker et al., 2020) or TROPOMI (?)(Lorente et al., 2021). This is because XCH_4 signals are strongly affected by vertical shifts of the tropopause altitude, i.e. their use for investigating CH_4 absorption and release at ground depends on the correct consideration of the tropopause altitude by model simulations (Pandey et al., 2016).

This manuscript is organised as follows. Section 3 briefly discusses 2 briefly presents the used IASI and TROPOMI products (generated by two individual retrievals),. Section 3 presents the equations for the optimal a posteriori combination of the two independent retrieval outputs (level 2 product combination), and performs a theoretical evaluation of the individual and combined products. Section 4 validates the total column and tropospheric and UTLS (upper tropospheric/lower stratospheric) partial column products obtained by the individual IASI and TROPOMI retrievals and by the a posteriori combination . Section ?? discusses biases by an inter-comparison to reference data from TCCON, AirCore, and GAW. Section 5 discusses the global consistency of the products and its latitudinal consistencyshows global maps. Section 6 resumes the results of our study and briefly discusses upcoming possibilities. Furthermore, in Appendix A we provide extensive background information on give a brief overview on retrieval theory and in Appendix B we discuss the theory of our a posteriori combination method and

we show that the method is equivalent has strong similarities to performing a full multispectral optimal estimation retrieval. Appendix C introduces the operator for transferring logarithmic scale differentials into linear scale differentials. Appendix D presents the operators used for converting vertical profile data into total and partial column data. Appendix E examines the dislocation error, i.e. to what extent the temporal and spatial dislocation of the IASI and TROPOMI observations (the two sensors are on two different satellites having different orbits) impacts the combined data product. Appendix F explains how we assess the comparability of the satellite products with the reference data and reveals the reasonable agreement between the characteristics of the satellite products and the results of the validation study.

2 A posteriori combination of MUSICA IASI CH_4 and TROPOMI XCH_4 productsSatellite data

In this section we present the method for combining CH_4 profiles derived from IASI thermal nadir spectra and briefly present the satellite data products that are use for the combination procedure. These are the XCH_4 data obtained from the analysis of the near and short wave infrared (SWIR and NIR) spectra measured by TROPOMI . and the CH_4 profiles derived from IASI thermal nadir (TIR) spectra. In addition, we explain the criteria used for collocating the two satellite observations.

2.1 RemoTeC TROPOMI XCH_4

The TROPOMI XCH_4 data used in this study are generated by the RemoTeC algorithm (Butz et al., 2011), which is used for the operational processing of Sentinel 5 Precursor/TROPOMI XCH_4 data (Hu et al., 2016; Hasekamp et al., 2019; Landgraf et al., 2019). The current operational processing algorithm version is 1.2Here we work with data of the operational processing algorithm version 2.2.0 . Here we use data from version 1.3.0 with the improvements as presented and validated in ?. It is foreseen to become the operational processing version with the operational processor update in April 2021. (which has been presented and v . The TROPOMI output files provide the XCH_4 data together with the used a priori data (constructed from simulations of the global chemistry-transport model TM5, Krol et al., 2005), the column averaging kernels, and the error values. In order to filter out data with reduced quality, here we only use TROPOMI data , for which the variable `qa_value` has values larger than 0.5. This filter is consistent to the filtering as suggested in Table A1 of ?Here we work with all TROPOMI data that pass the standard quality filtering (TROPOMI output variable `qa_value` must be equal to 1.0, which means a filtering according to Table A1 of Lorente et . In addition, we remove observations over ground covered by snow (which show a high bias as discussed in Lorente et al., 2021) by requiring a blended albedo (A_b, calculated from the NIR, A_{NIR}, and SWIR, A_{SWIR}, albedos according to Wunch et al., 2011b, as $A_b =$ of smaller than 0.85.

2.2 MUSICA IASI CH_4 profiles

As IASI CH_4 data product we use the data generated by the retrieval processor MUSICA (MUlti-platform remote Sensing of Isotopologues for investigating the Cycle of Atmospheric water, a European Research Council project between 2011 and 2016). The MUSICA IASI data full retrieval product encompasses trace gas profiles of H_2O, the HDO/H_2O ratio, N_2O, CH_4, and HNO_3. The data have been validated in several previous studies (Schneider et al., 2016; Borger et al., 2018; Gar-

cía et al., 2018), and it has been shown that the CH_4 product can ~~very well~~ detect the CH_4 signals originating in the upper troposphere/lower stratosphere particularly well. MUSICA IASI data using processor versions 3.2.1 and 3.3.0/1 are currently available for the 2014 to ~~2020 time~~ 2021 period and are presented in ~~?~~Schneider et al. (2022). This MUSICA IASI data set is best suited for a posteriori data reusage (e.g. Diekmann et al., 2021), because in addition to the retrieved trace gas profiles it contains full information on retrieval settings (a priori states and constraints) and on averaging kernel and error covariance matrices. In ~~oder~~ order to ensure highest MUSICA IASI data quality, here we require the flag variable `musica_fit_quality_flag` to be set to 3 (the spectral fit of the MUSICA IASI retrieval has a good quality and the spectral ~~rediduals~~ residuals are close to the instrumental noise level). Furthermore, we only use MUSICA IASI data for which the flag variable `eumetsat_cloud_summary_flag` is set to 1, which guarantees that the IASI instrumental field of view is cloud-free.

A particularity of the MUSICA IASI processor is that the trace gas inversions are performed on a logarithmic scale. In Appendix B of ~~?~~ Schneider et al. (2022) it is shown that the MUSICA IASI retrieval can be considered as a moderately non-linear problem, in particular if the differentials (averaging kernels and covariances) are used on the logarithmic scale. In the following equations we take special care on the correct usage of the corresponding logarithmic scale differentials. Nevertheless, all equations are also applicable for retrievals made on linear scale by replacing in the following the operator $\mathbf{L}$ (which is introduced in Appendix C) by the identity operator.

2.3 Collocation of TROPOMI and IASI observations

As temporal collocation criterion we use 6 hours, for a valid horizontal collocation the centres of the TROPOMI and IASI ground pixels must be closer than 50 km, and the difference between the ground pressure at the TROPOMI and IASI ground pixels must be within 50 hPa. Generally multiple TROPOMI/IASI ground pixel pairs fulfill the aforementioned criteria. In such case we use the pair with the smallest distance metric. This metric is defined as the Euclidean distance that considers a norm of 12 hours for the temporal distance, a norm of 50 km for the horizontal distance, and a norm of 5 hPa for the vertical distance. The possible small difference in the TROPOMI and IASI ground pixel pressures is taken into account by correcting the TROPOMI XCH_4 values according to Appendix B of Sha et al. (2021).

3 Presentation and characterisation of the combination method

3.1 Calculation of the combined state vector

For this study we use the CH_4 a priori profile as provided by the TROPOMI product as the common a priori for all products (these are simulations of the global chemistry-transport model TM5, Krol et al., 2005). For this purpose we modify the MUSICA IASI product and bring it in line with the TROPOMI a priori profile choice by applying Eq. (B13).

For updating the IASI CH_4 profile product using the TROPOMI XCH_4 observation we apply a Kalman filter and obtain the combined CH_4 state as:

$$\hat{\boldsymbol{x}}^{l}_{\boldsymbol{C}} = \hat{\boldsymbol{x}}^{l}_{\boldsymbol{I}} + \mathbf{L}^{-1}\boldsymbol{m}[\hat{x}^{*}_{T} - \boldsymbol{a}^{*}_{\boldsymbol{T}}{}^{T}\hat{\boldsymbol{x}}_{\boldsymbol{I}}] - \mathbf{L}^{-1}\boldsymbol{m}(\boldsymbol{w}^{*}{}^{T} - \boldsymbol{a}^{*}_{\boldsymbol{T}}{}^{T})\boldsymbol{x}_{\boldsymbol{a}}. \quad (1)$$

Here the vector $\hat{\boldsymbol{x}}_{\boldsymbol{I}}$ and scalar ~~$\hat{x}_T$~~ $\hat{x}^{*}_{T}$ are the MUSICA IASI CH_4 profile and the TROPOMI XCH_4 column averaged products. The row vector $\boldsymbol{a}^{*}_{\boldsymbol{T}}{}^{T}$ is the total column averaged mixing ratio kernel of the TROPOMI product interpolated to the vertical grid used by the MUSICA IASI processor and the row vector $\boldsymbol{w}^{*}{}^{T}$ is the operator for converting mixing ratio vertical profiles into total column averaged mixing ratios (for details on the interpolation see Appendix D). The state vector $\hat{\boldsymbol{x}}^{\boldsymbol{l}}_{\boldsymbol{C}}$ represents the logarithmic scale combined CH_4 profile product ~~in logarithmic scale~~ (i.e. the MUSICA IASI CH_4 data updated with the TROPOMI XCH_4 observation). The superscript '^{l}' used with $\hat{\boldsymbol{x}}^{\boldsymbol{l}}_{\boldsymbol{C}}$ and $\hat{\boldsymbol{x}}^{\boldsymbol{l}}_{\boldsymbol{I}}$ indicates the use of the logarithmic scale. Here and in the following we will mark scalars, vectors or matrix operators that are in logarithmic scale by the superscript '^{l}'. The matrix $\mathbf{L}$ is the operator for the transformation of differentials or small changes (as given by averaging kernels or error covariances) from the logarithmic to the linear scale (for more details see Appendix C).

The column vector $\boldsymbol{m}$ is the Kalman gain operator and it is given by:

$$\boldsymbol{m} = \mathbf{L}\mathbf{S}^{\mathbf{l}}_{\hat{\boldsymbol{x}}_{\boldsymbol{I}}}\mathbf{L}^{T}\boldsymbol{a}^{*}_{\boldsymbol{T}}(\boldsymbol{a}^{*}_{\boldsymbol{T}}{}^{T}\mathbf{L}\mathbf{S}^{\mathbf{l}}_{\hat{\boldsymbol{x}}_{\boldsymbol{I}}}\mathbf{L}^{T}\boldsymbol{a}^{*}_{\boldsymbol{T}} + S_{\hat{\boldsymbol{x}}_{T},n}{}^{*}_{\hat{x}_{T},n})^{-1}, \quad (2)$$

with the matrix $\mathbf{S}^{\mathbf{l}}_{\hat{\boldsymbol{x}}_{\boldsymbol{I}}}$ and the scalar ~~$S_{\hat{\boldsymbol{x}}_T,n}$~~ $S^{*}_{\hat{x}_T,n}$ being the logarithmic scale ~~retrieval noise error~~ a posteriori covariance of the MUSICA IASI CH_4 product and the noise error variance of the TROPOMI XCH_4 product, respectively. The vector operator $\boldsymbol{a}^{*}_{\boldsymbol{T}}$ is the transpose of the TROPOMI column averaging kernel, i.e. $\boldsymbol{a}^{*}_{\boldsymbol{T}} = (\boldsymbol{a}^{*}_{\boldsymbol{T}}{}^{T})^{T}$.

Except for the logarithmic scale transformation, the Eqs. (1) and (2) are analogous to Eqs. (B9) and (B10). As demonstrated in Appendix B this kind of Kalman filter application ~~is equivalent~~ has a strong similarity to an optimal estimation retrieval that uses a combined IASI and TROPOMI measurement vector (synergetic use of level 1 data). The application of this Kalman filter is possible because the MUSICA IASI data are provided with full information on a priori states, constraints, error covariances, and averaging kernels ~~(?)~~(Schneider et al., 2022), and because the TROPOMI data are provided together with their a priori state, averaging kernel, and retrieval noise error ~~(?)~~(Lorente et al., 2021).

The Kalman Gain according to Eq. (2) describes how differences between the MUSICA IASI and TROPOMI XCH_4 product are used to update the MUSICA IASI CH_4 profile. An example for a Kalman Gain operator is depicted in Fig. 1. It shows that a positive difference of $+1$ ppb of ~~$[\hat{x}_T - \boldsymbol{a}^{*}_{\boldsymbol{T}}{}^{T}\hat{\boldsymbol{x}}_{\boldsymbol{I}}]$~~ $[\hat{x}^{*}_{T} - \boldsymbol{a}^{*}_{\boldsymbol{T}}{}^{T}\hat{\boldsymbol{x}}_{\boldsymbol{I}}]$ will lead to a combined CH_4 profile product that has been modified with respect to the MUSICA IASI CH_4 product by almost $+3$ ppb in the lowermost troposphere, by about -0.5 ppb at 10 km, and by about ~~$+1$~~$+1.5$ ppb above 20 km.

3.2 ~~Collocation of TROPOMI~~ Vertical resolution and ~~IASI observations~~representativeness

~~As temporal collocation criterion we use four hours, for a valid horizontal collocation the centres of the TROPOMI and IASI ground pixels must be closer than 50 km, and the difference between the ground pressure at the TROPOMI and IASI ground pixels must be within 50 hPa. Generally multiple TROPOMI/IASI ground pixel pairs fulfill the aforementioned criteria. In~~

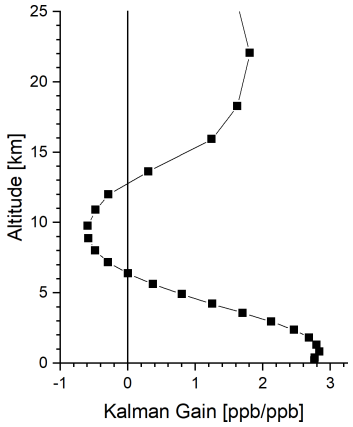

Figure 1. Visualisation of a Kalman Gain operator for optimally combining TROPOMI XCH_4 data with MUSICA IASI CH_4 profile data. This is the column vector $\boldsymbol{m}$ according to Eq. (2). The example shown is for a late summer atmosphere (27 September 2018) over Central Europe.

~~such case we use the pair with the smallest spatial distance, which we define as the Euclidean distance that considers a norm of 40 km for the horizontal distance and a norm of 5 hPa for the vertical distance. TROPOMI and IASI observations already belonging to a valid collocation pair are disregarded for further collocations. This ensures that an individual IASI or TROPOMI observation can only belong to a single collocation pair. The possible small difference in the TROPOMI and IASI ground pixel pressures is taken into account by correcting the TROPOMI XCH_4 values, respectively.~~

3.3 ~~Sensitivity and vertical resolution~~

In this section we compare the vertical resolution and representativeness of the individual retrieval products with those achieved when combining the two retrieval products. According to Eq. 1 the averaging kernels for the combined data product can be calculated as:

$$\mathbf{A}_\mathbf{C}^\mathbf{l} = \mathbf{A}_\mathbf{I}^\mathbf{l} + \mathbf{L}^{-1}\boldsymbol{m}(\boldsymbol{a}_\boldsymbol{T}^{*\,T} - \boldsymbol{a}_\boldsymbol{T}^{*\,T}\mathbf{L}\mathbf{A}_\mathbf{I}^\mathbf{l}\mathbf{L}^{-1})\mathbf{L}. \quad (3)$$

Here $\mathbf{A}_\mathbf{I}^\mathbf{l}$ and $\mathbf{A}_\mathbf{C}^\mathbf{l}$ are the logarithmic scale averaging kernels of the MUSICA IASI CH_4 product and of the combined product (the MUSICA IASI CH_4 product after being updated with the information provided by the TROPOMI XCH_4 ~~data~~ product), respectively. These are the kernels for the profile products represented in nal (nal: number of atmospheric levels) levels, i.e. they are matrices of dimension $nal \times nal$. Logarithmic scale kernels are also called fractional or relative averaging kernels (e.g. Keppens et al., 2015).

Figure 2 depicts the rows of typical averaging kernels for the MUSICA IASI product (~~panel~~ Fig. 2a) and the combined data product (~~panel~~ Fig. 2b). Adding the information provided by TROPOMI clearly improves the sensitivity in the lower troposphere: for the MUSICA IASI product the lower tropospheric kernels generally peak at the upper limit of the lower troposphere (at about 5 km a.s.l.). For the combined product these peak values are obtained at significantly lower altitudes (at

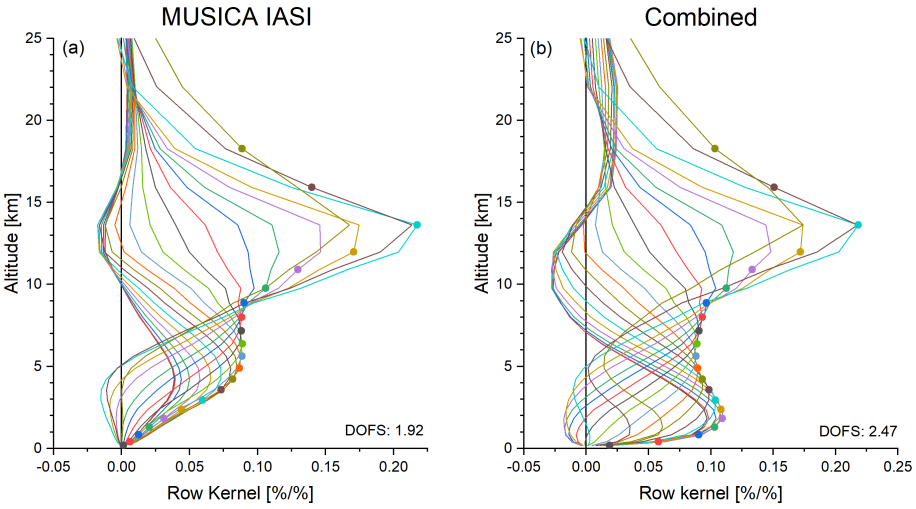

Figure 2. Logarithmic scale row kernels for (a) the MUSICA IASI and (b) the combined product for the same late summer observations as used in the context of Figs. 1 and 3. The symbols mark the kernel values at the nominal altitude.

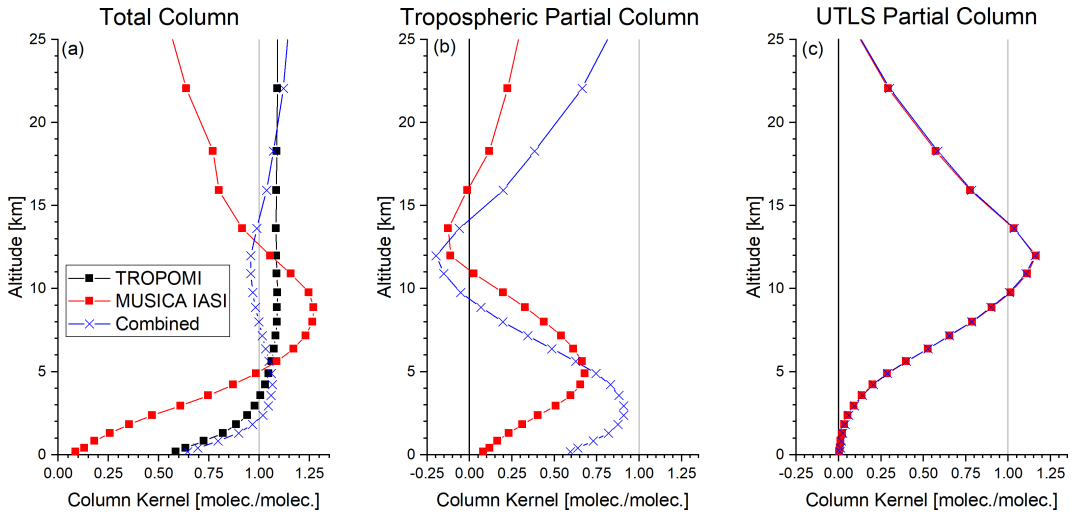

Figure 3. Total column amount and partial column amount kernels corresponding to the TROPOMI, MUSICA IASI, and combined product for the same late summer observation as used in Figs. 1 and 2: (a) total column amount kernels; (b) lower tropospheric partial column amount kernels, surface - 6 km a.s.l.; (c) upper tropospheric/lower stratospheric (UTLS) partial column amount kernels, 6 - 20 km a.s.l.

about ~~2.5~~2 km a.s.l.). In the ~~upper troposphere/lower stratosphere (UTLS)~~ UTLS we see no significant difference between the kernels.

~~Time series of the relative contribution of the a priori data to the retrieved products (example for Central Europe). Black squares: TROPOMI; red dots: MUSICA IASI; blue crosses: Combined product. (a) Total column; (b) tropospheric partial~~

~~column; (c) UTLS partial column.~~ In this work we focus on the total column and the partial columns between the surface and 6 km a.s.l. (the tropospheric partial column) and between 6 km a.s.l. and 20 km a.s.l. (the UTLS partial column). The total and partial column kernels are calculated from $\mathbf{A}_\mathbf{I}^\mathbf{l}$ and $\mathbf{A}_\mathbf{C}^\mathbf{l}$ by their transformation on linear scale (see Appendix C) and the vertical resampling as explained in Appendix D. Figure 3 depicts the total and partial column kernels corresponding to the row kernels of Fig. 2.

Total column amount kernels are available for all three products (see Fig. 3a): the TROPOMI, the MUSICA IASI, and the combined product. The TROPOMI kernel is close to unity for all altitudes, documenting the good sensitivity for CH_4 at all altitudes. The combined total column amount kernel is ~~very similar to~~ even closer to unity than the respective TROPOMI kernel~~(even correcting the overshoot at 4-6 km) and~~ , which means that the combined retrieval product does also well reflect the actual atmospheric total column amounts. The MUSICA IASI kernel has relatively low values in the lower troposphere and above 15 km, only in the UTLS region the kernel values are between 0.75 and 1.25. This means that MUSICA IASI can actually not well detect total column amounts, because it lacks sensitivity in the lower troposphere. The altitude regions where the MUSICA IASI product has reduced sensitivities are the regions where TROPOMI's total column information has the strongest impact on the combined product (see Fig. 1).

Partial column amount kernels are only available for profile products, i.e. the MUSICA IASI and the combined product (MUSICA IASI updated with information from TROPOMI). Figure 3b shows tropospheric partial column amount kernels. For the MUSICA IASI product we observe values that are generally lower than 0.5. The highest values are achieved around 6 km a.s.l., i.e. at the upper boundary of the vertical layer we defined as the tropospheric partial column. The kernel of the combined product shows a good sensitivity with peak values of almost 0.95 at 2.5 km a.s.l. and values above 0.75 for almost all altitudes between the surface and 6 km a.s.l.

UTLS partial column amount kernels are depicted in ~~Figure~~ Fig. 3c. The values are ~~close~~ closest to unity for ~~most of~~ the altitudes that we attributed to the UTLS layer (altitudes between 6 km and 20 km a.s.l.). There is almost no difference between the MUSICA IASI and the combined kernels, meaning that the information provided by TROPOMI has almost no effect on the UTLS partial column, which is because the MUSICA IASI product is already very sensitive to this altitude region.

~~According to Eqs. and for the MUSICA IASI and combined retrievaldata we can write~~ The example kernels document that the combined product allows for detecting tropospheric CH_4 largely independent from CH_4 in the UTLS, which is not possible by the IASI product alone. Figure 4 shows a time series of the degree of freedom for signal (DOFS: it is calculated as the trace of the averagi . It documents that the combination of TROPOMI with IASI improves the profiling capability of IASI rather consistently throughout all seasons. Here we also show the DOFS values of the TROPOMI retrieval, but please note that only the total column data are made available, i.e. there is no profile information in the provided TROPOMI CH_4 data product.

An optimal estimation retrieval updates the a priori knowledge with information provided by a measurement. The a posteriori uncertainty is the uncertainty achieved by optimally combing the a priori knowledge (captured by the inverse of the a priori covariance matrix, i.e. $\mathbf{S_a}^{-1}$) with the measurement. As shown in Appendix A the a posteriori uncertainty covariance is the sum of the noise covariance and the representativeness error covariance (called "smoothing error" covariance in Rodgers, 2000) . According to Eq. (A7) the representativeness error matrix is calculated from the averaging kernel ($\mathbf{A}$) and the a priori

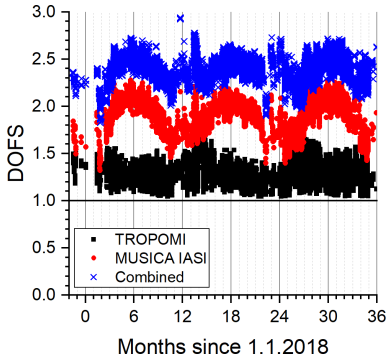

Figure 4. Time series of the degree of freedom for signal (DOFS, example for Central Europe). Black squares: TROPOMI (please note that only the total column data are made available); Red dots: MUSICA IASI; blue crosses: combined product.

covariance ($\mathbf{S_a}$) as

$$\mathbf{S}^{\mathbf{l}}_{\hat{\mathbf{x}},\mathbf{r}} = \mathbf{A}^{\mathbf{l}}(\mathbf{I}\mathbf{A}^{\mathbf{l}} - \mathbf{I})\mathbf{S}^{\mathbf{l}}_{\mathbf{a}}(\mathbf{A}^{\mathbf{l}} - \mathbf{I})^{T}, \tag{4}$$

with $\mathbf{I}$ being the identity operator. By using the kernels $\mathbf{A}^{\mathbf{l}}_{\mathbf{i}}$ and ~~$\boldsymbol{x}^{\boldsymbol{l}}$ the actual atmospheric state in logarithmnic scale. Equation reveals that the term $(\mathbf{I} - \mathbf{A}^{\mathbf{l}})\boldsymbol{x}^{\boldsymbol{l}}_{\boldsymbol{a}}$ captures the relative contribution of the a priori to the retrieved product~~ $\mathbf{A}^{\mathbf{l}}_{\mathbf{C}}$ we can calulate the representativeness error for the MUSICA IASI and the combined product, respectively. The resampling of ~~this term~~ $\mathbf{S}^{\mathbf{l}}_{\hat{\mathbf{x}},\mathbf{r}}$ on total and partial columns is made according to Eq. (D7). For the TROPOMI total column averaged mixing ratios we can calculate the ~~apriori contribution by $(\boldsymbol{w}^{*T} - \boldsymbol{a}^{*T}_{\boldsymbol{T}})\boldsymbol{x}_{\boldsymbol{a}}$~~ representativeness error by $(\boldsymbol{w}^{*T} - \boldsymbol{a}^{*T}_{\boldsymbol{T}})\mathbf{S}_{\mathbf{a}}(\boldsymbol{w}^{*T} - \boldsymbol{a}^{*T}_{\boldsymbol{T}})^{T}$. For more details see Appendix D.

Figure 5 depicts the ~~a priori contribution~~ representativeness error relative to the retrieved values for the total column, the tropospheric and UTLS partial columns. Shown are time series for measurements over Central Europe, which confirm the observations made in the context of the example kernels of Fig. 3: for the total column (Fig. 5a) the ~~a priori contribution~~ representativeness error on the TROPOMI and the combined products are rather small and can be neglected, i.e. both products can detect total column signals. In contrast the MUSICA IASI ~~total column product is significantly affected by the a priori data~~ representativeness error is much larger and the respective data do not well represent the total column, i.e. ~~provides no independent observation~~ provide no independent observations of the total column. Concerning partial column products (Fig. 5b and c) we can compare the MUSICA IASI and the combined product (the TROPOMI product has no information on the vertical distribution). The tropospheric MUSICA IASI partial column ~~is significantly affected by the a priori, but~~ has a significant representativeness error (and a seasonal cycle with highest values of about 3% in winter). In the combined product ~~is largely independent on the a priori data~~this error is throughout all seasons generally smaller than 1%. In the UTLS both the MUSICA IASI and combined products are ~~largely independent on the apriori data~~well representative for the actual atmospheric methane concentration signals (representativeness error is generally between 0.5 and 1%). In summary, ~~with~~ TROPOMI only provides

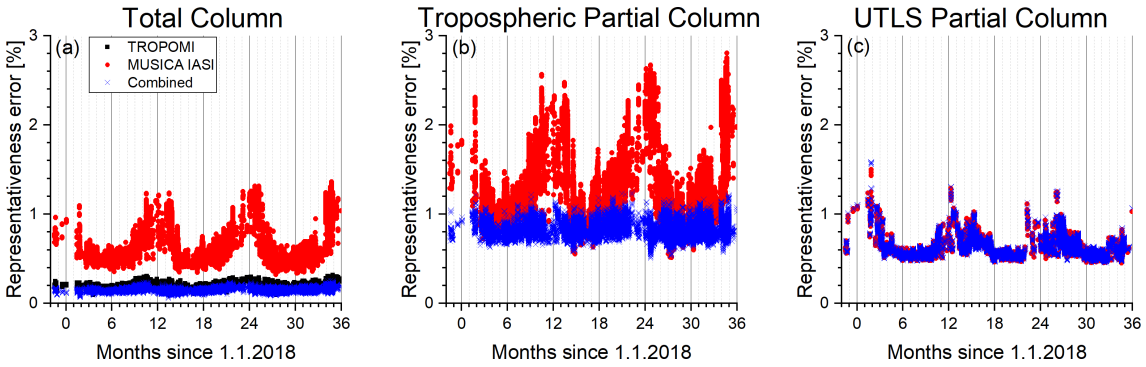

Figure 5. Time series of the representativeness error (example for Central Europe). Black squares: TROPOMI; red dots: MUSICA IASI; blue crosses: combined product. (a) Total column; (b) tropospheric partial column; (c) UTLS partial column.

total column data. With IASI alone we can well detect signals in the UTLS, but not in the lower troposphere. The detection of signals in both altitude regions independently from the a priori information is only possible by using the combined product.

3.3 Retrieval noise error

~~In this section we~~ After documenting the representativeness error in the previous subsection, here we investigate the retrieval noise error. We compare the retrieval noise errors of the individual retrieval products with those achieved when combining the two retrieval products. According to Eq. (1) we can calculate the retrieval noise covariance matrix for the combined data product by

$$\mathbf{S}^{\mathbf{l}}_{\hat{\mathbf{x}}_{\mathbf{C}},\mathbf{n}} = (\mathbf{I}-\mathbf{L}^{-1}\boldsymbol{m}\boldsymbol{a}^{*T}_{\boldsymbol{T}})\mathbf{L}\mathbf{S}^{\mathbf{l}}_{\hat{\mathbf{x}}_{\mathbf{I}},\mathbf{n}}\mathbf{L}^{T}(\mathbf{I}-\mathbf{L}^{-1}\boldsymbol{m}\boldsymbol{a}^{*T}_{\boldsymbol{T}})^{T}+(\mathbf{L}^{-1}\boldsymbol{m})S_{\hat{x}_T,n\hat{x}^{*}_T,n}(\mathbf{L}^{-1}\boldsymbol{m})^{T}. \quad (5)$$

Here $\mathbf{S}^{\mathbf{l}}_{\hat{\mathbf{x}}_{\mathbf{I}},\mathbf{n}}$ is the retrieval noise covariance matrix of the MUSICA IASI retrieval. The error covariances resampled to the total and partial columns are then determined according to Appendix D. Figure 6 shows the retrieval noise errors (which are the square root values of the error variances) relative to the retrieved values for the total column and the tropospheric and UTLS partial columns.

The errors for the total columns (Fig. 6a) are generally below 0.2% for the TROPOMI product. For the MUSICA IASI product they are rather stable at about 0.6%. Concerning the combined product the retrieval noise error is very similar to the retrieval noise error of the TROPOMI data.

For the tropospheric partial columns (Fig. 6b) the error is in general above 1% for the MUSICA IASI product and below 1% for the combined product. For the UTLS partial columns (Fig. 6c) we observe an error of generally below 1% and no significant difference between the MUSICA IASI and the combined data products. This suggests that the error in the combined product is dominated by the error in the MUSICA IASI data, which reveals the very limited impact of the TROPOMI data on the combined UTLS data product.

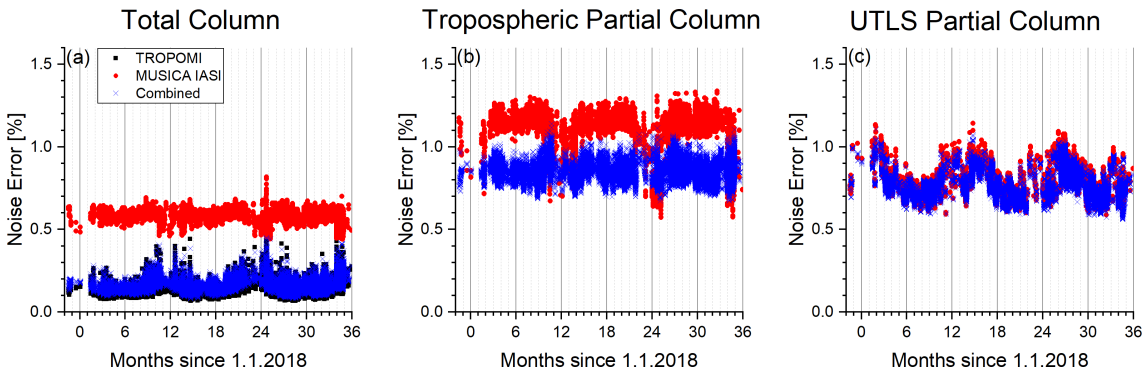

Figure 6. Time series of estimated relative noise error for the retrieved products (example for Central Europe). Colours are as in Fig. 5. (a) Total column; (b) tropospheric partial column; (c) UTLS partial column.

3.4 Dislocation error

As mentioned in Sect. 2.3 we allow for small dislocations between the TROPOMI and IASI observations of up to 6 hours and 50 km. As derived in Appendix E the dislocation error covariance matrix is calculated by

$$\mathbf{S}^{\mathbf{l}}_{\hat{\mathbf{x}}_{\mathbf{C,dl}}} = \mathbf{A}^{\mathbf{l}}_{\mathbf{C,dl}} \mathbf{S}^{\mathbf{l}}_{\mathbf{\Delta_{dl}}} {\mathbf{A}^{\mathbf{l}}_{\mathbf{C,dl}}}^{T}, \tag{6}$$

where $\mathbf{A}^{\mathbf{l}}_{\mathbf{C,dl}}$ is the dislocation kernel and $\mathbf{S}^{\mathbf{l}}_{\mathbf{\Delta_{dl}}}$ is the covariance matrix for the CH_4 dislocation uncertainty, whose main characetristics are visualised in Figs. E1 and E2. The low entries of the dislocation kernel at low altitudes (typical example see Fig. E4), reduces the impact of the spatial and temporal dislocation on the total and tropospheric partial columms of combined product.

Over Central Europe we estimate an error in the combined product due to the dislocations between IASI and TROPOMI as shown in Fig. 7. For the total column the error is below 0.1% and for the tropospheric and UTLS partial columns it is generally below 0.8%. If compared to the noise error (see Fig. 6), the dislocation error is of secondary importance. Details on the estimation of these dislocation errors and examples for other locations are given in Appendix E.

4 Validation

In this section we ~~compare the~~ empirically evaluate the quality of the TROPOMI, MUSICA IASI, and combined products by their inter-comparison to different reference data products. As reference for the total column averaged mixing ratio (XCH_4) we use TCCON (Total Carbon Column Observing Network, Wunch et al., 2011a) ground-based remote sensing data from ~~six~~ 14 sites located in different climate zones. As reference for the total and the partial columns we use in-situ profiles measured by the AirCore system (Karion et al., 2010) at two geophysically different European locations. Furthermore, we use in-situ data measured at two nearby Central European Global Atmospheric Watch (GAW) mountain stations.

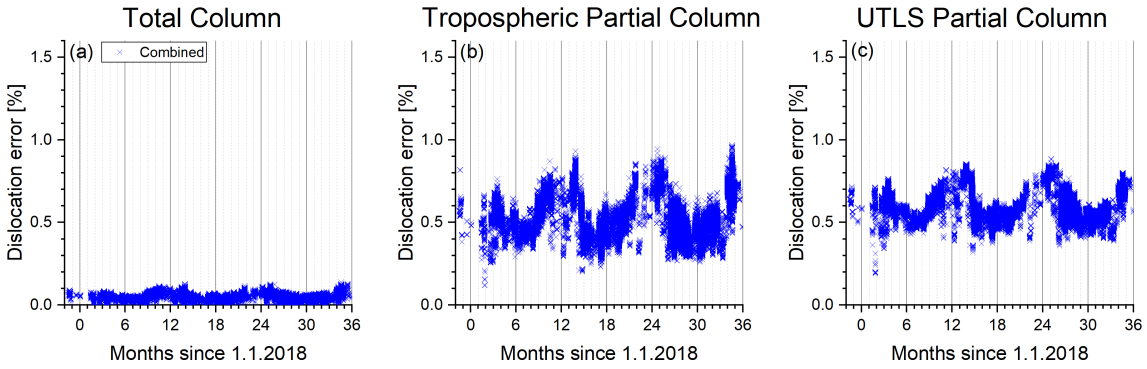

Figure 7. Time series of estimated relative dislocation error for the combined product due to temporal and spatial dislocation of the TROPOMI and IASI satellite ground pixels (example for Central Europe). (a) Total column; (b) tropospheric partial column; (c) UTLS partial column.

~~Map showing the location of the European reference measurements and the areas accepted for valid horizontal collocation. Blue crosses and circles: sites with AirCore measurements and circles with 500 km radius. Red crosses and grey dots: sites with TCCON and GAW measurements, respectively, and circles with 150 km radius.~~ Figure 8 depicts the geographical location of the ~~European~~ reference observations. ~~We consider the European TCCON stations at Sodankylä (Finland)and Karlsruhe (Germany). They are indicated as red crosses together with~~ Figure 8a shows that the considered TCCON stations are distributed around the globe (more detailed information on these sites is given in Table 1). Figure 8b gives details on the different European reference sites and the areas accepted for a valid collocation. For collocation with TCCON the satellite ground pixels should fall within a circle around the stations with a radius of ~~150~~100 km ~~indicating the spatial collocation criteria: only satellite observations with ground pixels inside this circle are compared to the TCCON data . Blue crosses and circles represent the locations of AirCore measurements (at Trainou, France, and Sodankylä, Finland)and their spatial collocation criteria, respectively. Here~~ (red crosses and circles). For the comparison to the GAW data the collocation circle has a radius of 150 km (grey circle) and is centred in the middle of the two GAW stations (Jungfraujoch in Switzerland and Schauinsland in South-western Germany indicated by the grey dots). For the comparison with AirCore we relax the radius of the collocation circle to 500 km in order to achieve a sufficient high number of coincidences between AirCore and satellite observations. The two ~~grey dots indicate the locations of the two GAW stations (Jungfraujoch in Switzerland and Schauinsland in South-western Germany~~AirCore sites (Trainou in France and Sodankylä in Finnland) and the ~~respective grey spatial collocations circle around the middle distance point of the two stations has a radius of 150 km.~~collocation circles are indicated by the blue stars and circles.

Appendix F reveals that the following validation results are in reasonable agreement with sensitivities and errors of the different satellite data products as shown in Sects. 3.3 - 3.4.

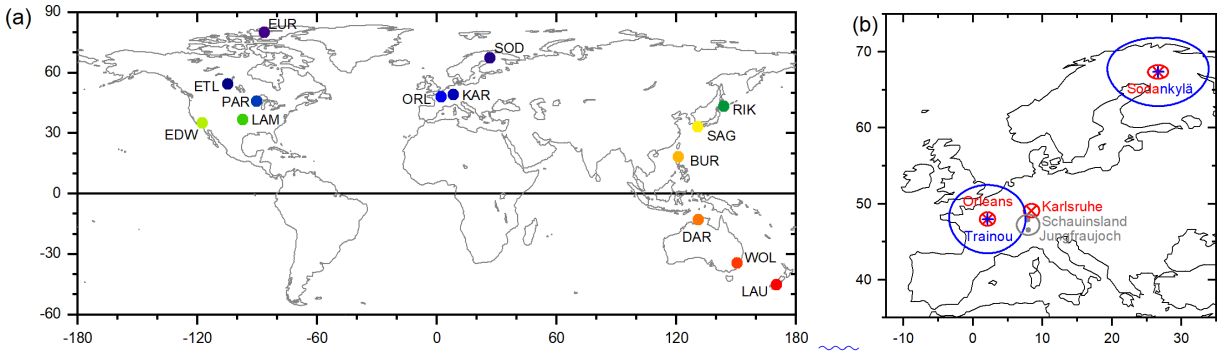

Figure 8. Maps showing the location of the reference measurements used for the validation. (a) Global map with the 14 TCCON stations (more detailed information on these sites is given in Table 1). (b) Map indicating the areas accepted for valid horizontal collocations in the sourroundings of the European reference stations: TCCON sites and the 100 km collocation radius (red crosses and circles), AirCore sites and the spatial collocation circles with 500 km radius (blue stars and circles), and GAW sites and the collocation circle with 150 km radius (grey dots and circle).

4.1 TCCON XCH_4

We use TCCON ground-based remote sensing data from ~~six exemplary~~ 14 sites located in different climate zones representative for high, mid and low latitudes. ~~The Sodankylä site is located at high latitudes, Karlsruhe and Lauder are located in~~ Details on the locations of these sites, the respective data amounts, and references are given in Table 1. We use the TROPOMI a priori setting for the comparison between the ground-based TCCON and the ~~northern and southern hemispheric mid-latitudes, Wollongong is located in the subtropics, and Burgos and Darwin are located in~~ satellite-based remote sensing products. For this purpose the TCCON product is adjusted to the TROPOMI a priori settings according to Eq. (B13), which ensures the usage of the same a priori data for all the remote sensing products. As spatial collocation criteria we require the TROPOMI and IASI ground pixels to be located within 100 km of the TCCON station (where we consider the viewing direction of the TCCON spectrometer by using as location, the TCCON's line of sight {latitude,longitude} at 5 km altitude). Differences in the satellite and TCCON ground pressures are taken into account by correcting the TCCON XCH_4 values according to Appendix B of Sha et al. (2021). For collocation with respect to time, we use as TCCON reference the median XCH_4 value calculated from all TCCON data measured within 2 hours of the TROPOMI observation. Furthermore, we require stable conditions for atmospheric CH_4. This is achieved by performing the comparisons only, if there are at least 3 individual TCCON observations that fullfil the collocation criterion and if the timestamps of these observations have a 1σ standard deviation of 1 hour and the ~~tropics. More details on the locations of these sites and references and amount of the used data sets are given in Table 1~~ 1σ standard deviation of the respective XCH_4 data is smaller than 0.5%.

~~We use the TROPOMI apriori setting for the comparison between the ground-based TCCON and the satellite-based remote sensing products.For this purpose the TCCON product is adjusted to the TROPOMI a priori settings according to Eq. , which ensures the usage of the same a priori data for all the remote sensing products. As spatial collocation criteria we require that~~

Table 1. Locations of TCCON sites~~and references and~~ , amount of the ~~TCCON~~ satellite data ~~used in this study~~compared to TCCON, and references. "~~N~~Number" gives the total number of ~~collocations with~~ single satellite ~~footprints~~ footprint collocations and "Days" the number of days with collocations.

~~Name and Country~~ Station (ID)	~~Latitude~~ Location	~~Longitude~~ Period
~~Sodankylä, Finland~~ Eureka (EUR)	80.1°N; 86.4°W; 610 m a.s.l.	06/2020 - 06/2020
Sodankylä (SOD)	67.4°N; 26.6°E; 190 m a.s.l.	~~Kivi et al. (2014); Kivi and Heikkinen (2016)~~ 05/2018 - 0
~~Karlsruhe, Germany~~		
East Trout Lake (ETL)	54.4°N; 105.0°W; 500 m a.s.l.	02/2018 - 08/2020
Karlsruhe (KAR)	49.1°N; 8.4°E; 120 m a.s.l.	~~Hase et al. (2015)~~ 02/2018 - 11/2020
~~Burgos, Philippines~~ Orleans (ORL)	~~18.5~~48.0°N~~120.7~~; 2.1°E~~40~~; 130 m a.s.l.	~~Velazco et al. (2017)~~02/2018 - 09/2020
~~Darwin, Australia~~ Park Falls (PAR)	~~12.5~~46.0°~~S 130.9~~N; 90.3°~~E 40~~W; 440 m a.s.l.	~~Griffith et al. (2014a)~~11/2017 - 12/2020
~~Wollongong, Australia~~ Rikubetsu (RIK)	~~34.4~~43.5°~~S 150.9~~N; 143.8°E~~30~~; 380 m a.s.l.	~~Griffith et al. (2014b)~~11/2017 - 09/2019
~~Lauder, New Zealand~~ Lamont (LAM)	~~45.0~~36.6°~~S 169.7~~N; 97.5°~~E 610~~W; 320 m a.s.l.	~~Sherlock et al. (2014); Pollard et al. (2019)~~12/2017 - 12/
Edwards (EDW)	35.0°N; 118.9°W; 700 m a.s.l.	06/2018 - 12/2020
Saga (SAG)	33.2°N; 130.3°E; 10 m a.s.l.	11/2017 - 12/2020
Burgos (BUR)	18.5°N; 120.7°E; 40 m a.s.l.	11/2018 - 03/2020
Darwin (DAR)	12.5°S; 130.9°E; 40 m a.s.l.	06/2018 - 04/2020
Wollongong (WOL)	34.4°S; 150.9°E; 30 m a.s.l.	03/2018 - 06/2020
Lauder (LAU)	45.0°S; 169.7°E; 610 m a.s.l.	11/2017 - 12/2020

~~the ground pixels of the TROPOMI and the IASI measurement fall within a circle with a radius of 150 km around the TCCON sites. For collocation with respect to time, TCCON, TROPOMI, and IASI observations have to be made within at least 6 hours. Furthermore, we require that the altitude differences between the TCCON stations and the satellite ground pixels are within 250 m .~~

~~We estimate the reliability of the TCCON data as reference for the satellite observations.For this estimation we consider the TCCON retrieval noise errors, the incomparableness of TCCON and satellite data caused by their different averaging kernels, and the collocation mismatch. The total column uncertainty variance (the scalar S_{ref}) for using the TCCON data as reference for the satellite data can be estimated by:~~

$$S_{\mathrm{ref}} = S_{\Delta \mathrm{TC}} + (\boldsymbol{a}^{*T} - \boldsymbol{a}^{*}_{\mathbf{TC}}{}^{T})\mathbf{S}_{\mathbf{\Delta a}}(\boldsymbol{a}^{*T} - \boldsymbol{a}^{*}_{\mathbf{TC}}{}^{T})^{T} + \boldsymbol{a}^{*}_{\mathbf{TC}}{}^{T}(\mathbf{S}_{\mathbf{\Delta}_{\mathrm{t}}} + \mathbf{S}_{\mathbf{\Delta}_{\mathrm{h}}})\boldsymbol{a}^{*}_{\mathbf{TC}},$$

~~The first term (the scalar $S_{\Delta \mathrm{TC}}$) is the TCCON retrieval error covariance (the TCCON error is provided with the TCCON data is typically 1).The second term accounts for the different averaging kernels.The row vectors $\boldsymbol{a}^{*T}$ and $\boldsymbol{a}^{*}_{\mathbf{TC}}{}^{T}$ are the total column averaged mixing ratio kernels of the satellite and the TCCON retrievals, respectively (calculated according to Appendix D) . The matrix $\mathbf{S}_{\mathbf{\Delta a}}$ describes the uncertainty covariances of the used a priori data. We determine these uncertainty covariances~~

from the TM5 CH_4 simulations (Krol et al., 2005), which are provided in the TROPOMI data set as the a priori data. For this purpose we assume a hypothetical out-of-phase of the model of 24 hours and in addition ahorizontal mismatch of the modeled CH_4 fields of 500 km.The covariances obtained for the differences between the original TM5 model fields and the TM5 fields with the hypothetical model deficits are then used as the uncertainty covariances.We found an a priori uncertainty covariance $\mathbf{S_{\Delta a}}$ having largest values close to the surface but even there, the uncertainty variance is smaller than $(4‰)^2$. Due to this good a priori knowledge the effect of the different averaging kernels on the comparison is less than 0.5 (even for the comprison between the TCCON and the MUSICA IASI products, where the difference in the averaging kernels is most significant) . The third term takes into account that TCCON and the satellites might detect different air masses.The respective uncertainty covariances are again estimated with the TM5 CH_4 simulations. We determine the covariances between out-of-phase model fields and the correct model fields for different out-of-phase time intervals. Similarly we calculate the covariances between model fields that have a horizontal mismatch and the correct model fields for different horizontal mismatch intervals. The temporal collocation uncertainty covariance ($\mathbf{S_{\Delta t}}$) and the horizontal collocation uncertainty covariance ($\mathbf{S_{\Delta h}}$) are then the covariances interpolated to the actual temporal and horizontal mismatch of the satellite and the TCCON measurements.The effect of this collocation mismatch on the comparison of the total columns is estimated to be smaller than 0.5.In summary, we estimate the reliability of the TCCON data as reference for the satellite total column observations to be within 2.

In Fig. 9 the TROPOMI, MUSICA IASI, and combined XCH_4 products are compared to the TCCON XCH_4 data. The crosses represent the daily mean data and the filled symbols in the background show all data corresponding to all individual valid collocations (between all single pixel satellite observations and individual TCCON observations). Figure 9a-c show time series of the differences with respect to the TCCON references. The daily mean data have error bars, which is the 1σ standard deviation of the data used for calculating the daily mean.

Statistics in form of mean difference and 1σ standard devation (scatter) around the mean the median of the difference and the scatter around the median difference are given in each panel (for statistics using daily mean data in black fonts and for statistics using all individual valid collocations in grey fonts). We use here the median in order to be less affected by outliers. For the same reason we use as metric for the scatter the half inter-percentile range between the 15.9 and 84.1 percentiles (hIPR68.2, which is analogous to the 1σ standard deviation in case of a pure Gaussian distribution). Concerning TROPOMI (Fig. 9a) we observe – in line with ? – a very a good agreement. For daily mean data as well as for the statistics based on all individual differences, the mean median difference is within 0.560.1% and the scatter lies below 0.9%. A very 0.7%.

A similar good agreement and low values for mean median difference and scatter are is also achieved for the combined product (Fig. 9c). For the MUSICA IASI product (Fig. 9b) we have reduced sensitivity in the lower troposphere (see Figs. 3 and 5)and the observed good . Because of uncertainties in the a priori assumptions the agreement with the TCCON XCH_4 data can be partly explained by the reliable a priori data. is weaker (uncertainties in the a priori assuption are less well detected, see Fig. F2). We observe no significant systematic negative or positive difference for the satellite versus TCCON comparisons, i.e. the satellite data sets seem to be in good absolute agreement with TCCON. In general the observed scatter values are within the range that can be expected from the data uncertainties and the data comparability (for more details see Appendix F).

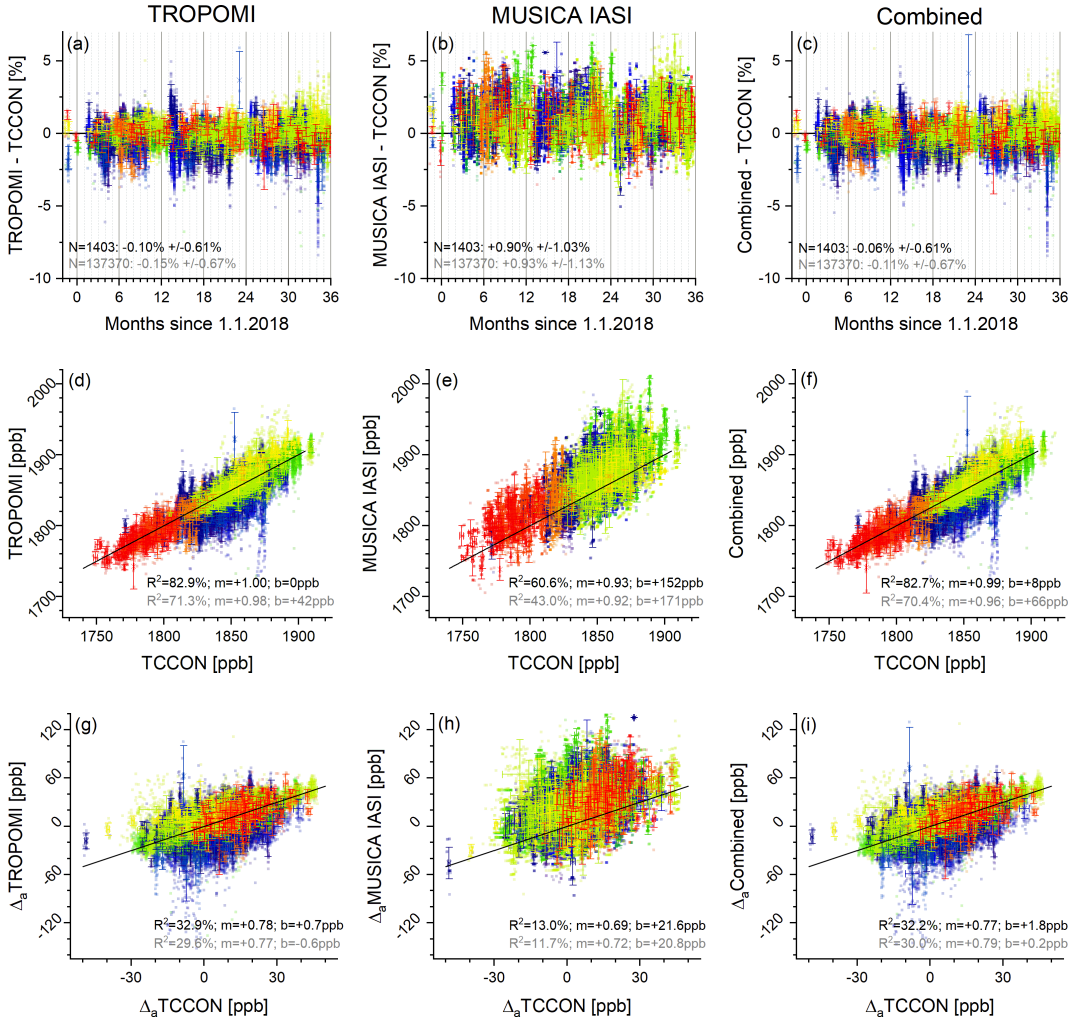

Figure 9. Comparison of the different XCH_4 satellite products with TCCON XCH_4 data from ~~five~~ 14 globally representative stations (the different colours correspond to the stations as ~~given~~ shown in ~~the legend~~Fig.8a). Data for all individual coincidences are plotted in the background as squares and daily mean data are depicted as crosses with error bars representing the 1σ standard deviation (daily means are only calculated if there are at least 3 observations per day): (a)-(c) ~~shows~~ time series of the differences~~, text in dark and pale fonts report mean and 1σ standard deviation~~ . ~~(scatter) determined from daily mean data and from all individual collocations, respectively; (~~d)-(f) ~~visualises the correlations~~ Correlations between TCCON and satellite data (the black line is the one-to-one diagonal)~~, ~~. (g)-(i) Correlations between the a priori free TCCON data (Δ_aTCCON = XCH_4(TCCON) − XCH_4(apriori)) and the a priori free satellite data (Δ_aSatellite = XCH_4(Satellite) − XCH_4(apriori)). The inserted text ~~in dark~~ reports median and ~~pale fonts report coefficients of determination~~ scatter (~~R^2~~hIPR68.2, a-c) and the coefficients of determination, the slope, and the intercept of the robust linear regression ~~line~~ model (R^2, m, and b, d-i)~~obtained~~. Black and grey fonts represent the values for ~~a linear least squares fit on~~ the daily mean data and ~~on~~ for data from all individual collocations, respectively.

Figure 9d-f depicts the correlation plots. In order to reduce the effect of outliers, we apply a robust linear regression model (the iteratively reweighted least-squares algorithm with Tukey's bisquare weight function and the respective tuning parameter set to the commonly used value of 4.685). For daily mean data the obtained coefficients of determination (R^2) are ~~about 62~~larger than 80% for the TROPOMI and the combined product. The slope of the obtained linear regression line is ~~slightly closer to unityfor the combined data product than for the TROPOMI data product~~very close to unity. When considering all individual coincidences the R^2 values are about ~~30~~70%. The error bars on the daily mean data are the 1σ standard deviations of the data used for calculating the daily mean. For the MUSICA IASI product, we observe a similar good correlation ~~than~~ as for the TROPOMI and the combined products. However, concerning the MUSICA IASI data, part of the common signal might be due to the a priori on which the MUSICA IASI total column product is not independent (the MUSICA IASI data have a reduced sensitivity, i.e. an increased representativeness error, see Fig. 5a).

~~The different satellite XCH_4 data products show a very good agreement with the TCCON data (within 0.9%-1.1% concerning the comparison of single satellite pixel data with individual reference data). Figure F3 shows the correlations between the theoretically predicted scatter – considering the reference uncertainty according to Eq. and the~~ Figure 9g-i reveals the information gained by the satellite ~~products' noise error (see Fig. 6) – and the actually observed scatter. For the comparison of the MUSICA IASI product with TCCON (red square) we observe a larger scatter than for the comparison of the TROPOMI and combined products with TCCON (black and blue squares). The relatively larger scatter for the MUSICA IASI comparison is also theoretically predicted and mainly due to the increased noise error of this product (see Fig. 6a). Nevertheless, for all satellite products there is a systematic difference between the theoretically predicted and actually observed scatter values. Because it is consistently seen in all satellite products we assume that it is due to an underestimation of the reference uncertainty calculated according to Eq.~~ data with respect to the a priori data. ~~Theoretically predicted and observed 1σ scatter for the comparison of single pixel satellite data with individual TCCON and AirCore reference data. Black, red and blue colours represent TROPOMI, MUSICA IASI, and combined satellite data, respectively. The squares and vertical crosses are for XCH_4 comparisons with TCCON and AirCore references, respectively. The diagonal crosses and stars are for tropospheric and UTLS partial column comparisons, respectively, with AirCore references.~~

~~We observe small systematic negative and positive differences for the TROPOMI versus TCCON and the MUSICA IASI versus TCCON comparisons, respectively. Although these systematic differences are not significant (within the observed standard deviation), they might indicate to a bias between the TROPOMI and MUSICA IASI XCH_4 products of about 1%~~It depicts the correlation between the collocated a priori free TCCON data ($\Delta_a\mathrm{TCCON} = \mathrm{XCH_4(TCCON)} - \mathrm{XCH_4(apriori)}$) and the a priori free satellite data ($\Delta_a\mathrm{Satellite} = \mathrm{XCH_4(Satellite)} - \mathrm{XCH_4(apriori)}$). It shows the same data as in 9d-f but with the a priori knowledge removed. We find that the TROPOMI and the combined data product adds a significant amount of information to the a priori knowledge (R^2 values for the respective linear correlations of above 32%). This information gain is much smaller in the case of the MUSICA IASI data, which confirms that the good correlation as observed in Fig. 9e is to a large extent due to the good quality of the a priori data.

4.2 Air-Core in-situ CH_4 profiles

We use the AirCore balloon borne in-situ measurements (Karion et al., 2010) as the reference for CH_4 total columns as well as for the CH_4 vertical distribution. The AirCore system samples the vertical distribution of CH_4 with a much better vertical resolution than the satellite remote sensing systems. For this reason we can generate an AirCore profile ($\hat{\boldsymbol{x}}_{\mathrm{AC}}$) that has the same vertical sensitivity and resolution characteristics as the remote sensing data. According to Eqs. (A2) and (A4) for the MUSICA IASI and the combined retrieval data we can write:

$$\hat{\boldsymbol{x}}^{\boldsymbol{l}}{}_{\mathrm{AC}} = \boldsymbol{x}^{\boldsymbol{l}}_{\boldsymbol{a}} + \mathbf{A}^{\mathbf{l}}(\boldsymbol{x}^{\boldsymbol{l}}{}_{\mathrm{AC}} - \boldsymbol{x}^{\boldsymbol{l}}_{\boldsymbol{a}}). \tag{7}$$

Here $\mathbf{A}^{\mathbf{l}}$ and $\boldsymbol{x}^{\boldsymbol{l}}_{\boldsymbol{a}}$ are the logarithmic scale averaging kernels and the logarithmic scale a priori state of the satellite retrieval, respectively, $\boldsymbol{x}^{\boldsymbol{l}}{}_{\mathrm{AC}}$ is the measured logarithmic scale AirCore profile regridded to the atmospheric model grid used for the satellite retrievals. The resampling of these data on total and partial columns is made with the linear scale data according to Eq. (D5). For the TROPOMI total column averaged mixing ratios we ~~calcuated~~ calcuate the adjusted AirCore total column averaged mixing ratio (a scalar) by ~~$\hat{x}_{\mathrm{AC}} = \boldsymbol{w}^{*T}\boldsymbol{x}_{\boldsymbol{a}} + \boldsymbol{a}^{*T}_{\boldsymbol{T}}(\boldsymbol{x}_{\mathrm{AC}} - \boldsymbol{x}_{\boldsymbol{a}})$~~ $\hat{x}^{*}_{\mathrm{AC}} = \boldsymbol{w}^{*T}\boldsymbol{x}_{\boldsymbol{a}} + \boldsymbol{a}^{*T}_{\boldsymbol{T}}(\boldsymbol{x}_{\mathrm{AC}} - \boldsymbol{x}_{\boldsymbol{a}})$. For more details see Appendix D.

As spatial collocation criteria we require that the ground pixels of the TROPOMI and ~~the~~ IASI measurement fall within a circle with a radius of 500 km around the mean horizontal location of the AirCore system when sampling between the 450 and 550 hPa pressure levels. The temporal collocation requirements for both satellite observations is 6 hours. AirCore data are typically not available close to the ground and above the burst altitude of the balloon (approximately 25 hPa). At low altitudes we extend the profile with the concentrations closest to the ground. At high altitudes we extend the profile with the TM5 model data, with a smooth transition between the measured values and the modelled data.

~~Similar to the TCCON data we estimate the reliability of the AirCore profile data as reference for the satellite observations. For this estimation we consider an AirCore measurement noise covariance ($\mathbf{S}_{\mathbf{\Delta}\mathrm{AC,n}}$). It is calculated assuming an uncertainty for altitudes with AirCore CH_4 data of 0.3% (Karion et al., 2010) and the uncertainty according to $\mathbf{S}_{\mathbf{\Delta a}}$ from Sect.4.1 for all other altitudes. The outer diagonal elements are determined by assuming the same vertical correlation as derived for $\mathbf{S}_{\mathbf{\Delta a}}$. In addition, we consider uncertainties in the height attribution, which is according to Wagenhäuser et al. (2021) below 10 m close to ground, about 200 m at 20 km a.s.l. and about 1 km at 27 km a.s.l. For some AirCore soundings there was a problem with the electronic board. For those measurements information on pressure, altitude and temperature had to be reconstructed from the radiosonde data and we use for all altitude levels an additional height attribution uncertainty value of 500 m. We construct a respective height attribution uncertainty covariance ($\mathbf{S}_{\mathbf{\Delta}\mathrm{AC,v}}$) by assuming a very strong correlation of the height attribution uncertainties between different altitude levels. The temporal and spatial collocation uncertainty covariance between the AirCore and the satellite observations ($\mathbf{S}_{\mathbf{\Delta}\mathrm{t}}$ and $\mathbf{S}_{\mathbf{\Delta}\mathrm{h}}$, respectively) are calculated as described in Sect. 4.1.~~

~~All the aforementioned uncertainties are independent and we can calculate the total uncertainty as:~~

$$\mathbf{S}_{\mathbf{\Delta}\mathrm{AC}} = \mathbf{S}_{\mathbf{\Delta}\mathrm{AC,n}} + \mathbf{S}_{\mathbf{\Delta}\mathrm{AC,v}} + \mathbf{S}_{\mathbf{\Delta}\mathrm{t}} + \mathbf{S}_{\mathbf{\Delta}\mathrm{h}}.$$

~~The reliability of the AirCore data – after its adjustment according to Eq. – as reference for the MUSICA IASI and combined satellite data can then be estimated by:~~

$$\mathbf{S}^{\mathbf{l}}_{\mathrm{ref}} = \mathbf{A}^{\mathbf{l}}\mathbf{S}^{\mathbf{l}}_{\mathbf{\Delta}\mathrm{AC}}{\mathbf{A}^{\mathbf{l}}}^{T}.$$

~~Here and in Eq. the covariances are determined for the full vertical profile. Respective covariances for total or partial columns can be derived according to Appendix D. The reliability for the TROPOMI total column averaged mixing ratio data can be calculated by $S_{\mathrm{ref}} = \boldsymbol{a}^{*}_{\boldsymbol{T}}{}^{T}\mathbf{S}_{\mathbf{\Delta}\mathrm{AC}}\boldsymbol{a}^{*}_{\boldsymbol{T}}$.~~

~~List with information about the AirCore flights. P_{min},$P_{\mathrm{max}}$is the pressure range covered by the AirCore measurements. N is the number of collocated satellite observations (one collocation of IASI and TROPOMI counts as one). $P_{\mathrm{max}} = \overline{P^{\mathrm{Sat.}}_{\mathrm{GND}}} - P_{\mathrm{max}}$ is the mean difference between AirCore maximum pressure value and the pressure values for the collocated satellite ground pixels. $\overline{\Delta h}$ is the mean horizontal distance between the AirCore system (location for AirCore system at 450-550 hPa) and the locations of the satellite ground pixels. $\overline{\Delta t} = \overline{t^{\mathrm{Sat.}}} - t$ is the mean time difference between the AirCore observations (time for AirCore system at 450-550 hPa) and the satellite observations. $\overline{\mathrm{\Delta AC_{tot}}}$, $\overline{\mathrm{\Delta AC_{tro}}}$, and $\overline{\mathrm{\Delta AC_{utls}}}$ are the square roots of the variances (determined according to Eq. and the column calculations according to Appendix D). These are the estimated uncertainties for using the adjusted AirCore data as reference for the satellite data: for the total column (index: 'tot') and the tropospheric and UTLS partial columns (indices 'tro' and 'utls', respectively). ID Location Date P_{min} P_{max} N $\overline{\Delta P_{\mathrm{max}}}$ $\overline{\Delta h}$ $\overline{\Delta t}$ $\overline{\mathrm{\Delta AC_{tot}}}$ $\overline{\mathrm{\Delta AC_{tro}}}$ $\overline{\mathrm{\Delta AC_{utls}}}$YYYYMMDDhPahPahPakmmin%%%0-1 Trainou 20180523 29.0 962.3 68 +43.4 409 -41 0.4 0.4 0.41-2 20180525 26.4 972.2 23 -2.7 363 -47 0.3 0.4 0.32-3 20190220 21.9 983.4 240 +14.1 301 -76 0.6 0.5 0.73-4 20190220 19.2 940.5 183 +58.3 305 -1380.3 0.4 0.34-5 20190221 19.8 902.7 433 +92.5 284 -76 0.6 0.5 0.75-6 20190221 19.4 986.3 318 +11.6 266 -1180.3 0.4 0.46-7 20190617 20.5 910.9 399 +64.2 357 -2270.5 0.4 0.67-8 20190618 23.8 972.8 31 +66.8 375 -1040.6 0.5 0.78-9 20190621 44.6 869.1 2 +141.6 216 -47 0.6 0.5 0.69-10 20191011 38.1 914.8287 +64.2 313 -82 0.5 0.5 0.610-11 Sodankylä 20180417 19.8 963.9 16 +20.2 281 -141 0.3 0.3 0.411-12 20180528 36.3 959.1 167 +43.3 401 +9 0.3 0.3 0.412-13 20180618 32.9 937.5 12 +57.2 411 -39 0.3 0.3 0.413-14 20180620 19.7 929.7 5 +66.4 316 -106 0.3 0.3 0.414-15 20180625 24.3 935.1 58 +67.3 360 -99 0.3 0.3 0.415-16 20180702 78.2 952.0 1171 +33.9 280 -127 0.3 0.3 0.316-17 20180801 15.8 962.6 452 +31.7 303 -203 0.5 0.4 0.617-18 20181003 13.0 916.5 1 +64.9 433 +61 0.3 0.3 0.418-19 20190410 15.1 975.7 51 +24.3 282 +39 0.3 0.3 0.419-20 20190628 16.6 952.8 18 +53.5 343 -9 0.3 0.3 0.420-21 20190724 16.8 961.1 207 +34.8 323 -13 0.5 0.4 0.621-22 20190801 16.3 957.8 10 +28.1 313 -14 0.3 0.3 0.322-23 20190828 13.8 966.1 680 +22.4 258 +9 0.3 0.3 0.323-24 20190909 24.0 968.0 161 +28.9 226 -43 0.3 0.3 0.3~~Table 2 gives an overview ~~on the~~ of the satellite data amount compared to the AirCore profiles measured at Trainou (France, 48.0°N, 2.1°E) and Sodankylä (Finland, 67.4°N, 26.6°E). In total we have ~~24~~ 36 individual AirCore profiles ~~with~~ measured on 31 different days for which collocated satellite observations exist. The total number of collocated single pixel satellite observations is ~~4993.~~ 34784. We estimate that the AirCore data can serve as reliable references for the ~~satellite data validation . The three columns on the right report the uncertainties determined according to Eq. . For the reliability – according to Eq. – we get very similar values (exept for the total column and the partial tropospheric column of the MUSICA IASI product, because of the limited sensitivity). It is 3-6, 3-5, and 3-7, for the total column, the tropospheric partial column and the UTLS partial column, respectively. In the troposphere the reliability depends~~

Table 2. Locations of AirCore sites and amount of satellite data compared to AirCore. "Number" gives the total number of single satellite footprint collocations, "Days" the number of days with collocations, and "AC number" the number of collocated AirCore profiles.

Station	Location	Period	Number	Days	AC number
Sodankylä	67.4°N; 26.6°E	04/2018 - 08/2020	16326	14	14
Trainou	48.0°N; 2.1°E	01/2018 - 11/2020	18458	17	22

mainly on the availability of AirCore data close to the ground and in the UTLS uncertainties of the altitude attribution have a dominating influence. validation of the total column as well as for the validation of the tropospheric and UTLS partial columns (see Appendix F).

The comparison between the TROPOMI satellite and the AirCore XCH_4 data is shown in Fig. ??10. The differences of collocated measurements are shown in Fig. ??aFigs. 10a-c. The agreement between TROPOMI the different satellite products and AirCore is very goodand the mean difference and the 1σ sigma standard deviation (scatter) around the mean difference is good: the scatter around the median difference is low and similar to the comparison between TROPOMI and TCCON. Considering the mean values for all coincidences corresponding to the same AirCore flight, we observe a coefficient of determinarion (with TCCON. Furthermore, we observe no significant bias in none of the satellite data, which demonstrates the good consistency between the RemoTeC TROPOMI and MUSICA IASI XCH_4 data.

Figure 10d-f depicts the correlation between the satellite and the adjusted AirCore data. Here we apply the same iteratively reweighted least-squares as in Sect. 4.1. The obtained R^2) of about 30% . This is values are high (for all products above 60% for daily mean data), although a bit lower than the R^2 value achieved for the correlation with TCCON data; however, we have to consider that the amplitude in the analysed total column signals is much smaller in the AirCore data set (data from two northern hemispheric sites only) if compared to the TCCON data set .

Same as Fig. ??, but for comparisons with the MUSICA IASI XCH_4, tropospheric CH_4, and UTLS CH_4 products: (a)-(c) shows the series of differences order by flight number; (d)-(f) visualises the correlation. Figure ?? presents the comparison between the MUSICA IASI and AirCore total column and tropospheric and UTLS partial column data . The differences between both data sets are depicted (data from 14 globally distributed sites). As for the comparison to TCCON we examine the correlation between the a priori free reference data ($\Delta_a\mathrm{AirCore} = \mathrm{XCH_4(AirCore)} - \mathrm{XCH_4(apriori)}$) and the a priori free satellite data ($\Delta_a\mathrm{Satellite} = \mathrm{XCH_4(Satellite)} - \mathrm{XCH_4(apriori)}$). These correlations are visualised in Fig. ??a-c10g-i. We find a very good agreement for the UTLS partial column data (mean difference of about 0.6% and a scatter of about 1%). Because at this altitude region the MUSICA IASI productis almost independent from reasonable correlation for the daily mean TROPOMI and combined data products, but no significant correlation for the daily mean IASI product. This indicates that the correlation as observed between the IASI and the adjusted AirCore data in Fig. 10e is mainly due to the a priori assumption (see Sect. 3.3), data, i.e. IASI adds almost no information with respect to XCH_4 to what is already known by the a priori effect

on $\hat{\boldsymbol{x}}_{\mathrm{AC}}$ from Eq. 7 can also be neglected and we compare here two independent datasets. For the total column we also see a good agreement (model. These findings are in line with the vertical resolution and representativeness analyses of Sect. 3.3.

Figure 11 presents the comparison between the AirCore and satellite tropospheric partial column CH_4 data. The differences between the satallite and the AirCore data are depicted in Fig. **??**a). However according to Sect. 3.3 the MUSICA IASI total column products are significantly affected by the a priori data and so is $\hat{\boldsymbol{x}}_{\mathrm{AC}}$ from Eq. 7, i.e. here we actually do not compare two independent data sets and a significant part of the good agreement might be due to 11a and b. If compared to the common a priori effect. For the tropospheric partial columns (Fig. **??**b)the agreement worsens a bit. We get a mean difference of about 2.4% and a scatter around the mean differences of about 1.3%(for data averaged per flight). The increased mean difference total column data the agreement worsens a bit (increased median difference and scatter). Nevertheless, the agreement is still good and close to what can be expected from the uncertainty and the comparability of the different data (see Appendix F). Concerning the daily mean data the combined product has a median difference and hIPR68.2 scatter of below about 0.9%. These values increase to about 1.25% for the IASI product. These results might indicate a weak systematic bias in the MUSICA IASI lower tropospheric partial columns, which might also explain the increased scatter: the bias will depend on the actual sensitivity of the MUSICA IASI product, which in turn varies with the conditions present during the observation (mainly the surface temperature and the vertical temperature and humidity profiles). .

Figure **??**d-f shows respective 11c and d show the correlation plots. We get very high In particular for the combined product we observe a reasonable correlation (R^2 values for the UTLS partial column, where the two data sets are largly independent (almost not affected by of about 26% for daily mean data obtained by using the robust linear regression model). For the IASI product the a priori data). This demonstrates that the MUSICA IASI product reliably captures the actual atmospheric CH_4 signals in the UTLS. Concerning the total column and the tropospheric partial column the MUSICA IASI and the adjusted AirCore data are not independent, neverthless the correlation strength is reduced (R^2 values are lower than for the UTLS partial coloumns. This is due to a low amplitude of the respective signals (total column) and due to varying MUSICA IASI sensitivities, which causes a varying impact of a possible systematic bias (tropospheric partial column). of about 18% for daily mean data). Furthermore, we have to consider that the IASI product has a rather limited tropospheric sensitivity (see Sect. 3.3), which means that a large part of the observed correlation is due to the a priori data: according to Eq. (7) for low entries in $\mathbf{A}^1$ the variability in the satellite data as well as in the adjusted AirCore data is determined by the variability in the a priori ($\boldsymbol{x}_{\boldsymbol{a}}^{\boldsymbol{l}}$). This is confirmed by Figs. 11e and f, which show the correlations after removing the a priori data. We observe still a good correlation for the combined product (R^2 of about 44% and regression line slope of 0.93 for daily mean data), but only a weak correlation for the IASI daily mean data (R^2 of about 11%). This clearly documents the importance of combining IASI and TROPOMI in order to be sensitive to and reliably detect tropospheric CH_4 variations.

Same as Fig. **??**, but for comparisons with the combined data products. All combined products (total column and tropospheric and UTLS partial columns) are practically independent from the a priori assumptions (see Fig. 5). Figure **??**a-c illustrates the differences between AirCore data and the combined products.For the total column we achieve values for the scatter that are similar to the comparison of the respective TROPOMI product. However, we observe a mean difference that is outside the 1σ scatter and also outside the uncertainty estimated for the AirCore references (see Table 2), which might indicate to a positive

bias in the total columns of the combined dataproduct. For the tropospheric partial column we observe a low scatter, but also mean difference of about 1.4% that is slightly outside the 1σ scatter of about 1.2%(for data averaged per flight). For the Concerning the UTLS partial column we find a very good agreement between the adjusted AirCore data and the mean difference and scatter values are similar to the comparison of the respective MUSICA IASI product.

The correlation plots (IASI and combined satellite data products (see Fig. **??**d-f)allow similar conclusions: the combined product can capture total column signals as reliable as the TROPOMI product (apart from a possible weak bias) and UTLS partial columns signals as reliable as the MUSICA IASI product. Concerning the tropospheric partial column we observe higher 12a and b): median difference calculated from the daily mean data are about -0.3% and the scatter values are within about 0.5%. We find no indication of a bias in the satellite data product. The scatter observed between the AirCore and satellite data is even better than what we estimate from the data uncertainty and the data comparability analysis (see Appendix F). Figure 12c and d show that in the UTLS the AirCore and satellite data are strongly correlated (for daily mean data and when using the robust linear regression model, we get R^2 values than for the respective correlation with MUSICA IASI data; however, only when correlating the mean values for all coincidences corresponding to the same AirCore flight. When correlating all individual coincidences the R^2 values are even lower than values of up to about 82% and regression line slopes of very close to unity). In this altitude region the MUSICA IASI and the already low R^2 values achieved for the respective correlation with MUSICA IASI data (compare Fig. **??**c with Fig. **??**e). The low values for R^2 are explained by the low CHcombined products have a very good sensitivity (see Sect. 3.3). This means that the entries in $\mathbf{A}^1$ of Eq. (7) are large and any deviation between the a priori and the actual CH_4 variability encountered during the 24 individual AirCore profiles.

Figure F3 shows the correlations between the theoretically predicted scatter – considering the reference uncertainty according to Eqs. and and the satellite products ' noise error (see Fig. 6)– and the actually observed scatter values. The black, red and blue vertical crosses are for the scatter in the XCH_4 data, and concentrations in the UTLS are well captured by the adjusted AirCore and satellite data products. Nevertheless, the red and blue diagonal crosses and stars for the scatter in the tropospheric and UTLS partial column data. There are large similarities to the scatter values obtained for the comparison with TCCON. Firstly, observation and theory agree concerning the relative scatter increases: lower scatter values for TROPOMI and combined data productsthan for MUSICA IASI data product. Secondly, for XCHcorrelation strength observed for the a priori free data (Fig. 12e and f) is relatively weak (R^2 values of 20%-23% for daily mean data). This indicates that the a priori model does generally capture well the actual variation of the CH_4 as well as for the tropospheric partial column the observed scatter is significantly larger than the theoretically predicted scatter. For the UTLS partial column we find a very good agreement in the absolut values of the theoretically predicted and actually obsereved scatter. Because the observed scatter is consistently higher than the theoretically predicted scatter independent from the kind of XCH_4 or tropospheric partial column satellite data product and also independent from the reference data (AirCore or TCCON) , it is very reasonable to assume that close to ground we underestimate the temporal collocation uncertainty covariance ($\mathbf{S}_{\Delta t}$)and the horizontal collocation uncertainty covariance ($\mathbf{S}_{\Delta h}$). These are the only terms used consistently for all the different theoretical scatter predictions.

Similar to the TCCON comparisons, the AirCore study suggests a systematic bias between the TROPOMI and MUSICA IASI XCH_4 products of slightly above 1%, which seems to be mainly due to a positive bias of about 2% in the MUSICA IASI

~~tropospheric data product. In the UTLS we observe no significant bias in the MUSICA IASI data~~concentration in the UTLS above France and northern Scandinavia.

4.3 GAW surface in-situ CH_4 measurements

At many globally distributed sites atmospheric trace gas in-situ measurements are made continuously ~~with~~ within the Global Atmospheric Watch (GAW, https://community.wmo.int/activity-areas/gaw) programme. Appendix A of Sepúlveda et al. (2014) presents a method for filtering common signals in night time CH_4 data of the two nearby mountain GAW stations Jungfraujoch (46.5°N, 8.0°E, 3580 m a.s.l.) and Schauinsland (47.9°N, 7.9°E, 1205 m a.s.l.). Data were retained as common signals when deviations of observations (after correction for vertical gradient, i.e. application of an offset, and a temporal shift in the annual cycles) at both sites were below a certain threshold. Sepúlveda et al. (2014) showed that the common signals are well representative for a broader layer in the lower free troposphere. Here we follow this approach and use the mean of the Jungfraujoch and Schauinsland CH_4 mixing ratio – whenever identified as a common signal – as a validation reference for the remote sensing data in South-western Germany and Northern Switzerland (indicated by the grey circle in Fig. 8b). We assume that the signals obtained from this GAW data filtering are well representative for the tropospheric partial column averaged mixing ratios (surface - 6 km a.s.l.) and compare these data directly to different satellite products as a fully independent data set: we do not adjust the data to a common a priori data usage as in Sects. 4.1~~and Sect. 4.2~~, because the in-situ data represent absolute measurements and do not depend on any a priori information. Furthermore, we do not adjust sensitivities as in Sect. 4.2 (see Eq. (7)), which means that we validate here also the sensitivities of the products.

~~Comparison of GAW measurements made at Jungfraujoch and Schauinsland with the TROPOMI XCH_4, the IASI tropospheric CH_4, and the Combined tropospheric CH_4 product. Data for all individual coincidences are shown in the background as squares and daily averages are depicted as crosses with error bars representing the estimated uncertainty: (a)-(c) shows the time series of differences, text in dark and pale coloured fonts report mean and 1σ standard deviation (scatter) determined from daily mean data and from all individual collocations, respectively; (d)-(f) visualises the correlation (the black line is the one-to-one diagonal), text in normal and bright coloured fonts report coefficients of determination (R^2) and the slope of the linear regression line (m) obtained for a linear least squares fit on daily mean data and on data from all individual collocations, respectively.~~ In order to be able to compare TROPOMI data to the GAW data, we calculate from the TROPOMI XCH_4 data a proxy (f_T(TROPOMI)) that represents the tropospheric column averaged mixing ratios:

$$\begin{aligned} \mathrm{troXCH_4(TROPOMI)} &\approx f_\mathrm{T}(\mathrm{TROPOMI}) \\ &= \frac{\mathrm{X_{air}}}{\mathrm{troX_{air}}}\left[\mathrm{XCH_4(TROPOMI)} - \mathrm{XCH_4(apriori)}\right] + \mathrm{troXCH_4(apriori)}. \end{aligned} \tag{8}$$

In Eq. (8) X_{air} and $troX_{air}$ are the dry air total and tropospheric partial columns, respectively, and $troXCH_4$(apriori) is the tropospheric column averaged CH_4 a priori. In the case that the CH_4 a priori in the UTLS is of very good quality, this proxy is well representative for the tropospheric CH_4 variations.

Figure 13 shows the comparison with the different satellite products. ~~Concerning the comparison with TROPOMI~~ For the tropospheric proxy product calculated from the XCH_4 ~~data we observe a very large~~ product of TROPOMI we observe no systematic difference and ~~very low values for R^2~~ a scatter of the daily mean differences of within 1.3% (Fig. 13a~~and d). This indicates that the total column (XCH_4)signals are not a good proxy for lower tropospheric CH_4 signals, instead the former are strongly~~). However, the correlation is rather weak (from the robust linear regression model we get R^2 values of about 10% and regression line slope m of below 0.5, see Fig. 13d), which might suggest that this proxy is affected by signals in the UTLS, where CH_4 values are ~~strongly affected~~ dominated by shifts of the tropopause height.

For the MUSICA IASI tropospheric partial column averaged mixing ratio product (Fig. 13b and e) we observe a smaller ~~mean~~ median difference than for the ~~TROPOMI XCH~~comparison with the TROPOMI tropospheric proxy CH_4 ~~comparison~~data, but at the same time an increased ~~1σ standard deviation (scatter) around the mean~~scatter. The R^2 values are larger than for the correlation of TROPOMI proxy data; however, we have to be careful, because ~~the lower tropospheric~~ in the lower troposphere the MUSICA IASI CH_4 data ~~are significantly affected by the a priori assumptions~~ have a limited sensitivity (see Fig. 5b). This means that the respective data are significantly affected by the a priori assumptions and the observed correlation might actually be due to a correlation with the tropospheric a priori data. ~~Furthermore, the slope of the linear regression line is significantly larger than unity~~This is confirmed by Fig. 13h, which shows the correlation after removing the a priori data. Then the correlation strength is weaker if compared to the data that include the a priori information (R^2 decreases from about 25% to 20% and from about 20% to 10% for correlations with daily mean and all individual data, respectively).

The combined ~~tropospheric~~ product has a good sensitivity in the troposphere (see Fig. 5b), i.e. the respective partial column averaged mixing ratio product is practically independent from the a priori assumptions~~(see Fig. 5b). The~~ . We find a good agreement and correlation between the GAW data and the combined products as illustrated in Fig. 13c and f: for instance, for daily mean data the difference and scatter is $+0.28\% \pm 1.05\%$, the R^2 value is about 37%, and the regression line slope very close to 1.0. This demonstrates that the combined product can reliably capture actual tropospheric CH_4 ~~signals~~ variations independently from the UTLS CH_4 ~~signals. For~~ variations and from the a priori assumption. The latter is confirmed by Fig. 13i, which shows the correlation after removing the tropospheric a priori information. We observe that the good correlation remains even after removing the a priori information (for daily mean data ~~we find a mean difference of about 1.2%, a 1σ scatter of also about 1.2%, an~~ the R^2 value ~~of almost 35% , and a slope of the linear regression line of very close to unity.~~ is about 39% and the regression line slope close to 1.0). A similar good correlation is not achieved by the TROPOMI tropospheric proxy and the IASI product.

5 ~~Bias discussion~~Global data

5.1 ~~Global validity of the observed bias~~The AirCore comparison of Sect. 4.2 indicates to a positive bias of about +1% ~~for the combined tropospheric CH_4 data product and suggests~~ Discussion on global data consistency

The TCCON and AirCore comparisons of Sects. 4.1 and 4.2 suggest that the combined total column and UTLS partial column products have no significant bias ~~for the combined UTLS dataproduct; however, the study~~ with respect to reference data.

However, there might be a weak bias in the troposphere (see discussions in the context of Fig. 11). In general we have to consider that the study on biases in the profile data is limited to ~~a middle and high northern latitude site, respectively. Nevertheless, in this section~~ the two sites where AirCore references are available: Sodankylä in northern Scandinavia and Trainou in France. In this section, we argue that it is reasonable to assume similar insignificant or low biases also for other locations.

According to Eq. (A2) a varying error in the a priori state together with a poor sensitivity (i.e. an averaging kernel being very different from an identity matrix) can cause a varying bias. If the error in the a priori state is ~~latitudinal~~ latitudinally dependent the bias will also be ~~latitudinal dependent. Furthermore~~latitudinally dependent. Similarly, a systematic error source (like an error in a spectroscopic parameter) can have a variable impact on the remote sensing product, if the sensitivity is variable. If the sensitivity has a dependency on latitude, a systematic error source can thus also cause a ~~latitudinal~~ latitudinally dependent bias. In this context, variabilities (e.g. latitudinal dependencies) of biases are likely for a low or variable sensitivity. In contrast, inconsistencies in the bias are unlikely in case of a high and constant sensitivity (as observed in Fig. 5 for the total column and tropospheric and UTLS partial ~~column~~ columns of the combined data product).

~~Statistics based on the comparisons between satellite and TCCON data of the overall mean XCH_4 values obtained for the six TCCON sites of Table 1. Product Difference (mean±std) R^2 Slope (m)TROPOMI -0.29%±0.43% 94.4% 1.04MUSICA IASI +0.45%±0.66% 85.0% 0.84Combined +0.23%±0.39% 96.3% 1.09~~Figure 14 depicts the overall mean total and partial column values obtained at the ~~six~~ 14 TCCON and and two AirCore observation sites. For total column data (Fig. 14a) we achieve a good latitudinal coverage by the TCCON observation sites and can investigate possible latitudinal inconsitencies in the satellite data products. We find that the TROPOMI and the combined satellite data product capture ~~practically the same latitudinal dependency as~~ a latitudinal dependency that is similar to the dependency as seen in the TCCON data.

Figures 3a and 5a reveal that for ~~these data~~ the TROPOMI and the combined XCH_4 products the sensitivities are very high and stable, in contrast to the MUSICA IASI data product, which has a relatively weak and seasonally (and supposed latitudinally) varying sensitivity. This explains that in Fig. 14a the latitudinal dependency of the MUSICA IASI XCH_4 data is ~~slightly~~ different from the TCCON data. Table 3 resumes the statistics made with the overall mean XCH_4 values obtained for the ~~six~~ 14 TCCON observation sites. For the TROPOMI and the combined data product the 1σ standard deviation calculated from the mean difference of the ~~six~~ 14 stations is about 0.4%. ~~The~~ A standrad linear least squares fit results in R^2 values of almost 100% and ~~the~~ regression line slope values of close to unity~~confirm~~ , which confirms the very good latitudinal data consistency of the TROPOMI and combined data products. The MUSICA IASI ~~data~~ XCH_4 product shows poorer performance with regard to the values of standard deviation ~~,~~ and R^2, ~~and regression line slope,~~ which is in line with its weak and varying sensitivity.

A similar study of the ~~latititudinal~~ latitudinal consistency of the partial column data products is compromised by the lack of profile references for low latitudes and southern hemispheric sites (Fig. 14b). Nevertheless, because the combined product has a rather high and constant sensitivity for the tropospheric as well as the UTLS partial column (see Figs. 3 and 5), we expect – as for XCH_4 – a good latitudinal consistency, i.e. a bias at low and/or southern latitudes that is ~~similar to the bias of about +1%~~

Table 3. Statistics based on the comparisons between satellite and TCCON data of the overall mean XCH_4 values obtained for the 14 TCCON sites of Table 1.

Product	Difference (mean±std)	R^2	Slope (m)	Intercept (b)
TROPOMI	-0.04%±0.41%	94.2%	1.09	-174 ppb
MUSICA IASI	+0.71%±0.67%	79.2%	0.88	$+237$ ppb
Combined	+0.02%±0.41%	94.2%	1.09	-173 ppb

~~as observed at~~ similarly insignificant or low as the biases observed at for two AirCore station in the middle and high northern latitudes.

5.2 ~~MUSICA IASI and TROPOMI~~ Example of global maps

The proposed synergetic use method needs no extra retrievals, and is thus computationally very efficient. This makes it ideal for combining the large TROPOMI and IASI data sets on global scale. Figure 15 shows monthly mean global maps ($1° \times 1°$ resolution) of TROPOMI XCH_4 data ~~inconsistencyThe validation study of Sect. 4 suggest a small positive bias of about +1% of the MUSICA IASI XCH~~and the tropospheric and UTLS partial column CH_4 data ~~product with respect to the TROPOMI XCH~~of the combined product. The maps are generated from about 1.62 million and 3.77 million individual data points in January and July 2020, respectively. These are the data that remain after requiring collocation of the quality filtered IASI and TROPOMI data according to Sect. 2.

TROPOMI alone only reports the XCH_4 data (Fig. 15a and b). We observe low XCH_4 ~~data product. This bias affects the term $[\hat{x}_T - \boldsymbol{a}_T^{*T}\hat{\boldsymbol{x}}_I]$ of Eq. and can introduce artefacts into the combined data product.For a constant Kalman gain operator the bias will mainly have a systematic effect on the combined product and will not cause variable artificial signals: the variability of~~ values at high latitudes. The lowest values are encountered in the sumertime southern hemisphere. The highest XCH_4 ~~is rather small (about 2%) and a bias of 1% only causes an artificial signal in the term $[\hat{x}_T - \boldsymbol{a}_T^{*T}\hat{\boldsymbol{x}}_I]$ of $1\% \times 2\% = 0.02\%$. However, the Kalman gain operator varies from observation to observation and in consequence the impact of a 1% bias on~~ values are present between northern low and middle latitudes. Here Fig. 15a and b shows the TROPOMI data, the XCH_4 data of the combined product ~~is very likely also variable. Furthermore, if the reason of the bias is a systematic error source (e. e. an error in a spectroscopic parameter) the varying sensitivity of the MUSICA IASI data products (see~~ are very similar.

The combined product offers the most reliable tropospheric partial columns. Respective maps are shown in Fig. ~~5) can cause variable signals in the term $[\hat{x}_T - \boldsymbol{a}_T^{*T}\hat{\boldsymbol{x}}_I]$ that are misinterpreted by the combination method.~~

~~In summary, by reducing the systematic inconsistency between the TROPOMI and MUSICA IASI~~ 15c and d. We observe partial column averaged CH_4 mixing ratios that are almost monotonically increasing from south to north. In norther hemispheric winter (January 2020) this gradient is significantly stronger than in northern hemispheric summer (July 2020). The latitudinal patterns of tropospheric CH_4 is significantly different from the respective patterns of XCH_4~~data we might be able to further~~

improve the quality of the combined data product. Assuming that this inconsistency is mainly due to a positive bias in the lower/middle tropospheric MUSICA IASI , which might indicate to an extra potential of this tropospheric CH_4 data (see Sect. 4.2), follow-up studies can focus on removing the MUSICA IASI bias (for instance, by an approach as discussed in Sect. 3.4 of Kulaw and in documenting the impact of the bias removal on the quality of the when investigating the CH_4 sources and sinks.

Figure 15e and f shows the respective maps of the UTLS partial columns (here we depict the combined data product. However, such studies are currently compromised by the lack of high quality CH_4 profile data , the respective MUSICA IASI data are very similar). We observe highest partial column averaged mixing ratios at low latitudes over land for the period after October 2017 (period with operating TROPOMI and IASI instruments). (in January 2020 around the equator and in July 2020 in the northern subtropics). The mixing ratios are lowest in high latitudes. This latitudinal pattern is in line with the tropopause hight, which increases from high to low latitudes.

6 Summary and outlook

We present a method for a synergetic use of TROPOMI total column and combination of the IASI vertical profile and TROPOMI total column level 2 retrieval products. The method is It is computationally very efficient, because it is based on simple linear algebra calculations , i.e. the execution of computationally expensive dedicated combined retrievalsis not neededthat works with the output already available from individual IASI and TROPOMI retrievals. Nevertheless, theoretically it approximates closely to a dedicated combined optimal estimation retrievalusing the combined computationally expensive multispectral retrieval, that use the TROPOMI and IASI measurements level 1 data (see Appendix B). We apply the method to CH_4 datalevel 2 products. By providing a compilation with all important equations we support the application of this method its application to other data products.

We theoretically examine the sensitivity, vertical resolution, and errors of the individual TROPOMI and IASI products and of the combined product. The TROPOMI product consists of reliable total column CH_4 data, but does not offer information on the vertical distribution. The IASI product offers some information on the vertical distribution and has best sensitivity in the UTLS region, but lacks sensitivity in the lower troposphere , i.e. it is not well sensitive and in consequence to the total column. We show that the combined product combines both strengths: it is a reliable reference for the total column and also for the UTLS partial column. In addition, we found as a clear synergetic effect that the combined product is also theoretically able to distinguish variations of CH_4 that take place in the troposphere from variations at higher altitudes (it is a reliable reference for the tropospheric partial column.

We generate the combined CHcolumns). We empirically demonstrate the functionality of the synergetic use method by comparing the different satellite CH_4 product for the time period between November 2017 and December 2019 and compare the individual and combined products to reference data of TCCON, AirCore and GAW. TCCON data are available for the different latitudes

The TCCON data offer good references for XCH_4. In this study we use data from 14 stations covering different climate regions in the northern and southern hemisphereand offer good references . For the TROPOMI and the combined data products,

which are well sensitive for XCH_4. ~~We~~ , we get an agreement ~~of all satellite XCH_4 products~~ with the TCCON data within ~~1% . This comparison reveals a good reliability of the TROPOMI and the combined XCH_4 products, because of their independency on the a priori data (the comparison of the IASI data is affected by the a priori data and thus cannot be directly interpreted). We found that the AirCore data are a very good reference for the consistent validation of~~ about 0.7% (the ~~CH~~agreement is slightly poorer with the IASI satellite product due its reduced sensitivity).

AirCore offers XCH_4 ~~total column amounts and the~~ references as well as references for the vertical distribution of CH_4 ~~vertical distribution; however, they are limited to~~ . For this study 36 individual AirCore profiles measured at two sites in the northern hemispheric high and middle latitudes ~~. Concerning total column comparison we get a very low 1σ scatter between the satellite products and the AirCore reference data (within 1%, which is similar to the comparison with TCCON). For the UTLS partial columns the scatter is also within 1% and for the tropospheric partial columns it is 1.1%- 1.7%. While the comparison to TCCON shows no significant bias, the comparsion to AirCore reveals a significant positive bias in the MUSICA IASI XCH_4 and tropospheric partial column data (significant in the sense that the systematic difference is outside the 1σ scatter and that it can also be not explained by the uncertainty of the AirCore references). For the combined tropospheric partial column product we report a slightly significant positive bias of about +1.4%.~~

~~We have only 24 AirCore profiles measured in collocation to satellite observations.A statistically more robust validation of the tropospheric partial column products can be achieved by using continuous CH~~are available. Concerning XCH_4 ~~observations from two nearby GAW stations. The CH~~, the comparisons to AirCore data confirm the results obtained by the comparison to TCCON data, and in addition demonstrate a very good consistency between the TROPOMI and the IASI product. Concerning CH_4 ~~signals that are common at both stations are a good validation reference for the troposphere. We get collocations between the GAW data and satellite observations for 100 individual days and the comparison to the tropospheric partial column averaged mixing ratios generated from the combined dataproduct confirms and widens the conclusions based on the comparison with the AirCore data: for the comparison~~ in the UTLS – where the MUSICA IASI and the combined data product are well sensitive – we find that both products agree well with the respective AirCore references (agreement within 0.7%).

The validation study with the TCCON and AirCore references shows that the total column and the UTLS partial column of the combined product has almost the same good quality as the respective products of TROPOMI and MUSICA IASI. This allows two conclusions: firstly, the assumption of the moderate non-linearity – required for a reliable functionality of the level 2 product combination according to Eq. (1) – is valid and secondly, the combined product's tropospheric data are also of good quality (good total column and UTLS data quality is an indirect proof of a good tropopsheric data quality).

The good quality of the combined product in the troposphere is in addition directly proven by the comparison to tropospheric reference data. We find an agreement of the daily mean ~~data we get a mean difference and~~ tropospheric AirCore and combined product data within 1σ ~~scatter of +1.2%$\pm$1.2%, which is in good agreement to the comparison with the AirCore data (i.e. the combined product agrees very well with reference data , but we find indications of a weak positive bias~~%. This validation result is confirmed by the statistically very robust comparison with CH_4 data observed continuously at two nearby GAW stations (the collocated GAW reference data cover all seasons for more than 3 years and represent more than 186 different days). The ~~continuous GAW CH~~GAW and the combined product's data capture very similar tropospheric CH_4 ~~reference data~~

cover seasonal cycle signals and have a larger amplitude than the AirCore data. We demonstrate that the lower tropospheric partial column averaged mixing ratio generated from the combined data productis able to capture these signals much better than the respective IASI product or the TROPOMI total column averaged product.

There might be a chance to further improve the quality of the combined data product by performing detailed investigations on the inconsistency between the TROPOMI and the MUSICA IASI XCH_4 data short term variabilities and seasonal cycles. Similar good agreements are not achieved by comparisons to the individual MUSICA IASI or TROPOMI data products, i.e.The availability of additional CH_4 profile reference data for low latitudes (e.g. obtained by the AirCore system) would be very beneficial for such purpose we empirically and directly prove the synergetic effect of the level 2 product combination.

The proposed method takes benefit from the outputs generated by the dedicated individual TROPOMI and IASI retrievals, it needs no extra retrievals, and is thus computationally very efficient. This makes it is ideal for an application at large scale, and allows the combination of operational operational combination of IASI and TROPOMI products in an efficient and sustained manner. This has a particular attraction, because IASI and TROPOMI successor instruments will be jointly aboard the upcoming Metop (Meteorological operational) Second Generation satellites (guaranteeing observations from the 2020s to the 2040s). There will be several 100,000 globally distributed and perfectly collocated IASI and TROPOMI successor instruments will have globally-distributed and perfectly-collocated observations (over land) of IASI and TROPOMI successor instruments in the order of several hundred thousands per day, for which a combined product can be generated in a computationally very efficient way.

Data availability. Access to the MUSICA IASI data is provided via http://www.imk-asf.kit.edu/english/musica-data.php. The TROPOMI XCH_4 data used in this study are available for download at ftp://ftp.sron.nl/open-access-data-2/TROPOMI/tropomi/ch4/14_14_Lorente_et_al_2020_AMTD/. TCCON data are made available via the TCCON Data Archive, hosted by CaltechDATA, California Institute of Technology, California (USA), http://tccondata.org. For Trainou AirCore data please contact Michel Ramonet (michel.ramonet@lsce.ipsl.fr) and for Sodankylä AirCore data please contact Huilin Chen (huilin.chen@rug.nl). The GAW surface in-situ data are available via the World Data Centre for Greenhouse Gases (WDCGG), https://gaw.kishou.go.jp/search/.

Appendix A: Theoretical considerationsBasics on retrieval theory

In this appendix, we give a brief overview on the theory of optimal estimation remote sensing methods and follow the notation as recommended by the TUNER activity (von Clarmann et al., 2020), which is closely in line with the notation used by Rodgers (2000). The overview focuses on the equations that are important for our work, i.e. the optimal a posteriori combination of two independently retrieved optimal estimation remote sensing products. We show analytically that our method of combining two individually retrieved optimal estimation products by means of a posteriori calculations, is in most cases equivalent to a combined optimal estimation retrieval that uses a combined measurement vector.

For a more detailed and general insight into the theory of optimal estimation remote sensing methods we refer to Rodgers (2000)and for a general introduction on vector and matrix algebra dedicated textbooks are recommended. .

A1 ~~Basics on retrieval theory~~

~~If we assume a moderately non-linear problem (according to Chapter 5 of Rodgers, 2000), the retrieved optimal estimation product (the retrieved atmospheric state vector $\hat{x}$)can be written as:~~

$$\hat{x} = x_a + \mathbf{G}[\mathbf{K}(x - x_a)].$$

~~Here x and x_a are~~ Atmospheric remote sensing instruments measure radiance spectra (written as state vector y), which can be well simulated by models (F) whenever the actual atmospheric state ~~vector and~~ (the vector x) is known. Using the a priori atmospheric state vector ~~, respectively.~~ x_a we can linearise and write:

$$F(x) - F(x_a) = \Delta y = \mathbf{K}(x - x_a). \tag{A1}$$

Here, $\mathbf{K}$ is the Jacobian matrix, i~~,e,~~e. derivatives that capture how the measurement vector (the measured radiances) will change for changes of the atmospheric state (the atmospheric state vector x). A remote sensing retrieval inverts Eq. (A1) and provides an estimation of the difference between the atmospheric state and the a priori atmospheric state. For a moderately non-linear problem (according to Chapter 5 of Rodgers, 2000), the retrieved optimal estimation product ($\hat{x}$) can be written as:

$$\hat{x} - x_a = \mathbf{G}\Delta y = \mathbf{G}[\mathbf{K}(x - x_a)]. \tag{A2}$$

$\mathbf{G}$ is the gain matrix ~~, i. e.,~~ and realises the inversion from the measurement domain (radiances) to the domain of the atmospheric states. It consists of derivatives that capture how the retrieved atmospheric state vector will change for changes in the measurement vector:

$$\begin{aligned} \mathbf{G} &= (\mathbf{K}^T {\mathbf{S_{y,n}}}^{-1} \mathbf{K} + {\mathbf{S_a}}^{-1})^{-1} \mathbf{K}^T {\mathbf{S_{y,n}}}^{-1} \\ &\equiv \mathbf{S_a} \mathbf{K}^T (\mathbf{K} \mathbf{S_a} \mathbf{K}^T + \mathbf{S_{y,n}})^{-1}, \end{aligned} \tag{A3}$$

with $\mathbf{S_{y,n}}$ and ~~$\mathbf{S_a}^{-1}$~~ $\mathbf{R} = {\mathbf{S_a}}^{-1}$ being the retrieval's noise covariance and the constraint matrices ~~, respectively. In~~ (in a strict optimal estimation sense, the constraint matrix is the inverse of the a priori covariance matrix $\mathbf{S_a}$), respectively. The equivalence of both lines in Eq. (A3) is demonstarted in Chapter 4.1 of Rodgers (2000), where the first line is called the n-form and the second line the m-form.

The averaging kernel

$$\mathbf{A} = \mathbf{G}\mathbf{K}, \tag{A4}$$

is an important component of a remote sensing retrieval, because according to Eq. (A2) it reveals how changes of the ~~real~~ actual atmospheric state vector x affect the retrieved atmospheric state vector $\hat{x}$.

~~Very useful is also~~ A valuable diagnostic quantity is the a posteriori covariance matrix, which can be calculated as follows:

$$\mathbf{S}_{\hat{x}} = (\mathbf{K}^T {\mathbf{S_{y,n}}}^{-1} \mathbf{K} + {\mathbf{S_a}}^{-1})^{-1}. \tag{A5}$$

The linearised formulation of the retrieval solution according to (A2) is very useful for the analytic characterisation of the product. The retrieval state's noise error covariance matrix for noise can be analytically calculated as:

$$\mathbf{S}_{\hat{\mathbf{x}},\mathbf{n}} = \mathbf{G}\mathbf{S}_{\mathbf{y},\mathbf{n}}\mathbf{G}^T,$$

$$\begin{aligned} \mathbf{S}_{\hat{\mathbf{x}},\mathbf{n}} &\approx \mathbf{G}\mathbf{S}_{\mathbf{y},\mathbf{n}}\mathbf{G}^T \\ &\approx \mathbf{S}_{\hat{\boldsymbol{x}}}\mathbf{K}^T{\mathbf{S}_{\mathbf{y},\mathbf{n}}}^{-1}\mathbf{K}\mathbf{S}_{\hat{\boldsymbol{x}}}, \end{aligned} \tag{A6}$$

where $\mathbf{S}_{\mathbf{y},\mathbf{n}}$ is the covariance matrix for noise on the measured radiances $\boldsymbol{y}$.

~~Further very helpful equations are the relations between the a posteriori covariance, the averaging kernel, the constraint (or the a priori covariance), and the retrieval's state noise error covariance matrices:~~

$$\mathbf{S}_{\hat{\boldsymbol{x}}} = (\mathbf{I} - \mathbf{A})\mathbf{S}_{\mathbf{a}},$$

~~and~~

$$\mathbf{S}_{\hat{\boldsymbol{x}},\mathbf{n}} = \mathbf{A}\mathbf{S}_{\hat{\boldsymbol{x}}},$$

The second line of Eq. (A6) is obtained by substituting $\mathbf{G}$ by $\mathbf{S}_{\hat{\boldsymbol{x}}}\mathbf{K}^T{\mathbf{S}_{\mathbf{y},\mathbf{n}}}^{-1}$ according to Eqs. (A3) and (A5). The representativeness error reveals the deficit of the retrieval product in representing the actual variations of the state vector $\boldsymbol{x}$. In Chapter 3 of Rodgers (2000) it is called the smoothing error and can be calculated as (with $\mathbf{I}$ being the identity matrix):

$$\begin{aligned} \mathbf{S}_{\hat{\mathbf{x}},\mathbf{r}} &\approx (\mathbf{A} - \mathbf{I})\mathbf{S}_{\mathbf{a}}(\mathbf{A} - \mathbf{I})^T \\ &\approx \mathbf{S}_{\hat{\boldsymbol{x}}}{\mathbf{S}_{\mathbf{a}}}^{-1}\mathbf{S}_{\hat{\boldsymbol{x}}}. \end{aligned} \tag{A7}$$

The second line of Eq. (A7) is obtained using:

$$\mathbf{S}_{\hat{\boldsymbol{x}}} = (\mathbf{I} - \mathbf{A})\mathbf{S}_{\mathbf{a}}, \tag{A8}$$

which in turn follows from Eqs. (A3) - (A6).

Using Eqs. (A5) - (A7) reveals that the a posteriori covariance is the sum of the noise error covariance and the representativeness error covariance:

$$\mathbf{S}_{\hat{\boldsymbol{x}}} = \mathbf{S}_{\hat{\mathbf{x}},\mathbf{n}} + \mathbf{S}_{\hat{\mathbf{x}},\mathbf{r}}. \tag{A9}$$

A1 ~~Optimal combination of retrieval data products~~

Appendix B: Theory on the optimal combination of retrieval data products

In this ~~subsection~~ section, we discuss an optimal estimation retrieval that uses a combined measurement vector (two measurements from different instruments). ~~Then we briefly introduce the Kalman filter and~~ First we show that the ~~Kalman~~

~~filter formalism enables us to combine two individually retrieved remote sensing data products in equivalence to the optimal estimation retrieval using~~ retrieval output of two profile retrievals performed on the same vertical grid can be used in a way that yields to the same results as performing a retrieval with the combined measurement vector. Then we present an approach for combining the outputs of a retrieval that provides profiles and another retrieval that provides column data. We show that the combination of profile and column data can be realised in a computationally efficient manner via a Kalman filter. Finally, we discuss the validity of the methods and the requirements on the individual retrieval products.

B0.1 ~~Optimal estimation using a combined measurement vector~~

B1 Inversion of a combined measurement vector

According to Eqs. (A2), (A3), and (A5) the retrieval product obtained from ~~a combined measurement vector $\{\boldsymbol{y_1}, \boldsymbol{y_2}\}$~~ measurement $\boldsymbol{y}$ can be written as:

$$\hat{\boldsymbol{x}} - \boldsymbol{x_a} = (\mathbf{K}^T \mathbf{S_{y,n}}^{-1} \mathbf{K} + \mathbf{S_a}^{-1})^{-1} \mathbf{K}^T \mathbf{S_{y,n}}^{-1} \mathbf{K} (\boldsymbol{x} - \boldsymbol{x_a}). \tag{B1}$$

In the case of two individual measurements (measurement 1 and 2), we obtain from using a combined measurement vector $\{\boldsymbol{y_1}, \boldsymbol{y_2}\}$:

$$\begin{aligned} \hat{\boldsymbol{x}} - \boldsymbol{x_a} &= (\mathbf{K_1}^T \mathbf{S_{y_1,n}}^{-1} \mathbf{K_1} + \mathbf{K_2}^T \mathbf{S_{y_2,n}}^{-1} \mathbf{K_2} + \mathbf{S_a}^{-1})^{-1} (\mathbf{K_1}^T \mathbf{S_{y_1,n}}^{-1} \mathbf{K_1} + \mathbf{K_2}^T \mathbf{S_{y_2,n}}^{-1} \mathbf{K_2}) (\boldsymbol{x} - \boldsymbol{x_a}) \\ &= (\mathbf{S_{\hat{x}_1}}^{-1} + \mathbf{S_{\hat{x}_2}}^{-1} - \mathbf{S_a}^{-1})^{-1} (\mathbf{K_1}^T \mathbf{S_{y_1,n}}^{-1} \mathbf{K_1} + \mathbf{K_2}^T \mathbf{S_{y_2,n}}^{-1} \mathbf{K_2}) (\boldsymbol{x} - \boldsymbol{x_a}), \end{aligned} \tag{B2}$$

where $\mathbf{S_{y_1,n}}$ and $\mathbf{S_{y_2,n}}$ are the respective measurement noise covariances, $\mathbf{K_1}$ and $\mathbf{K_2}$ the respective Jacobians and $\mathbf{S_{\hat{x}_1}}$ and $\mathbf{S_{\hat{x}_2}}$ the respective a posteriori covariances. The second line follows from Eq. (A5). According to Eqs. (A3) - (A5) we can substitute $\mathbf{K}^T \mathbf{S_{y,n}}^{-1} \mathbf{K} (\boldsymbol{x} - \boldsymbol{x_a})$ by $\mathbf{S_{\hat{x}}}^{-1} (\hat{\boldsymbol{x}} - \boldsymbol{x_a})$ and write Eq. (B2) as

$$\hat{\boldsymbol{x}} - \boldsymbol{x_a} = (\mathbf{S_{\hat{x}_1}}^{-1} + \mathbf{S_{\hat{x}_2}}^{-1} - \mathbf{S_a}^{-1})^{-1} [\mathbf{S_{\hat{x}_1}}^{-1} (\hat{\boldsymbol{x}}_1 - \boldsymbol{x_a}) + \mathbf{S_{\hat{x}_2}}^{-1} (\hat{\boldsymbol{x}}_2 - \boldsymbol{x_a})]. \tag{B3}$$

Using Eq. (B3) we can realise an optimal combination of the two retrieval products that only needs the a priori covariance, the a posteriori covariances, and the two retrieval products. The Jacobians are not needed. This combination is mathematically equivalent to using the Jacobians of a combined measurement vector $\{\boldsymbol{y_1}, \boldsymbol{y_2}\}$, i.e. within a linear subspace (validity of moderate non-linearities), it is equivalent to a synergetic use of level 1 data in form of a multispectral retrieval.

B1.1 ~~Linear Kalman filter~~

B2 Combining profile and column data products

Equation (B3) requires two retrieval results on the same vertical grid and can be used to combine two profile products. Here we will develop a method for combining a profile and a column data product. For a column retrieval we can write in analogy to Eq. (A1)

$$\Delta x^* = \boldsymbol{a^*}^T (\boldsymbol{x} - \boldsymbol{x_a}), \tag{B4}$$

where $\boldsymbol{a}^{*T}$ is the column averaged mixing ratio according to Appendix D2. Equation (B4) poses an inverse problem of the same kind as Eq. (A1) and in order to optimally estimate a profile from an available column product we can apply the same solution approach as in Eqs. (A2) and (A3). A similar application of this approach is also presented in Sect. 4.2 of Rodgers and Connor (2003). For the application here we substitute in Eq. (A3) $\mathbf{K}$ by $\boldsymbol{a}^{*T}$ and $\mathbf{S_{y,n}}$ by the scalar $S^*_{\hat{x},n}$ (the noise error variance of the column data product) and get the profile

$$\begin{aligned}\hat{\boldsymbol{x}} - \boldsymbol{x_a} &\approx (\boldsymbol{a}^* {S^*_{\hat{x},n}}^{-1} \boldsymbol{a}^{*T} + \mathbf{S_a}^{-1})^{-1} \boldsymbol{a}^* {S^*_{\hat{x},n}}^{-1} \boldsymbol{a}^{*T} (\boldsymbol{x} - \boldsymbol{x_a}) \\ &\approx (\boldsymbol{a}^* {S^*_{\hat{x},n}}^{-1} \boldsymbol{w}^{*T} \mathbf{S_{\hat{x}}} \mathbf{K}^T \mathbf{S_{y,n}}^{-1} \mathbf{K} + \mathbf{S_a}^{-1})^{-1} \boldsymbol{a}^* {S^*_{\hat{x},n}}^{-1} \boldsymbol{w}^{*T} \mathbf{S_{\hat{x}}} \mathbf{K}^T \mathbf{S_{y,n}}^{-1} \mathbf{K} (\boldsymbol{x} - \boldsymbol{x_a}). \end{aligned} \quad \text{(B5)}$$

For the second line of Eq. (B5) we use $\boldsymbol{a}^{*T} = \boldsymbol{w}^{*T}\mathbf{A}$ – according to Eq. (D6) – and $\mathbf{A} = \mathbf{S_{\hat{x}}}\mathbf{K}^T\mathbf{S_{y,n}}^{-1}\mathbf{K}$ – according to Eqs. (A3) - (A5). We write this second line to discuss similarities with Eq. (B1). The comparison of Eq. (B5) with Eq. (B1) reveals that for a retrieval providing only a column product, the Jacobian information provided by $\mathbf{K}$ is vertically aggregated according to the operator $\boldsymbol{a}^* {S^*_{\hat{x},n}}^{-1} \boldsymbol{w}^{*T} \mathbf{S_{\hat{x}}}$. The term $\mathbf{S_{\hat{x}}}$ is the vertically resolved a posteriori covariance, which exist for a retrieval that internally inverts profiles, but only distributes the column products; however, it is only an internal measure of the retrieval, and actually not available.

Instead of the term of Eq. (B4) we now invert the term $\Delta x^* = \boldsymbol{a_2^*}^T(\boldsymbol{x} - \hat{\boldsymbol{x}}_\mathbf{1})$, i.e. we replace $\boldsymbol{x_a}$ by the profile product $\hat{\boldsymbol{x}}_\mathbf{1}$ of a first retrieval (retrieval 1) on the right side of (B4) and use $\boldsymbol{a_2^*}^T$ and $S^*_{\hat{\boldsymbol{x}}_\mathbf{2},n}$ for the column averaging kernel and the noise error variance of a second retrieval (retrieval 2), respectively. Here and in the following, retrieval 1 is the profile retrieval and retrieval 2 the retrieval that provides only column products. The solution can easily be achieved by substituting in (B5) $\mathbf{S_a}$ by $\mathbf{S}_{\hat{\boldsymbol{x}}_\mathbf{1}}$, which is the a posteriori covariance of retrieval 1:

$$\hat{\boldsymbol{x}} - \hat{\boldsymbol{x}}_\mathbf{1} \approx (\boldsymbol{a_2^*} {S^*_{\hat{x}_2,n}}^{-1} \boldsymbol{a_2^*}^T + \mathbf{S}_{\hat{\boldsymbol{x}}_\mathbf{1}}{}^{-1})^{-1} \boldsymbol{a_2^*} {S^*_{\hat{x}_2,n}}^{-1} \boldsymbol{a_2^*}^T (\boldsymbol{x} - \hat{\boldsymbol{x}}_\mathbf{1}). \quad \text{(B6)}$$

We modify Eq. (B6) by using $\hat{\boldsymbol{x}}_\mathbf{1} = \mathbf{A_1}(\boldsymbol{x} - \boldsymbol{x_a}) + \boldsymbol{x_a}$:

$$\begin{aligned}\hat{\boldsymbol{x}} - \boldsymbol{x_a} &\approx \mathbf{A_1}(\boldsymbol{x} - \boldsymbol{x_a}) + (\mathbf{S}_{\hat{\boldsymbol{x}}_\mathbf{1}}{}^{-1} + \boldsymbol{a_2^*} {S^*_{\hat{x}_2,n}}^{-1} \boldsymbol{a_2^*}^T)^{-1} \boldsymbol{a_2^*} {S^*_{\hat{\boldsymbol{x}}_\mathbf{2},n}}^{-1} \boldsymbol{a_2^*}^T (\mathbf{I} - \mathbf{A_1})(\boldsymbol{x} - \boldsymbol{x_a}) \\ &\approx (\mathbf{S}_{\hat{\boldsymbol{x}}_\mathbf{1}}{}^{-1} + \boldsymbol{a_2^*} {S^*_{\hat{x}_2,n}}^{-1} \boldsymbol{a_2^*}^T)^{-1} [\mathbf{S}_{\hat{\boldsymbol{x}}_\mathbf{1}}{}^{-1} \mathbf{A_1} + \boldsymbol{a_2^*} {S^*_{\hat{x}_2,n}}^{-1} \boldsymbol{a_2^*}^T](\boldsymbol{x} - \boldsymbol{x_a}) \\ &\approx (\mathbf{S}_{\hat{\boldsymbol{x}}_\mathbf{1}}{}^{-1} + \boldsymbol{a_2^*} {S^*_{\hat{x}_2,n}}^{-1} \boldsymbol{a_2^*}^T)^{-1} [\mathbf{S}_{\hat{\boldsymbol{x}}_\mathbf{1}}{}^{-1} (\hat{\boldsymbol{x}}_\mathbf{1} - \boldsymbol{x_a}) + \boldsymbol{a_2^*} {S^*_{\hat{x}_2,n}}^{-1} (\hat{x}_2^* - \boldsymbol{w}^{*T} \boldsymbol{x_a})]. \end{aligned} \quad \text{(B7)}$$

In the third line of Eq. (B7) we use the column product $\hat{x}_2^* = \boldsymbol{a_2^*}^T(\boldsymbol{x} - \boldsymbol{x_a}) + \boldsymbol{w}^{*T}\boldsymbol{x_a}$. Similarly to Eq. (B3) we can generate a combined product without the need of the Jacobian matrices. The combination is possible by using the profile and the column product ($\hat{\boldsymbol{x}}_\mathbf{1}$ and $\hat{x}_2^*$, respectively) together with the a posteriori covariance of the profile product and the noise error and averaging kernel of the column product.

If we substitute in the second line of Eq. (B7) $\mathbf{S_{\hat{x}_1}}^{-1}$ by $\mathbf{K_1}^T\mathbf{S_{y_1,n}}^{-1}\mathbf{K_1}+\mathbf{S_a}^{-1}$ – according to Eq. (A5), $\boldsymbol{a_2^{*T}}$ by $\boldsymbol{w^{*T}}\mathbf{A_2}$ – according to Eq. (D6), and then $\mathbf{A_2}$ by $\mathbf{S_{\hat{x}_2}}\mathbf{K_2}^T\mathbf{S_{y_2,n}}^{-1}\mathbf{K_2}$ – according to Eqs. (A3) - (A5), we get:

$$\begin{aligned}\hat{\boldsymbol{x}}-\boldsymbol{x_a} &\approx (\mathbf{K_1}^T\mathbf{S_{y_1,n}}^{-1}\mathbf{K_1}+\boldsymbol{a_2^*}S^*_{\hat{x}_2,n}{}^{-1}\boldsymbol{w^{*T}}\mathbf{S_{\hat{x}_2}}\mathbf{K_2}^T\mathbf{S_{y_2,n}}^{-1}\mathbf{K_2}+\mathbf{S_a}^{-1})^{-1}\\ &\quad [\mathbf{K_1}^T\mathbf{S_{y_1,n}}^{-1}\mathbf{K_1}+\boldsymbol{a_2^*}S^*_{\hat{x}_2,n}{}^{-1}\boldsymbol{w^{*T}}\mathbf{S_{\hat{x}_2}}\mathbf{K_2}^T\mathbf{S_{y_2,n}}^{-1}\mathbf{K_2}](\boldsymbol{x}-\boldsymbol{x_a}).\end{aligned} \tag{B8}$$

This equation has strong similarities to the first line of Eq. (B2), i.e. the retrieval product obtained when using the combined measurement vector $\{\boldsymbol{y_1},\boldsymbol{y_2}\}$. The only difference is that in Eq.(B8) the information provided by Jacobian $\mathbf{K_2}$ is vertically aggregated according to the operator $\boldsymbol{a_2^*}S^*_{\hat{x}_2,n}{}^{-1}\boldsymbol{w^{*T}}\mathbf{S_{\hat{x}_2}}$.

B3 Linear Kalman filter

Here we show that the approach developed in Appendix B2 is equivalent to a Kalman filter. An important application of a Kalman filter (Kalman, 1960; Rodgers, 2000) is data assimilation in the context of atmospheric modelling. There, the filter operates sequentially in different time steps. Kalman filter data assimilation methods determine the analysis state ($\hat{\boldsymbol{x}}^{\boldsymbol{a}}$) by optimally combining the background (or forecast) state ($\hat{\boldsymbol{x}}^{\boldsymbol{b}}$) with the information as provided by a new observation ($\hat{\boldsymbol{x}}^{\boldsymbol{o}}$):

$$\hat{\boldsymbol{x}}^{\boldsymbol{a}}=\hat{\boldsymbol{x}}^{\boldsymbol{b}}+\mathbf{M}[\hat{\boldsymbol{x}}^{\boldsymbol{o}}-\mathbf{H}\hat{\boldsymbol{x}}^{\boldsymbol{b}}]. \tag{B9}$$

Optimal means here that the uncertainties of both, the background state and the observation, are correctly taken into account by the Kalman gain matrix ($\mathbf{M}$):

$$\mathbf{M} = \mathbf{S}_{\hat{\boldsymbol{x}}^{\boldsymbol{b}}}\mathbf{H}^T(\mathbf{H}\mathbf{S}_{\hat{\boldsymbol{x}}^{\boldsymbol{b}}}\mathbf{H}^T+\mathbf{S}_{\hat{\boldsymbol{x}}^{\boldsymbol{o}},\mathbf{n}})^{-1}=(\mathbf{H}+\mathbf{S}_{\hat{\boldsymbol{x}}^{\boldsymbol{o}}_{\boldsymbol{n}}}\mathbf{H}^{-T}\mathbf{S}_{\hat{\boldsymbol{x}}^{\boldsymbol{b}}}{}^{-1})^{-1}, \tag{B10}$$

with $\mathbf{S}_{\hat{\boldsymbol{x}}^{\boldsymbol{b}}}$ and $\mathbf{S}_{\hat{\boldsymbol{x}}^{\boldsymbol{o}},\mathbf{n}}$ being the uncertainty covariances of background state and the new measurement, respectively. The matrix $\mathbf{H}$ is the measurement forward operator, which maps the background domain into the measurement domain.

~~The similarity between Eqs. and , on the one hand,~~ By rearranging the n-form of (B6) as the m-form – in analogy to Eq. (A3) – and by using again $\hat{\boldsymbol{x}}_1=\mathbf{A_1}(\boldsymbol{x}-\boldsymbol{x_a})+\boldsymbol{x_a}$ and $\hat{x}_2^*=\boldsymbol{a}^{*T}(\boldsymbol{x}-\boldsymbol{x_a})+\boldsymbol{w}^{*T}\boldsymbol{x_a}$ we get

$$\begin{aligned}\hat{\boldsymbol{x}} &\approx \hat{\boldsymbol{x}}_1+\mathbf{S}_{\hat{\boldsymbol{x}}_1}\boldsymbol{a_2^*}(\boldsymbol{a_2^{*T}}\mathbf{S}_{\hat{\boldsymbol{x}}_1}\boldsymbol{a_2^*}+S^*_{\hat{x}_2,n})^{-1}\boldsymbol{a_2^{*T}}(\boldsymbol{x}-\hat{\boldsymbol{x}}_1)\\ &\approx \hat{\boldsymbol{x}}_1+\mathbf{S}_{\hat{\boldsymbol{x}}_1}\boldsymbol{a_2^*}(\boldsymbol{a_2^{*T}}\mathbf{S}_{\hat{\boldsymbol{x}}_1}\boldsymbol{a_2^*}+S^*_{\hat{x}_2,n})^{-1}[\hat{x}_2^*-\boldsymbol{a_2^{*T}}\hat{\boldsymbol{x}}_1-(\boldsymbol{w}^{*T}\boldsymbol{x_a}-\boldsymbol{a_2^{*T}}\boldsymbol{x_a})]\\ &\approx \hat{\boldsymbol{x}}_1+\boldsymbol{m}(\hat{x}_2^*-\boldsymbol{a_2^{*T}}\hat{\boldsymbol{x}}_1)-\boldsymbol{m}(\boldsymbol{w}^{*T}\boldsymbol{x_a}-\boldsymbol{a_2^{*T}}\boldsymbol{x_a})\end{aligned} \tag{B11}$$

with

$$\boldsymbol{m}=\mathbf{S}_{\hat{\boldsymbol{x}}_1}\boldsymbol{a_2^*}(\boldsymbol{a_2^{*T}}\mathbf{S}_{\hat{\boldsymbol{x}}_1}\boldsymbol{a_2^*}+S^*_{\hat{x}_2,n})^{-1}. \tag{B12}$$

Disregarding the term that accounts for the a priori information ($\boldsymbol{m}(\boldsymbol{w}^{*T}\boldsymbol{x_a}-\boldsymbol{a_2^{*T}}\boldsymbol{x_a})$), the Eqs. ~~and , on the other hand, reveals that remote sensing optimal estimation and Kalman filter data assimilation methods use the same mathematical formalism.~~

B3.1 ~~Optimal a posteriori combination of individually retrieved data products~~

~~We have a first estimation of the atmospheric state (the first retrieval product $\hat{\boldsymbol{x}}_1$) and we want to optimally improve this estimation by using a second retrieval product ($\hat{\boldsymbol{x}}_2$). This is a typical data assimilation problem and we can use the Kalman filter formalism. We make the following settings:~~

$$\begin{aligned}
\mathbf{S}_{\hat{\boldsymbol{x}}^b} &\equiv \mathbf{S}_{\hat{\boldsymbol{x}}_1} \\
&\equiv (\mathbf{K_1}^T \mathbf{S_{y_1,n}}^{-1} \mathbf{K_1} + \mathbf{S_a}^{-1})^{-1}
\end{aligned}$$

$$\begin{aligned}
\mathbf{S}_{\hat{\boldsymbol{x}}^o,\mathbf{n}} &\equiv \mathbf{S}_{\hat{\boldsymbol{x}}_2,\mathbf{n}} \\
&\equiv (\mathbf{K_2}^T \mathbf{S_{y_2,n}}^{-1} \mathbf{K_2} + \mathbf{S_a}^{-1})^{-1} \mathbf{K_2}^T \mathbf{S_{y_2,n}}^{-1} \mathbf{K_2} (\mathbf{K_2}^T \mathbf{S_{y_2,n}}^{-1} \mathbf{K_2} + \mathbf{S_a}^{-1})^{-1} \\
&\equiv \mathbf{S}_{\hat{\boldsymbol{x}}_2} \mathbf{K_2}^T \mathbf{S_{y_2,n}}^{-1} \mathbf{K_2} \mathbf{S}_{\hat{\boldsymbol{x}}_2}
\end{aligned}$$

$$\begin{aligned}
\mathbf{H} &\equiv \mathbf{A_2} \\
&\equiv (\mathbf{K_2}^T \mathbf{S_{y_2,n}}^{-1} \mathbf{K_2} + \mathbf{S_a}^{-1})^{-1} \mathbf{K_2}^T \mathbf{S_{y_2,n}}^{-1} \mathbf{K_2} \\
&\equiv \mathbf{S}_{\hat{\boldsymbol{x}}_2} \mathbf{K_2}^T \mathbf{S_{y_2,n}}^{-1} \mathbf{K_2}
\end{aligned}$$

$$\begin{aligned}
\hat{\boldsymbol{x}}^b &\equiv \hat{\boldsymbol{x}}_1 - \boldsymbol{x}_a \\
&\equiv (\mathbf{K_1}^T \mathbf{S_{y_1,n}}^{-1} \mathbf{K_1} + \mathbf{S_a}^{-1})^{-1} \mathbf{K_1}^T \mathbf{S_{y_1,n}}^{-1} \mathbf{K_1} (\boldsymbol{x} - \boldsymbol{x}_a) \\
&\equiv \mathbf{S}_{\hat{\boldsymbol{x}}_1} \mathbf{K_1}^T \mathbf{S_{y_1,n}}^{-1} \mathbf{K_1} (\boldsymbol{x} - \boldsymbol{x}_a)
\end{aligned}$$

$$\begin{aligned}
\hat{\boldsymbol{x}}^o &\equiv \hat{\boldsymbol{x}}_2 - \boldsymbol{x}_a \\
&\equiv (\mathbf{K_2}^T \mathbf{S_{y_2,n}}^{-1} \mathbf{K_2} + \mathbf{S_a}^{-1})^{-1} \mathbf{K_2}^T \mathbf{S_{y_2,n}}^{-1} \mathbf{K_2} (\boldsymbol{x} - \boldsymbol{x}_a) \\
&\equiv \mathbf{S}_{\hat{\boldsymbol{x}}_2} \mathbf{K_2}^T \mathbf{S_{y_2,n}}^{-1} \mathbf{K_2} (\boldsymbol{x} - \boldsymbol{x}_a).
\end{aligned}$$

~~In~~ (B11) and (B12) are the same as the Kalman filter Eqs. (B9) and (B10): retrieval 1 provides the background state and retrieval 2 the new observation. Compared to Eqs. ~~and we assume that the two individual retrievals use the same constraint ($\mathbf{S_a}^{-1}$). This is generally not the case and we can a posteriori modify a constraint and its effect on state vectors and covariances by the formalism as presented in Chapter 10.4 of Rodgers (2000) or Sect. 4.2 of Rodgers and Connor (2003). For our problem here this is of secondary importance, because we assume that TROPOMI total column data products are almost independent on the constraint (as long as the constraint is reasonable).~~(B7) and (B8) the form of Eq. (B11) has the advantage that no matrices have to be inverted only the scalar ($\boldsymbol{a}_2^{*T} \mathbf{S}_{\hat{\boldsymbol{x}}_1} \boldsymbol{a}_2^* + S^*_{\hat{x}_2,n}$).

~~In Eqs. and~~ We have shown that Eq. (B11) is mathematically the same as Eq. (B7) and Eq. (B8). The latter is in turn very similar to the synergetic use of level 1 data in form of a multispectral retrieval as discussed in the context of Eq. (B3).

B4 Discussion and requirements

In the Appendices B2 and B3, we assume the usage of the same a priori for the two individual retrievals. Since generally two indivudually individually performed retrievals use two different a priori settings we have to perform an a priori adjustment. Using the a priori of retrieval 2 as the reference ($\boldsymbol{x_{2,a} = x_a}$), we can adjust the output of retrieval 1 by (see Eq. (10) of Rodgers and Connor, 2003):

$$\hat{\boldsymbol{x}}_\mathbf{1}{}' = \hat{\boldsymbol{x}}_\mathbf{1} + (\mathbf{A_1} - \mathbf{I})(\boldsymbol{x_{1,a}} - \boldsymbol{x_{2,a}}), \tag{B13}$$

where $\boldsymbol{x_{1,a}}$ is the a priori used by retrieval 1.

Substitution of the settings from Eqs. - in For a combination according to Eq. gives:

$$\mathbf{M} = (\mathbf{S}_{\hat{\boldsymbol{x}}_1}{}^{-1} + \mathbf{S}_{\hat{\boldsymbol{x}}_2}{}^{-1} - \mathbf{S_a}^{-1})^{-1}\mathbf{S}_{\hat{\boldsymbol{x}}_2}{}^{-1},$$

where we use Eqs. and .

Substituting (B3) we need retrieval 1 and 2 outputs obtained by using the same constraint (the inverse of the a priori covariance $\mathbf{S_a}$). This has to be accounted for before applying Eq. together with the settings from Eqs. and in (B3), by adusting the contraint according to the formalism as presented in Chapter 10.4 of Rodgers (2000) or Sect. 4.2 of Rodgers and Connor (2003) . By applying Eq. finally yields:

$$\hat{\boldsymbol{x}}^{\boldsymbol{a}} - \boldsymbol{x_a} = (\mathbf{S}_{\hat{\boldsymbol{x}}_1}{}^{-1} + \mathbf{S}_{\hat{\boldsymbol{x}}_2}{}^{-1} - \mathbf{S_a}^{-1})^{-1}(\mathbf{K_1}^T\mathbf{S_{y_1,n}}^{-1}\mathbf{K_1} + \mathbf{K_2}^T\mathbf{S_{y_2,n}}^{-1}\mathbf{K_2})(\boldsymbol{x} - \boldsymbol{x_a}),$$

i.e. (B7) or the Kalman filter according to Eq. (B11) the common constraint is automatically set to the constraint of the analysis state is the same as the output $\hat{\boldsymbol{x}}$ of a retrieval with a combined measurement vector from Eq. . This means that we can a posteriori calculate the result that would be obtained by an optimal estimation retrieval using a combined measurement vectorretrieval 1 product and no extra modification is necesarry.

B4.1 Requirements

The optimal a posteriori combination of two remote sensing products The synergetic combination of remote sensing profile and column products according to Eq. (B7) or Eq. (B11) is possible, whenever: (1) the two remote sensing observations are made at the same time and detect the same location, (2) the problem problems is moderately non-linear (according to Chapter 5 of Rodgers, 2000), and (3) the individual retrieval output as listed by Eqs. to Eq. (B7) or Eq. (B11) is made available. This is for the first retrievalthe aposteriori : for the profile retrieval, we need the a posteriori covariances ($\mathbf{S}_{\hat{\boldsymbol{x}}}$, which might also be reconstracted from $\mathbf{A}$ and $\mathbf{R}$ $\mathbf{R} = \mathbf{S_a}^{-1}$ according to Eq. (A8)), the averaging kernels ($\mathbf{A}$), and the retrieved and a priori state vectors ($\hat{\boldsymbol{x}}$ and $\boldsymbol{x_a}$, respectively). For the second retrievalcolumn retrieval, we need the noise covariances ($\mathbf{S}_{\hat{\boldsymbol{x}},\mathbf{n}}$variances (the scalar $S^*_{\hat{x}^*,n}$), the column averaging kernels ($\mathbf{A}$), and the retrieved and a priori state vectors ($\hat{\boldsymbol{x}}$ and $\boldsymbol{x_a}$, respectively)the row vector $\boldsymbol{a}^{*T}$), the column product ($\hat{x}^*_2$), and the a priori column data ($\boldsymbol{w}^{*T}\boldsymbol{x_a}$), respectively.

Appendix C: Operator for transformation between linear and logarithmic scales

Linear scale differentials and logarithmic scale differentials are related by ~~$\Delta x = x \Delta \ln x$~~ $\partial x = x \partial \ln x$. For transforming differentials or covariances of a state vector with dimension nal (nal: number of atmospheric levels) from logarithmic to linear scale we define the $nal \times nal$ diagonal matrix $\mathbf{L}$:

$$\mathbf{L} = \begin{pmatrix} \hat{x}_1 & 0 & \cdots & 0 \\ 0 & \hat{x}_2 & \cdots & 0 \\ \vdots & \vdots & \ddots & \vdots \\ 0 & 0 & \cdots & \hat{x}_{nal} \end{pmatrix}. \tag{C1}$$

Here $\hat{x}_i$ is the value of the ith element of the retrieved state vector (i.e. in case of an atmospheric CH_4 state vector the CH_4 mixing ratios retrieved at the ith model level).

~~A~~ Approximatively, a logarithmic scale averaging kernel matrix $\mathbf{A}^{\mathbf{l}}$ can then be expressed in the linear scale as:

$$\mathbf{A} \approx \mathbf{L}\mathbf{A}^{\mathbf{l}}\mathbf{L}^{-1}. \tag{C2}$$

This is here an approximation, because on the right side the operator $\mathbf{L}$ should contain the actual instead of the retrieved mixing ratios. It is a valid approximation as long as the a priori is reasonable and there is no large bias in the retrieval data.

Similarly a logarithmnic scale covariance matrix $\mathbf{S}^{\mathbf{l}}$ can ~~then be~~ be approximately expressed in the linear scale as:

$$\mathbf{S} \approx \mathbf{L}\mathbf{S}^{\mathbf{l}}\mathbf{L}^{T}. \tag{C3}$$

Here the approximation is because $\Delta x \approx x \Delta \ln x$.

Appendix D: Operators for column data

This appendix explains the calculation of operators for partial (and total) column data. Although some sections are similar to Appendix C of ~~?~~ Schneider et al. (2022) we think it is ~~here~~ a very useful reference here, because it facilitates the reproducibility of our results.

For converting mixing ratio profiles into amount profiles we set up a pressure weighting operator $\mathbf{Z}$, as a diagonal matrix with the following entries:

$$Z_{i,i} = \frac{\Delta p_i}{g_i m_{\mathrm{air}} (1 + \frac{m_{\mathrm{H_2O}}}{m_{\mathrm{air}}} \hat{x}_i^{\mathrm{H_2O}})}. \tag{D1}$$

Using the pressure p_i at atmospheric grid level i we set $\Delta p_1 = \frac{p_2 - p_1}{2} - p_1$, $\Delta p_{nal} = p_{nal} - \frac{p_n al - p_{nal-1}}{2}$, and $\Delta p_i = \frac{p_{i+1} - p_i}{2} - \frac{p_i - p_{i-1}}{2}$ for $1 < i < nal$. Furthermore, g_i is the gravitational acceleration at level i, m_{air} and $m_{\mathrm{H_2O}}$ the molecular mass of dry air and water vapour, respectively, and $\hat{x}_i^{\mathrm{H_2O}}$ the retrieved or modelled water vapour mixing ratio at level i.

We define an operator ~~$\mathbf{W}$~~ $\mathbf{W}^T$ for resampling fine gridded atmospheric amount profiles into coarse gridded atmospheric partial column amount profiles. It has the dimension $c \times nal$, where c is the number of the resampled coarse atmospheric grid

levels and nal, the number of atmospheric levels of the original fine atmospheric grid. Each line of the operator has the value '1' for the levels that are resampled and '0' for all other levels:

$$\underset{\sim}{\mathbf{W}}^T = \begin{pmatrix} 1 & \cdots & 1 & 0 & \cdots & \cdots & \cdots & \cdots & 0 \\ 0 & \cdots & 0 & 1 & \cdots & 1 & 0 & \cdots & 0 \\ 0 & \cdots & \cdots & \cdots & \cdots & 0 & 1 & \cdots & 1 \end{pmatrix}. \tag{D2}$$

In analogy we can define a row vector $\boldsymbol{w}^T$ (with the dimension $1 \times nal$) with all elements having the value '1', which allows the resampling for the total column amounts.

D1 Column amounts

The kernel that discribes how a change in the amount at a certain altitude affects the retrieved partial (or total) colunm amount can be calculated as:

$$\mathbf{A}' = \underset{\sim}{\mathbf{W}}^T \mathbf{Z} \mathbf{A} \mathbf{Z}^{-1}. \tag{D3}$$

For the total column~~we replace $\mathbf{W}$~~, we replace $\underset{\sim}{\mathbf{W}}^T$ by $\boldsymbol{w}^T$ and get the row vector $\boldsymbol{a'}^T$ (dimension $1 \times nal$). This is the total column kernel provided by the TROPOMI data and it is typically written as $\boldsymbol{a}^T$. Figure 3 shows examples of such total and partial ~~columns~~ column amount kernels. The total column amount kernel can be interpolated to different altitude grids. For the applications in Sects. 3 and 4 we interpolate the TROPOMI total column amount kernel to the vertical grid used by the MUSICA IASI retrieval.

D2 Column averaged mixing ratios

We can also combine the operators $\mathbf{Z}$ and ~~$\mathbf{W}$~~ $\underset{\sim}{\mathbf{W}}^T$ for the calculation of a pressure weighted resampling operator by:

$$\underset{\sim}{\mathbf{W}^*}^T = (\underset{\sim}{\mathbf{W}}^T \mathbf{Z} \underset{\sim}{\mathbf{W}^T}^T)^{-1} \underset{\sim}{\mathbf{W}}^T \mathbf{Z}. \tag{D4}$$

This operator resamples linear scale mixing ratio profiles into linear scale partial column averaged mixing ratio profiles. ~~Its inverse is calculated as:~~

~~$\mathbf{W^*}^{-1} = \mathbf{Z}^{-1} \mathbf{W}^{-1} (\mathbf{W} \mathbf{Z} \mathbf{W}^T),$~~

~~with $\mathbf{W}^{-1} = (\mathbf{W}^T \mathbf{W})^{-1} \mathbf{W}^T$.~~ The respective total column ~~operators~~ operator $\boldsymbol{w^*}^T$ ~~and $(\boldsymbol{w^*}^T)^{-1}$~~ can be calculated in analogy to Eq. (D4) by replacing $\underset{\sim}{\mathbf{W}}^T$ by ~~replacing $\mathbf{W}$ by~~ $\boldsymbol{w}^T$ ~~.~~

~~With operator $\mathbf{W^*}$~~

With operator $\underset{\sim}{\mathbf{W^*}}^T$ we can calculate a coarse gridded partial column averaged state $\hat{\boldsymbol{x}}^*$ from the fine gridded linear mixing ratio state $\hat{\boldsymbol{x}}$ by:

$$\hat{\boldsymbol{x}}^* = \underset{\sim}{\mathbf{W}^*}^T \hat{\boldsymbol{x}}. \tag{D5}$$

The kernels matrix of the partial column averaged mixing ratio state can then be calculated from the fine gridded linear scale kernel matrix ($\mathbf{A}$) by:

$$\mathbf{A}^* = \mathbf{W}^{*T}\mathbf{A}. \tag{D6}$$

This kernel discribes how a change in the mixing ratio at a certain altitude affects the retrieved partial ~~column~~ column averaged mixing ratio. Covariances of the partial column averaged mixing ratio state can be calculated from the corresponding covariance matrices of the fine gridded linear scale ($\mathbf{S}$) by:

$$\mathbf{S}^* = \mathbf{W}^{*T}\mathbf{S}\mathbf{W}^{*T}. \tag{D7}$$

The respective calculations for total column averaged mixing ratios can be made by replacing ~~$\mathbf{W}^*$~~ $\mathbf{W}^{*T}$ by $\boldsymbol{w}^{*T}$. For the total column avereraged mixing ratios the covariance is a simple variance (the scalar ~~S^*~~ S^*) and the kernel has the dimension $1 \times nol$, i.e. it is a row vector $\boldsymbol{a}^{*T}$.

The total column amount kernel ($\boldsymbol{a_T}^T$) provided with the TROPOMI data set can be converted into a total column averaged mixing ratio kernel $\boldsymbol{a}_{\boldsymbol{T}}^{*T}$ by the following calculation ~~:~~ (using Eqs. (D3), (D4), and (D6)):

$$\boldsymbol{a}_{\boldsymbol{T}}^{*T} = \boldsymbol{w}^{*T}\mathbf{A}\mathbf{A}_{\mathbf{T}} = (\boldsymbol{w}^T\mathbf{Z}\boldsymbol{w})^{-1}\boldsymbol{a_T}^T\mathbf{Z}. \tag{D8}$$

The total column averaged mixing ratio kernel $\boldsymbol{a}_{\boldsymbol{T}}^{*T}$ used in Sects. 3 and 4 is valid for the vertical grid used by the MUSICA IASI retrieval. It is calculated from the TROPOMI total column amount kernel ($\boldsymbol{a_T}^T$) provided in the TROPOMI output files according to Eq. (D8), ~~but using a TROPOMI total column amount kernel ($\boldsymbol{a_T}$)that is interpolated onto the MUSICA IASI grid (see also Appendix D1)~~after its interpolation onto the MUSICA IASI grid (see also Appendix D1).

Appendix E: Dislocation of TROPOMI and IASI

IASI is on an orbit with descending node equator crossing at 9:30 mean local solar time. TROPOMI is on an orbit with ascending node equator crossing at 13:30 mean local solar time. In this work we require a temporal collocation within at least six hours. This requirement causes the following typical time difference (IASI - TROPOMI) for observing the same location: at northern high latitudes -0.6 to $+3.7$ hours, at northern middle latitudes -3.3 to -2.2 hours, at the equator -4.5 to -3.5 hours, at southern middle latitudes -5.4 to -4.3 hours, and at southern high latitudes -5.9 to -4.5 hours. This means that at all latitudes we find data that fullfil the temporal collocation requirements and that in the southern hemisphere the temporal collocation is typically larger than in the northern hemisphere. Furthermore, there are horizontal dislocations. In this work we use a horizontal collocation threshold of 50 km. In this appendix we estimate the impact of these spatial and temporal dislocations on the combined product.

E1 Uncertainty source

For investigating the spatial and temporal variability of the atmospheric CH_4 fields, we use the CAMS (Copernicus Atmospheric Monitoring service, https://atmosphere.copernicus.eu/) CH_4 forecast product at highest available resolution (≈ 9 km, Barré et al., 2021). By analysing the profiles forcasted for the same location but different timestamps, we can determine the temporal covariance of the vertical CH_4 fields. Similarly by analysing the profiles forecasted for the same timestamp but different locations we get the spatial covariance of the vertical CH_4 fields. The analyses are made with CAMS data between November 2017 and December 2020 for Central Europe in an area around Karlsruhe. The results are depicted in Figs. E1 to E3.

Figure E1 shows the root-mean-squares (RMS) of the difference between the forecasted reference methane profile and forecasted profiles that are dislocated with respect to the reference by different spatial distances and time differences. These are the square root values of the diagonal entries of the respective dislocation cavariance matrices ($\mathbf{S}^{l}_{\mathbf{\Delta}_{dl}}$, we use here the superscript 'l' for logarithmic scale, because we work with relative covariances: $\Delta \ln x \approx \Delta x/x$). The dashed black lines indicate our collocation threshold values used for the combination of TROPOMI and IASI (TROPOMI and IASI are only combined as long as the horizontal distance of their ground pixels is within 50 km and the time difference is within 6 hours). Naturally, the respective RMS values are increasing with increasing horizontal distance and time difference. The values are largest in a small layer close to the surface and in the stratosphere, but relatively small in the free troposphere. For a horizontal dislocation of 50 km the RMS value is about 2% very close to the surface, between 0.3 and 0.5% for the rest of the troposphere and then it increases again to about 2% above 25 km altitude. For a time difference of 6 hours the RMS value is about 2.5% in a very small layer above ground, 0.6-0.8% in the free troposphere below 10 km, and it reaches about 1.5% at 15 km and 3.5% at 30 km altitude.

Figure E2 reveals to what extend the dislocation uncertainties as shown in Fig. E1 are vertically correlated. Depicted are the vertical correlations for the example of a spatial dislocation of 50 km (Fig. E2a) and a temporal dislocation of 6 hours (Fig. E2b). We observe that for both spatial and temporal dislocations the vertical behavior of the vertical correlation length (distance where correlation coefficient decays to 0.5) is similar. The vertical correlation lengths are rather short close to the surface (only 100-200 m). They are larger for higher altitudes: in the middle/upper troposphere and in the stratosphere they increase to about 1000 m and 6000 m, respectively.

The dislocation error for total and partial columns can be calculated by resampling the spatial and temporal dislocation covariance matrices according to Eq. (D7) (more details see Appendix D). The result of these resampling calculations are shown for the spatial dislocation in Fig. E3a and for the temporal dislocation in Fig. E3b. Naturally the dislocation uncertainties increase for increasing horizontal distance and time difference. For our horizontal collocation threshold values of 50 km the uncertainty (RMS value is used as the metric) is about 0.2% for the total column data. For our time difference collocation threshold of 6 hours it is about 0.3% for the total column data. For the tropospheric and upper tropospheric / lower stratospheric partial columns the respective relative uncertainties values are slightly larger.

E2 Impact on the combined CH_4 product

For calculating the error in the combined profile due to the horizontal and spatial dislocation between IASI and TROPOMI we substitute $\hat{\boldsymbol{x}}_{\boldsymbol{I}}$ in Eq. (1) by $\hat{\boldsymbol{x}}_{\boldsymbol{I}} + \mathbf{A}_{\mathbf{I}}\mathbf{\Delta}_{dl}$, where $\mathbf{\Delta}_{dl}$ is the dislocation uncertainty of CH_4 as shown in Figs. E1 and E2. This

results in a new term in Eq. (1) that gives the dislocation error in the combined profile:

$$\boldsymbol{\Delta}_{dl}\hat{\boldsymbol{x}}_{C}^{l} = (\mathbf{I} - \mathbf{L}^{-1}\boldsymbol{m}\boldsymbol{a}_{\boldsymbol{T}}^{*\,T})\mathbf{A}_{\mathbf{I}}^{\mathbf{l}}\boldsymbol{\Delta}_{dl}^{l}. \tag{E1}$$

The respective error covariance matrix is

$$\mathbf{S}_{\hat{\mathbf{x}}_{\mathbf{C},\mathbf{dl}}}^{\mathbf{l}} = \mathbf{A}_{\mathbf{C},\mathbf{dl}}^{\mathbf{l}}\mathbf{S}_{\boldsymbol{\Delta}_{\mathbf{dl}}}^{\mathbf{l}}{\mathbf{A}_{\mathbf{C},\mathbf{dl}}^{\mathbf{l}}}^{T}, \tag{E2}$$

where $\mathbf{S}_{\boldsymbol{\Delta}_{\mathbf{dl}}}^{\mathbf{l}}$ is the covariance matrix for the CH_4 dislocation uncertainty whose main characetristics are visualised in Figs. E1 and E2. Here

$$\mathbf{A}_{\mathbf{C},\mathbf{dl}}^{\mathbf{l}} = (\mathbf{I} - \mathbf{L}^{-1}\boldsymbol{m}\boldsymbol{a}_{\boldsymbol{T}}^{*\,T})\mathbf{A}_{\mathbf{I}}^{\mathbf{l}} \tag{E3}$$

is the dislocation averaging kernel. Figure E4 shows an example of this dislocation averaging kernel. For the altitudes where the dislocation uncertainty of CH_4 are largest (close to ground and above 20 km, see Fig. E1) the dislocation kernel has rather low values (i.e. there the combination procedure has only limited sensitivity to the dislocation uncertainty).

We calculate the dislocation error covariance matrices according to Eq. (E2) for different locations and then determine the corresponding total and partial column dislocation errors by summing up the temporal and spatial dislocation covariances and performing an subsequent resampling of the covariance matrices according to Eq. (D7) (more details see Appendix D). Figure E5 depicts this dislocation error in comparison to the noise error (respective resampling of the covariance matrices obtained by Eq. (5), see also Fig. 6). We focus here on three different latitudinal locations: Sodankylä (northern high latitudes), Darwin (low latitudes), and Lauder (southern middle latitudes). We find that for the northern high latitude site (where horizontal and temporal dislocation are of similar importance) but also for the tropical and southern hemispheric middle latitude sites (where the temporal dislocation is dominating), the dislocation uncertainty is generally much smaller than the noise error.

Appendix F: Data comparability

The satellite data products are representative for broad vertical layers of the atmosphere (see averaging kernels as shown in Figs. 2 and 3). Also the TCCON and AirCore reference data are sensitive to atmospheric CH_4 at different vertical regions. If we furthermore assume that the TCCON and the AirCore data offer a stable absolute calibration reference, their inter-comparisons with the satellite data as shown in Sect. 4 can in principle be used for empirically validating the characteristics (sensitivity and error) of the satellite data products. The level of agreement that can be expected between the reference data and the satellite products depends on the reliability of the references and the characteristics of the satellite data products. In the following Appendices F1 and F2 we estimate the reliability of the TCCON and AirCore data, respectively, to serve as reference for the satellite data products. Then in Appendix F3 we show that the results of the inter-comparison as shown in the context of Figs. 9 to 12 are in a reasonable agreement with the reliability of the references and the characteristics of the different satellite data products. This confirms the validity of the sensitivity of the satellite data products as shown in Sect. 3.3 and the validity of the errors of the satellite data as documented in Sect. 3.3.

F1 TCCON versus satellite

For estimating the reliability of the TCCON data as reference for the satellite data products we consider the TCCON retrieval noise errors, the incomparableness of TCCON and satellite data caused by their different averaging kernels, and the collocation mismatch between the TCCON and the satellite observations. The total column uncertainty variance (the scalar S^*_{ref}) for using the TCCON data as reference for the satellite data can be estimated by:

$$S^*_{\mathrm{ref}} = S^*_{\Delta\mathrm{TC}} + (\boldsymbol{a}^{*T} - \boldsymbol{a}^{*}_{\mathbf{TC}}{}^{T})\mathbf{S}_{\mathbf{\Delta a}}(\boldsymbol{a}^{*T} - \boldsymbol{a}^{*}_{\mathbf{TC}}{}^{T})^T + \boldsymbol{a}^{*}_{\mathbf{TC}}{}^{T}(\mathbf{S}_{\mathbf{\Delta}_\mathrm{h}} + \mathbf{S}_{\mathbf{\Delta}_\mathrm{t}})\boldsymbol{a}^{*}_{\mathbf{TC}}, \tag{F1}$$

The first term (the scalar $S^*_{\Delta\mathrm{TC}}$) is the TCCON retrieval error variance (the TCCON error is provided with the TCCON data is typically 1‰). The second term accounts for the different averaging kernels. The row vectors $\boldsymbol{a}^{*T}$ and $\boldsymbol{a}^{*}_{\mathbf{TC}}{}^{T}$ are the total column averaged mixing ratio kernels of the satellite and the TCCON retrievals, respectively (calculated according to Appendix D). The matrix $\mathbf{S}_{\mathbf{\Delta a}}$ describes the uncertainty covariances of the used a priori data, and the matrices $\mathbf{S}_{\mathbf{\Delta}_\mathrm{h}}$ and $\mathbf{S}_{\mathbf{\Delta}_\mathrm{t}}$ the covariances for horizontal and temporal collocation mismatches.

For estimating $\mathbf{S}_{\mathbf{\Delta a}}$ we use the difference between the CH_4 state as modelled by TM5 ($\boldsymbol{x}_{\mathbf{TM5}}$) and provided by the high resolution CAMS forecast ($\boldsymbol{x}_{\mathbf{CAMS}}$, e.g., Barré et al., 2021). Figure F1 shows the results of these calculations for the surroundings of Karlsruhe documented by the RMS values of the differences in the vertical profiles (Fig. F1a) and the vertical correlation matrix of the differences (Fig. F1b). We estimate an uncertainty of the TM5 a priori model of about 6% close to the surface, about 2% up througout the middle troposphere, a gradual increase to about 7.5% between the UTLS and about 23 km altitude, and a maximum value of about 27% in the stratosphere at about 30 km. The vertical correlation lengths (altitude range where correlation coefficient decreases to about 0.5) is a few hundred metres close to the surface, about 5000 m in the middle troposphere, about 2500 m in the UTLS, and about 7500 m in the stratosphere above 30 km altitude. We find that this relatively large disagreement between the TM5 a priori data and the high resolution forecast of CAMS are significantly influenced by inconsistencies between TM5 and CAMS in the years 2019 and 2020: after 2018 the TM5 model shows an increase of about 1% per year, but the CAMS high resolution forecast shows no significant increase.

Figure F2 shows the value of the term $(\boldsymbol{a}^{*T} - \boldsymbol{a}^{*}_{\mathbf{TC}}{}^{T})(\boldsymbol{x}_{\mathbf{TM5}} - \boldsymbol{x}_{\mathbf{CAMS}})$ for the different satellite data products, i.e. it reveals the uncertainty in the comparison with TCCON data due to differences in the averaging kernels and the a priori model uncertainty, which in Eq. (F1) is represented by the square root value of the term $(\boldsymbol{a}^{*T} - \boldsymbol{a}^{*}_{\mathbf{TC}}{}^{T})\mathbf{S}_{\mathbf{\Delta a}}(\boldsymbol{a}^{*T} - \boldsymbol{a}^{*}_{\mathbf{TC}}{}^{T})^T$. Because the TROPOMI and the TCCON kernels have both a similar good column sensitivity throughout the troposphere, the respective uncertainty is generally within 0.1% (see black squares in Fig. F2). The same is true for the validation of the total column of the combined product (see blue crosses in Fig. F2). For the validation of the total column of the MUSICA IASI product this error is larger, because the total column sensitivity of IASI is significantly different from the respective sensitivity of the TCCON product and the other satellite products (see Fig. 3a). For the comparison of the IASI and TCCON total column data we estimate that the error due to the different sensitivities (of IASI and TCCON) can occasionally be even above 2% (see red dots in Fig. F2). This error is largest to the end of the time series, because then the TM5 a priori model error is largest (increasing difference between the TM5 model and the CAMS high resolution forecast after 2018).

The collocation mismatch covariances $\mathbf{S}_{\mathbf{\Delta}\mathrm{h}}$ and $\mathbf{S}_{\mathbf{\Delta}\mathrm{t}}$ are the linear scale versions of the matrices $\mathbf{S}^{\mathrm{l}}_{\mathbf{\Delta}_{\mathrm{dt}}}$ (characterised in Figs. E1 and E2) interpolated to the actual temporal and horizontal mismatch of the satellite and the TCCON measurements. The effect of this collocation mismatch on the comparison of the total columns (i.e. the term $\boldsymbol{a}^{*}_{\mathbf{TC}}{}^{T}(\mathbf{S}_{\mathbf{\Delta}\mathrm{h}}+\mathbf{S}_{\mathbf{\Delta}\mathrm{t}})\boldsymbol{a}^{*}_{\mathbf{TC}}$) is estimated to be between 0.1% and 0.4%.

F2 AirCore versus satellite

Similar to the TCCON data we estimate the reliability of the AirCore profile data as reference for the satellite observations. For this estimation we consider an AirCore measurement noise covariance ($\mathbf{S}_{\mathbf{\Delta}\mathrm{AC,n}}$). It is calculated assuming an uncertainty for altitudes with AirCore CH_4 data of 0.3% (Karion et al., 2010) and the uncertainty according to $\mathbf{S}_{\mathbf{\Delta}\mathrm{a}}$ from Sect. F1 for all other altitudes. The outer diagonal elements are determined by assuming the same vertical correlation as derived for $\mathbf{S}_{\mathbf{\Delta}\mathrm{a}}$. In addition, we consider uncertainties in the height attribution, which is according to Wagenhäuser et al. (2021) below 10 m close to ground, about 200 m at 20 km a.s.l. and about 1 km at 27 km a.s.l. We construct a respective height attribution uncertainty covariance ($\mathbf{S}_{\mathbf{\Delta}\mathrm{AC,v}}$) by assuming a very strong correlation of the height attribution uncertainties between different altitude levels. The temporal and spatial collocation mismatch covariance between the AirCore and the satellite observations ($\mathbf{S}_{\mathbf{\Delta}\mathrm{h}}$ and $\mathbf{S}_{\mathbf{\Delta}\mathrm{t}}$, respectively) are calculated as described in Sect. F1.

All the aforementioned uncertainties are independent and we can calculate the total uncertainty as:

$$\mathbf{S}_{\mathbf{\Delta}\mathrm{AC}} = \mathbf{S}_{\mathbf{\Delta}\mathrm{AC,n}} + \mathbf{S}_{\mathbf{\Delta}\mathrm{AC,v}} + \mathbf{S}_{\mathbf{\Delta}\mathrm{h}} + \mathbf{S}_{\mathbf{\Delta}\mathrm{t}}. \tag{F2}$$

The reliability of the AirCore data – after its adjustment according to Eq. (7) – as reference for the MUSICA IASI and combined satellite data can then be estimated by:

$$\mathbf{S}^{\mathrm{l}}_{\mathrm{ref}} = \mathbf{A}^{\mathrm{l}}\mathbf{S}^{\mathrm{l}}_{\mathbf{\Delta}\mathrm{AC}}\mathbf{A}^{\mathrm{l}^{T}}. \tag{F3}$$

Here and in Eq. (F2) the covariances are determined for the full vertical profile. Respective covariances for total or partial columns can be derived according to Appendix D. The reliability for the TROPOMI total column averaged mixing ratio data can be calculated by $S^{*}_{\mathrm{ref}} = \boldsymbol{a}^{*}_{\boldsymbol{T}}{}^{T}\mathbf{S}_{\mathbf{\Delta}\mathrm{AC}}\boldsymbol{a}^{*}_{\boldsymbol{T}}$.

In order to get a reasonable number of collocated AirCore data we relax the collocation criteria: we require a temporal collocation within 6 hours and a spatial collocation within 500 km (see Sect. 4.2). In particular loose spatial collocation requirement results in theoretically large collocation mismatch uncertainties. For instance, Fig. E3 reveals that a spatial mismatch of 400 km clearly dominates the temporal mismatch, whose threshold is set to 6 hours, but it is actually only in the southern hemisphere typically greater than 3 hours. The spatial mismatch uncertaintly also dominates AirCore uncertainties due to measurement noise and uncertain height attribution, i.e. it is the term that mostly affects the comparability of the AirCore and satellite measurements. We estimate a spatial mismatch error that has to be considered for the AirCore satellite inter-comparison of about 0.5% for the total column data and of about 0.6% for the tropospheric and UTLS partial column data.

F3 Summary

The sum of the uncertainty (co)variance of using TCCON or AirCore as the reference (S^*_{ref} or $\mathbf{S}^{\mathbf{1}}_{\mathrm{ref}}$, see Sects. F1 and F2, respectively) and the noise and dislocation error (co)varainces of the satellite data products (see Sect. 3.3 and 3.4, respectively) gives the covariance that can be theoretically expected for the scatter between the TCCON or AirCore reference data and the satellite data products.

Figure F3 shows the correlations between the theoretically expected scatter (mean value of the scatter expected for the individual data points) and the actually observed scatter (the hIPR68.2 of the individual differences between the reference data and the satellite data products). Shown is one data point for the XCH_4 comparisons with the TCCON references, for the XCH_4 comparisons with the AirCore references, and further data points for the comparisons of the tropospheric and UTLS partial columns with the AirCore references. A detailed contemplation suggests that the scatter observed for the total column data of the TROPOMI and the combined data products as well as the scatter observed for the tropospheric partial column data of the IASI and combined products are slightly larger than their theoretically expected counterparts. On the contrary, in the UTLS the scatter observed in the IASI and combined data products seems to be a bit smaller than the theoretically expected scatter values. However, the data points group reasonably well around the one-to-one diagonal, i.e. there is overall a good agreement between the theoretically expected scatter and the actually observed scatter. This means that the inter-comparison results as shown in Sect. 4 confirm the satellite data quality characterisation of Sects. 3.3 - 3.4.

Author contributions. Matthias Schneider developed the idea for the optimal a posteriori combination of the level 2 remote sensing products and he prepared the figures and the manuscript. Benjamin Ertl developed and performed the continuous MUSICA IASI data processing, where he was supported by Matthias Schneider, Christopher J. Diekmann, Farahnaz Khosrawi, Amelie N. Röhling, Omaira E. García, and Eliezer Sepúlveda. Frank Hase developed the PROFFIT-nadir retrieval code used for the MUSICA IASI processing. Quiansi Tu supported the use of the CAMS high resolution data. Tobias Borsdorff, Jochen Landgraf, Alba Lorente, and André Butz are responsible for the TROPOMI processing and made TROPOMI data available. Huilin Chen and Rigel Kivi are responsible for the AirCore profile measurements over Sodankylä. Thomas Laemmel, Michel Ramonet, Cyril Crevoisier, and Jérome Pernin are responsible for the AirCore profile measurements over Trainou. Martin Steinbacher and Frank Meinhardt are responsible for the GAW data of Jungfraujoch and Schauinsland, respectively. Rigel Kivi, Darko Dubravica, Frank Hase, Kimberly Strong, Debra Wunch, Thorsten Warneke, Coleen Roehl, Paul O. Wennberg, Isamu Morino, Laura T. Iraci, Kei Shiomi, Nicholas M. Deutscher, David W. T. Griffith, Voltaire A. Velazco, and David F. Pollard are responsible for the TCCON data. All authors supported the generation of the final version of this manuscript.

Competing interests. The authors declare that they have no conflict of interest

Acknowledgements. We would like to thank our colleague Thomas von Clarmann for his strong support in revising the equations in the Appendices of this manuscript.

This research has largely benefit from funds of the Deutsche Forschungsgemeinschaft (provided for the two projects MOTIV and TEDDY with IDs/Geschäftszeichen 290612604/GZ:SCHN1126/2-1 and 416767181/GZ:SCHN1126/5-1, respectively) and from support by the European Space Agency in the context the "Sentinel-5p+Innovation (S5p+I) - Water Vapour Isotopologues (H2O-ISO)" activities. Furthermore, we acknowledge funds from the Ministerio de Economía y Competividad from Spain for the project INMENSE (CGL2016-80688-P).

Important part of this work was performed on the supercomputer ForHLR funded by the Ministry of Science, Research and the Arts Baden-Württemberg and by the German Federal Ministry of Education and Research. We also acknowledge the contribution of Teide High-Performance Computing facilities. TeideHPC facilities are provided by the Instituto Tecnológico y de Energías Renovables (ITER), S.A (teidehpc.iter.es).

The TROPOMI data processing was carried out on the Dutch National e-Infrastructure with the support of the SURF cooperative. The presented material contains modified Copernicus data (2017, 2019).

The Eureka TCCON measurements were made at the Polar Environment Atmospheric Research Laboratory (PEARL) by the Canadian Network for the Detection of Atmospheric Change, primarily supported by NSERC, ECCC, and CSA. The East Trout Lake TCCON station is supported by CFI, ORF, and NSERC. The Karlsruhe TCCON station has been supported by the German Bundesministerium für Wirtschaft und Energie (BMWi) via DLR under grants 50EE1711A to E and by the Helmholtz Society via the research program ATMO. The ~~Burgos TCCON site is~~ Park Falls and Lamont TCCON sites are supported by and would like to acknowledge NASA's Carbon Cycle Science Program (grant # NNX17AE15G) and OCO-2/-3 projects (primary grant # NNN12AA01C), respectively. The Burgos and Rikubetsu TCCON sites are supported in part by the GOSAT series project. Burgos is supported in part by the Energy Development Corp. Philippines. ~~The Lauder TCCON programme is core funded by NIWA through New Zealand's Ministry of Business, Innovation and Employment~~Funding for the Edwards TCCON station is provided by NASA's Earth Science Division. NMD is funded by ARC Future Fellowship FT180100327. Darwin and Wollongong TCCON stations are supported by ARC grants DP160100598, LE0668470, DP140101552, DP110103118 and DP0879468, and Darwin through NASA grants NAG5-12247 and NNG05-GD07G. The Lauder TCCON programme is core funded by NIWA through New Zealand's Ministry of Business, Innovation and Employment.

The Trainou AirCore measurements have been supported by CEA, CNES, UVSQ, IPSL and the EU H2020 RINGO project (GA no. 730944), and are part of the French consortium for Aircore measurements (LMD, LSCE, GSMA, CNES). The Sodankylä TCCON and AirCore measurements have been supported via the ESA FRM4GHG project (under the grant agreement no. ESA-IPLPOE-LG-cl-LE-2015-1129) and the EU H2020 RINGO project.

The CH_4 observations at Jungfraujoch were established as part of the Swiss National Air Pollution Monitoring Network and are supported through ICOS-CH, which is funded by the Swiss National Science Foundation and in-house contributions.

We acknowledge the support by the Deutsche Forschungsgemeinschaft and the Open Access Publishing Fund of the Karlsruhe Institute of Technology.

References

Barré, J., Aben, I., Agustí-Panareda, A., Balsamo, G., Bousserez, N., Dueben, P., Engelen, R., Inness, A., Lorente, A., McNorton, J., Peuch, V.-H., Radnoti, G., and Ribas, R.: Systematic detection of local CH_4 anomalies by combining satellite measurements with high-resolution forecasts, Atmospheric Chemistry and Physics, 21, 5117–5136, https://doi.org/10.5194/acp-21-5117-2021, https://acp.copernicus.org/articles/21/5117/2021/, 2021.

Borger, C., Schneider, M., Ertl, B., Hase, F., García, O. E., Sommer, M., Höpfner, M., Tjemkes, S. A., and Calbet, X.: Evaluation of MUSICA IASI tropospheric water vapour profiles using theoretical error assessments and comparisons to GRUAN Vaisala RS92 measurements, Atmospheric Measurement Techniques, 11, 4981–5006, https://doi.org/10.5194/amt-11-4981-2018, https://www.atmos-meas-tech.net/11/4981/2018/, 2018.

Butz, A., Guerlet, S., Hasekamp, O., Schepers, D., Galli, A., Aben, I., Frankenberg, C., Hartmann, J.-M., Tran, H., Kuze, A., Keppel-Aleks, G., Toon, G., Wunch, D., Wennberg, P., Deutscher, N., Griffith, D., Macatangay, R., Messerschmidt, J., Notholt, J., and Warneke, T.: Toward accurate CO2 and CH4 observations from GOSAT, Geophysical Research Letters, 38, https://doi.org/https://doi.org/10.1029/2011GL047888, https://agupubs.onlinelibrary.wiley.com/doi/abs/10.1029/2011GL047888, 2011.

Ceccherini, S., Raspollini, P., and Carli, B.: Optimal use of the information provided by indirect measurements of atmospheric vertical profiles, Opt. Express, 17, 4944–4958, https://doi.org/10.1364/OE.17.004944, http://www.opticsexpress.org/abstract.cfm?URI=oe-17-7-4944, 2009.

Cortesi, U., Del Bianco, S., Ceccherini, S., Gai, M., Dinelli, B. M., Castelli, E., Oelhaf, H., Woiwode, W., Höpfner, M., and Gerber, D.: Synergy between middle infrared and millimeter-wave limb sounding of atmospheric temperature and minor constituents, Atmospheric Measurement Techniques, 9, 2267–2289, https://doi.org/10.5194/amt-9-2267-2016, https://amt.copernicus.org/articles/9/2267/2016/, 2016.

Costantino, L., Cuesta, J., Emili, E., Coman, A., Foret, G., Dufour, G., Eremenko, M., Chailleux, Y., Beekmann, M., and Flaud, J.-M.: Potential of multispectral synergism for observing ozone pollution by combining IASI-NG and UVNS measurements from the EPS-SG satellite, Atmospheric Measurement Techniques, 10, 1281–1298, https://doi.org/10.5194/amt-10-1281-2017, https://www.atmos-meas-tech.net/10/1281/2017/, 2017.

Cuesta, J., Eremenko, M., Liu, X., Dufour, G., Cai, Z., Höpfner, M., von Clarmann, T., Sellitto, P., Foret, G., Gaubert, B., Beekmann, M., Orphal, J., Chance, K., Spurr, R., and Flaud, J.-M.: Satellite observation of lowermost tropospheric ozone by multispectral synergism of IASI thermal infrared and GOME-2 ultraviolet measurements over Europe, Atmospheric Chemistry and Physics, 13, 9675–9693, https://doi.org/10.5194/acp-13-9675-2013, https://www.atmos-chem-phys.net/13/9675/2013/, 2013.

Diekmann, C. J., Schneider, M., Ertl, B., Hase, F., García, O., Khosrawi, F., Sepúlveda, E., Knippertz, P., and Braesicke, P.: The global and multi-annual MUSICA IASI $\{H_2O, \delta D\}$ pair dataset, Earth System Science Data, 13, 5273–5292, https://doi.org/10.5194/essd-13-5273-2021, https://essd.copernicus.org/articles/13/5273/2021/, 2021.

Fu, D., Worden, J. R., Liu, X., Kulawik, S. S., Bowman, K. W., and Natraj, V.: Characterization of ozone profiles derived from Aura TES and OMI radiances, Atmospheric Chemistry and Physics, 13, 3445–3462, https://doi.org/10.5194/acp-13-3445-2013, https://acp.copernicus.org/articles/13/3445/2013/, 2013.

García, O. E., Schneider, M., Ertl, B., Sepúlveda, E., Borger, C., Diekmann, C., Wiegele, A., Hase, F., Barthlott, S., Blumenstock, T., Raffalski, U., Gómez-Peláez, A., Steinbacher, M., Ries, L., and de Frutos, A. M.: The MUSICA IASI CH_4 and N_2O products and their comparison to HIPPO, GAW and NDACC FTIR references, Atmospheric Measurement Techniques, 11, 4171–4215, https://doi.org/10.5194/amt-11-4171-2018, https://www.atmos-meas-tech.net/11/4171/2018/, 2018.

Griffith, D. W., Deutscher, N. M., Velazco, V. A., Wennberg, P. O., Yavin, Y., Keppel-Aleks, G., Washenfelder, R. A., Toon, G. C., Blavier, J.-F., Paton-Walsh, C., Jones, N. B., Kettlewell, G. C., Connor, B. J., Macatangay, R. C., Roehl, C., Ryczek, M., Glowacki, J., Culgan, T., and Bryant, G. W.: TCCON data from Darwin (AU), Release GGG2014.R0, https://doi.org/10.14291/TCCON.GGG2014.DARWIN01.R0/1149290, https://data.caltech.edu/records/269, 2014a.

Griffith, D. W., Velazco, V. A., Deutscher, N. M., Paton-Walsh, C., Jones, N. B., Wilson, S. R., Macatangay, R. C., Kettlewell, G. C., Buchholz, R. R., and Riggenbach, M. O.: TCCON data from Wollongong (AU), Release GGG2014.R0, https://doi.org/10.14291/TCCON.GGG2014.WOLLONGONG01.R0/1149291, https://data.caltech.edu/records/291, 2014b.

Hase, F., Blumenstock, T., Dohe, S., Groß, J., and Kiel, M.: TCCON data from Karlsruhe (DE), Release GGG2014.R1, https://doi.org/10.14291/TCCON.GGG2014.KARLSRUHE01.R1/1182416, https://data.caltech.edu/records/278, 2015.

Hasekamp, O., Lorente, A., Hu, H., Butz, A., aan de Brugh, J., and Landgraf, J.: Algorithm Theoretical Baseline Document for Senitinel-5 Precursor methane retrieval, http://www.tropomi.eu/documents/atbd/, 2019.

Hu, H., Hasekamp, O., Butz, A., Galli, A., Landgraf, J., Aan de Brugh, J., Borsdorff, T., Scheepmaker, R., and Aben, I.: The operational methane retrieval algorithm for TROPOMI, Atmospheric Measurement Techniques, 9, 5423–5440, https://doi.org/10.5194/amt-9-5423-2016, https://amt.copernicus.org/articles/9/5423/2016/, 2016.

Iraci, L. T., Podolske, J. R., Hillyard, P. W., Roehl, C., Wennberg, P. O., Blavier, J.-F., Landeros, J., Allen, N., Wunch, D., Zavaleta, J., Quigley, E., Osterman, G. B., Albertson, R., Dunwoody, K., and Boyden, H.: TCCON data from Edwards (US), Release GGG2014.R1, https://doi.org/10.14291/TCCON.GGG2014.EDWARDS01.R1/1255068, https://data.caltech.edu/records/270, 2016.

Kalman, R. E.: A New Approach to Linear Filtering and Prediction Problems, Journal of Basic Engineering, 82, 35–45, https://doi.org/10.1115/1.3662552, https://doi.org/10.1115/1.3662552, 1960.

Karion, A., Sweeney, C., Tans, P., and Newberger, T.: AirCore: An Innovative Atmospheric Sampling System, Journal of Atmospheric and Oceanic Technology, 27, 1839 – 1853, https://doi.org/10.1175/2010JTECHA1448.1, https://journals.ametsoc.org/view/journals/atot/27/11/2010jtecha1448_1.xml, 2010.

Kawakami, S., Ohyama, H., Arai, K., Okumura, H., Taura, C., Fukamachi, T., and Sakashita, M.: TCCON data from Saga (JP), Release GGG2014.R0, https://doi.org/10.14291/TCCON.GGG2014.SAGA01.R0/1149283, https://data.caltech.edu/records/288, 2014.

Keppens, A., Lambert, J.-C., Granville, J., Miles, G., Siddans, R., van Peet, J. C. A., van der A, R. J., Hubert, D., Verhoelst, T., Delcloo, A., Godin-Beekmann, S., Kivi, R., Stübi, R., and Zehner, C.: Round-robin evaluation of nadir ozone profile retrievals: methodology and application to MetOp-A GOME-2, Atmospheric Measurement Techniques, 8, 2093–2120, https://doi.org/10.5194/amt-8-2093-2015, https://www.atmos-meas-tech.net/8/2093/2015/, 2015.

Kivi, R. and Heikkinen, P.: Fourier transform spectrometer measurements of column CO_2 at Sodankylä, Finland, Geoscientific Instrumentation, Methods and Data Systems, 5, 271–279, https://doi.org/10.5194/gi-5-271-2016, https://gi.copernicus.org/articles/5/271/2016/, 2016.

Kivi, R., Heikkinen, P., and Kyrö, E.: TCCON data from Sodankylä (FI), Release GGG2014.R0, https://doi.org/10.14291/TCCON.GGG2014.SODANKYLA01.R0/1149280, https://data.caltech.edu/records/289, 2014.

Krol, M., Houweling, S., Bregman, B., van den Broek, M., Segers, A., van Velthoven, P., Peters, W., Dentener, F., and Bergamaschi, P.: The two-way nested global chemistry-transport zoom model TM5: algorithm and applications, Atmospheric Chemistry and Physics, 5, 417–432, https://doi.org/10.5194/acp-5-417-2005, https://acp.copernicus.org/articles/5/417/2005/, 2005.

Kulawik, S. S., Worden, J. R., Payne, V. H., Fu, D., Wofsy, S. C., McKain, K., Sweeney, C., Daube Jr., B. C., Lipton, A., Polonsky, I., He, Y., Cady-Pereira, K. E., Dlugokencky, E. J., Jacob, D. J., and Yin, Y.: Evaluation of single-footprint AIRS CH_4 profile retrieval

uncertainties using aircraft profile measurements, Atmospheric Measurement Techniques, 14, 335–354, https://doi.org/10.5194/amt-14-335-2021, https://amt.copernicus.org/articles/14/335/2021/, 2021.

Landgraf, J. and Hasekamp, O. P.: Retrieval of tropospheric ozone: The synergistic use of thermal infrared emission and ultraviolet reflectivity measurements from space, Journal of Geophysical Research: Atmospheres, 112, https://doi.org/https://doi.org/10.1029/2006JD008097, https://agupubs.onlinelibrary.wiley.com/doi/abs/10.1029/2006JD008097, 2007.

Landgraf, J., Butz, A., Hasekamp, O., Hu, H., , and aan de Brugh, J.: Senitinel 5 L2 Prototype Processors, Algorithm Theoretical Baseline Document: Methane Retrieval, 2019.

Lorente, A., Borsdorff, T., Butz, A., Hasekamp, O., aan de Brugh, J., Schneider, A., Wu, L., Hase, F., Kivi, R., Wunch, D., Pollard, D. F., Shiomi, K., Deutscher, N. M., Velazco, V. A., Roehl, C. M., Wennberg, P. O., Warneke, T., and Landgraf, J.: Methane retrieved from TROPOMI: improvement of the data product and validation of the first 2 years of measurements, Atmospheric Measurement Techniques, 14, 665–684, https://doi.org/10.5194/amt-14-665-2021, https://amt.copernicus.org/articles/14/665/2021/, 2021.

Luo, M., Read, W., Kulawik, S., Worden, J., Livesey, N., Bowman, K., and Herman, R.: Carbon monoxide (CO) vertical profiles derived from joined TES and MLS measurements, Journal of Geophysical Research: Atmospheres, 118, 10,601–10,613, https://doi.org/https://doi.org/10.1002/jgrd.50800, https://agupubs.onlinelibrary.wiley.com/doi/abs/10.1002/jgrd.50800, 2013.

Morino, I., Yokozeki, N., Matsuzaki, T., and Horikawa, M.: TCCON data from Rikubetsu (JP), Release GGG2014.R2, https://doi.org/10.14291/TCCON.GGG2014.RIKUBETSU01.R2, https://data.caltech.edu/records/957, 2018.

Pandey, S., Houweling, S., Krol, M., Aben, I., Chevallier, F., Dlugokencky, E. J., Gatti, L. V., Gloor, E., Miller, J. B., Detmers, R., Machida, T., and Röckmann, T.: Inverse modeling of GOSAT-retrieved ratios of total column CH_4 and CO_2 for 2009 and 2010, Atmospheric Chemistry and Physics, 16, 5043–5062, https://doi.org/10.5194/acp-16-5043-2016, https://acp.copernicus.org/articles/16/5043/2016/, 2016.

Parker, R. J., Webb, A., Boesch, H., Somkuti, P., Barrio Guillo, R., Di Noia, A., Kalaitzi, N., Anand, J. S., Bergamaschi, P., Chevallier, F., Palmer, P. I., Feng, L., Deutscher, N. M., Feist, D. G., Griffith, D. W. T., Hase, F., Kivi, R., Morino, I., Notholt, J., Oh, Y.-S., Ohyama, H., Petri, C., Pollard, D. F., Roehl, C., Sha, M. K., Shiomi, K., Strong, K., Sussmann, R., Té, Y., Velazco, V. A., Warneke, T., Wennberg, P. O., and Wunch, D.: A decade of GOSAT Proxy satellite CH_4 observations, Earth System Science Data, 12, 3383–3412, https://doi.org/10.5194/essd-12-3383-2020, https://essd.copernicus.org/articles/12/3383/2020/, 2020.

Pollard, D. F., Robinson, J., and Shiona, H.: TCCON data from Lauder (NZ), Release GGG2014.R0, https://doi.org/10.14291/TCCON.GGG2014.LAUDER03.R0, https://data.caltech.edu/records/1220, 2019.

Rodgers, C.: Inverse Methods for Atmospheric Sounding: Theory and Praxis, World Scientific Publishing Co., Singapore, 2000.

Rodgers, C. and Connor, B.: Intercomparison of remote sounding instruments, J. Geophys. Res., 108, 4116–4129, https://doi.org/10.1029/2002JD002299, 2003.

Schneider, M., Wiegele, A., Barthlott, S., González, Y., Christner, E., Dyroff, C., García, O. E., Hase, F., Blumenstock, T., Sepúlveda, E., Mengistu Tsidu, G., Takele Kenea, S., Rodríguez, S., and Andrey, J.: Accomplishments of the MUSICA project to provide accurate, long-term, global and high-resolution observations of tropospheric $\{H_2O,\delta D\}$ pairs – a review, Atmospheric Measurement Techniques, 9, 2845–2875, https://doi.org/10.5194/amt-9-2845-2016, http://www.atmos-meas-tech.net/9/2845/2016/, 2016.

Schneider, M., Ertl, B., Diekmann, C. J., Khosrawi, F., Weber, A., Hase, F., Höpfner, M., García, O. E., Sepúlveda, E., and Kinnison, D.: Design and description of the MUSICA IASI full retrieval product, Earth System Science Data, 14, 709–742, https://doi.org/10.5194/essd-14-709-2022, https://essd.copernicus.org/articles/14/709/2022/, 2022.

Sepúlveda, E., Schneider, M., Hase, F., Barthlott, S., Dubravica, D., García, O. E., Gomez-Pelaez, A., González, Y., Guerra, J. C., Gisi, M., Kohlhepp, R., Dohe, S., Blumenstock, T., Strong, K., Weaver, D., Palm, M., Sadeghi, A., Deutscher, N. M., Warneke, T., Notholt, J., Jones,

N., Griffith, D. W. T., Smale, D., Brailsford, G. W., Robinson, J., Meinhardt, F., Steinbacher, M., Aalto, T., and Worthy, D.: Tropospheric CH_4 signals as observed by NDACC FTIR at globally distributed sites and comparison to GAW surface in situ measurements, Atmospheric Measurement Techniques, 7, 2337–2360, https://doi.org/10.5194/amt-7-2337-2014, https://amt.copernicus.org/articles/7/2337/2014/, 2014.

Sha, M. K., Langerock, B., Blavier, J.-F. L., Blumenstock, T., Borsdorff, T., Buschmann, M., Dehn, A., De Mazière, M., Deutscher, N. M., Feist, D. G., García, O. E., Griffith, D. W. T., Grutter, M., Hannigan, J. W., Hase, F., Heikkinen, P., Hermans, C., Iraci, L. T., Jeseck, P., Jones, N., Kivi, R., Kumps, N., Landgraf, J., Lorente, A., Mahieu, E., Makarova, M. V., Mellqvist, J., Metzger, J.-M., Morino, I., Nagahama, T., Notholt, J., Ohyama, H., Ortega, I., Palm, M., Petri, C., Pollard, D. F., Rettinger, M., Robinson, J., Roche, S., Roehl, C. M., Röhling, A. N., Rousogenous, C., Schneider, M., Shiomi, K., Smale, D., Stremme, W., Strong, K., Sussmann, R., Té, Y., Uchino, O., Velazco, V. A., Vigouroux, C., Vrekoussis, M., Wang, P., Warneke, T., Wizenberg, T., Wunch, D., Yamanouchi, S., Yang, Y., and Zhou, M.: Validation of methane and carbon monoxide from Sentinel-5 Precursor using TCCON and NDACC-IRWG stations, Atmospheric Measurement Techniques, 14, 6249–6304, https://doi.org/10.5194/amt-14-6249-2021, https://amt.copernicus.org/articles/14/6249/2021/, 2021.

Sherlock, V., Connor, B., Robinson, J., Shiona, H., Smale, D., and Pollard, D. F.: TCCON data from Lauder (NZ), 125HR, Release GGG2014.R0, https://doi.org/10.14291/TCCON.GGG2014.LAUDER02.R0/1149298, https://data.caltech.edu/records/281, 2014.

Strong, K., Roche, S., Franklin, J. E., Mendonca, J., Lutsch, E., Weaver, D., Fogal, P. F., Drummond, J. R., Batchelor, R., and Lindenmaier, R.: TCCON data from Eureka (CA), Release GGG2014.R3, https://doi.org/10.14291/TCCON.GGG2014.EUREKA01.R3, https://data.caltech.edu/records/1171, 2019.

Velazco, V. A., Morino, I., Uchino, O., Hori, A., Kiel, M., Bukosa, B., Deutscher, N. M., Sakai, T., Nagai, T., Bagtasa, G., Izumi, T., Yoshida, Y., and Griffith, D. W. T.: TCCON Philippines: First Measurement Results, Satellite Data and Model Comparisons in Southeast Asia, Remote Sensing, 9, https://doi.org/10.3390/rs9121228, https://www.mdpi.com/2072-4292/9/12/1228, 2017.

von Clarmann, T., Degenstein, D. A., Livesey, N. J., Bender, S., Braverman, A., Butz, A., Compernolle, S., Damadeo, R., Dueck, S., Eriksson, P., Funke, B., Johnson, M. C., Kasai, Y., Keppens, A., Kleinert, A., Kramarova, N. A., Laeng, A., Langerock, B., Payne, V. H., Rozanov, A., Sato, T. O., Schneider, M., Sheese, P., Sofieva, V., Stiller, G. P., von Savigny, C., and Zawada, D.: Overview: Estimating and reporting uncertainties in remotely sensed atmospheric composition and temperature, Atmospheric Measurement Techniques, 13, 4393–4436, https://doi.org/10.5194/amt-13-4393-2020, https://amt.copernicus.org/articles/13/4393/2020/, 2020.

Wagenhäuser, T., Engel, A., and Sitals, R.: Testing the altitude attribution and vertical resolution of AirCore measurements with a new spiking method, Atmospheric Measurement Techniques Discussions, 2021, 1–18, https://doi.org/10.5194/amt-2020-461, https://amt.copernicus.org/preprints/amt-2020-461/, 2021.

Warneke, T., Messerschmidt, J., Notholt, J., Weinzierl, C., Deutscher, N. M., Petri, C., and Grupe, P.: TCCON data from Orléans (FR), Release GGG2014.R1, https://doi.org/10.14291/TCCON.GGG2014.ORLEANS01.R1, https://data.caltech.edu/records/1301, 2019.

Warner, J. X., Yang, R., Wei, Z., Carminati, F., Tangborn, A., Sun, Z., Lahoz, W., Attié, J.-L., El Amraoui, L., and Duncan, B.: Global carbon monoxide products from combined AIRS, TES and MLS measurements on A-train satellites, Atmospheric Chemistry and Physics, 14, 103–114, https://doi.org/10.5194/acp-14-103-2014, https://acp.copernicus.org/articles/14/103/2014/, 2014.

Wennberg, P. O., Wunch, D., Roehl, C. M., Blavier, J.-F., Toon, G. C., and Allen, N. T.: TCCON data from Lamont (US), Release GGG2014.R1, https://doi.org/10.14291/TCCON.GGG2014.LAMONT01.R1/1255070, https://data.caltech.edu/records/279, 2016.

Wennberg, P. O., Roehl, C. M., Wunch, D., Toon, G. C., Blavier, J.-F., Washenfelder, R., Keppel-Aleks, G., Allen, N. T., and Ayers, J.: TCCON data from Park Falls (US), Release GGG2014.R1, https://doi.org/10.14291/TCCON.GGG2014.PARKFALLS01.R1, https://data.caltech.edu/records/295, 2017.

Worden, J., Liu, X., Bowman, K., Chance, K., Beer, R., Eldering, A., Gunson, M., and Worden, H.: Improved tropospheric ozone profile retrievals using OMI and TES radiances, Geophysical Research Letters, 34, https://doi.org/https://doi.org/10.1029/2006GL027806, https://agupubs.onlinelibrary.wiley.com/doi/abs/10.1029/2006GL027806, 2007.

Worden, J. R., Turner, A. J., Bloom, A., Kulawik, S. S., Liu, J., Lee, M., Weidner, R., Bowman, K., Frankenberg, C., Parker, R., and Payne, V. H.: Quantifying lower tropospheric methane concentrations using GOSAT near-IR and TES thermal IR measurements, Atmospheric Measurement Techniques, 8, 3433–3445, https://doi.org/10.5194/amt-8-3433-2015, https://amt.copernicus.org/articles/8/3433/2015/, 2015.

Wunch, D., Toon, G. C., Blavier, J.-F. L., Washenfelder, R. A., Notholt, J., Connor, B. J., Griffith, D. W. T., Sherlock, V., and Wennberg, P. O.: The Total Carbon Column Observing Network, Philosophical Transactions of the Royal Society A: Mathematical, Physical and Engineering Sciences, 369, 2087–2112, https://doi.org/10.1098/rsta.2010.0240, https://royalsocietypublishing.org/doi/abs/10.1098/rsta.2010.0240, 2011a.

Wunch, D., Wennberg, P. O., Toon, G. C., Connor, B. J., Fisher, B., Osterman, G. B., Frankenberg, C., Mandrake, L., O'Dell, C., Ahonen, P., Biraud, S. C., Castano, R., Cressie, N., Crisp, D., Deutscher, N. M., Eldering, A., Fisher, M. L., Griffith, D. W. T., Gunson, M., Heikkinen, P., Keppel-Aleks, G., Kyrö, E., Lindenmaier, R., Macatangay, R., Mendonca, J., Messerschmidt, J., Miller, C. E., Morino, I., Notholt, J., Oyafuso, F. A., Rettinger, M., Robinson, J., Roehl, C. M., Salawitch, R. J., Sherlock, V., Strong, K., Sussmann, R., Tanaka, T., Thompson, D. R., Uchino, O., Warneke, T., and Wofsy, S. C.: A method for evaluating bias in global measurements of CO_2 total columns from space, Atmospheric Chemistry and Physics, 11, 12 317–12 337, https://doi.org/10.5194/acp-11-12317-2011, https://acp.copernicus.org/articles/11/12317/2011/, 2011b.

Wunch, D., Mendonca, J., Colebatch, O., Allen, N. T., Blavier, J.-F., Roche, S., Hedelius, J., Neufeld, G., Springett, S., Worthy, D., Kessler, R., and Strong, K.: TCCON data from East Trout Lake, SK (CA), Release GGG2014.R1, https://doi.org/10.14291/TCCON.GGG2014.EASTTROUTLAKE01.R1, https://data.caltech.edu/records/362, 2018.

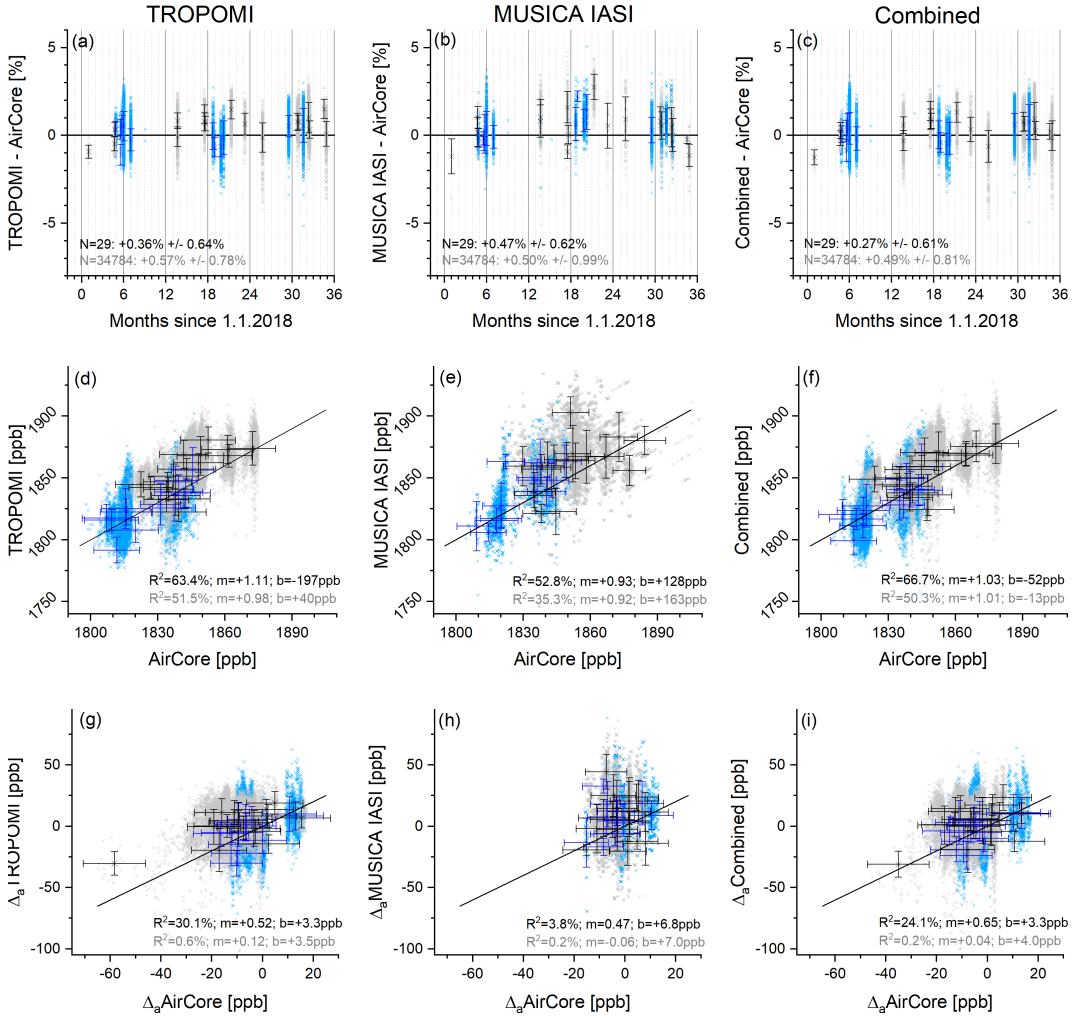

Figure 10. Comparison of the different satellite XCH_4 products with adjusted AirCore ~~measurements made~~ XCH_4 measured at Trainou (black) and Sodankylä (blue)~~with the TROPOMI XCH_4 product~~. Data for all individual coincidences are shown in the background as ~~squares~~ pale crosses and daily averages ~~per flight~~ are depicted as crosses with error bars ~~representing~~ (daily means are only calculated if there are at least 3 observations per day, which is the ~~estimated uncertainty:~~ case on 29 days of the total 31 days with AirCore observations). (a)~~shows the~~ -(c) Time series of the differences ~~ordered by flight number, text in dark and pale fonts report mean and 1σ~~ (error bars represent the daily 1σ standard deviation of the difference). (~~scatterd~~)~~determined from the averages per flight and from all individual collocations, respectively;~~ -(~~b~~f) ~~visualises the correlation~~ Correlation between AirCore and satellite data (the black line is the one-to-one diagonal~~)~~, ~~text in dark~~ x-axis error bars represent the mean uncertainty estimated for the AirCore data – according to Eq. (F3) – and ~~pale fonts report coefficients~~ y-axis error bars the daily 1σ standard deviation of ~~determination~~ the satellite data, respectively). (~~R^2~~g)-(i) Correlation between the a priori free AirCore and satellite data (error bars as in d-f). The inserted text reports median and scatter (hIPR68.2, a-c) and the coefficients of determination, the slope, and the intercept of the robust linear regression ~~line~~ model (R^2, m, and b, d-i)~~obtained~~. Black and grey fonts represent the values for ~~a linear least squares fit on~~ the ~~averages per flight~~ daily mean data and ~~on~~ for data from all individual collocations, respectively.~~Details about the corresponding AirCore flights are provided in Table 2.~~

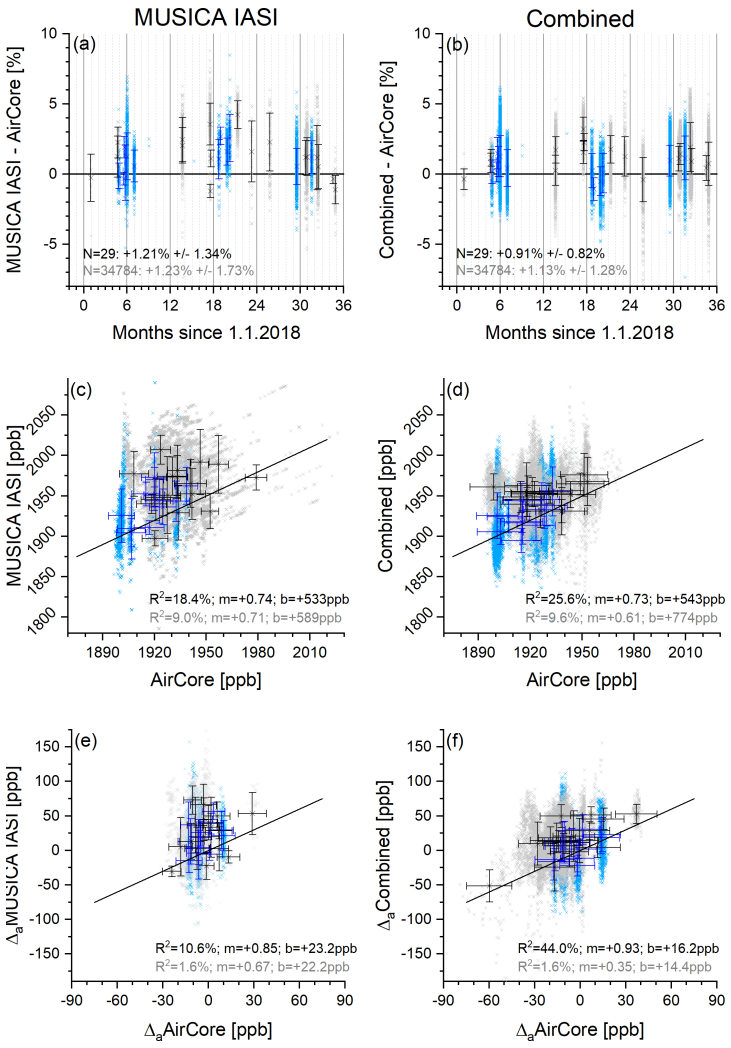

Figure 11. Same as Fig. 10, but for the comparisons of tropospheric partial column averaged CH_4 AirCore and satellite products (IASI and combined).

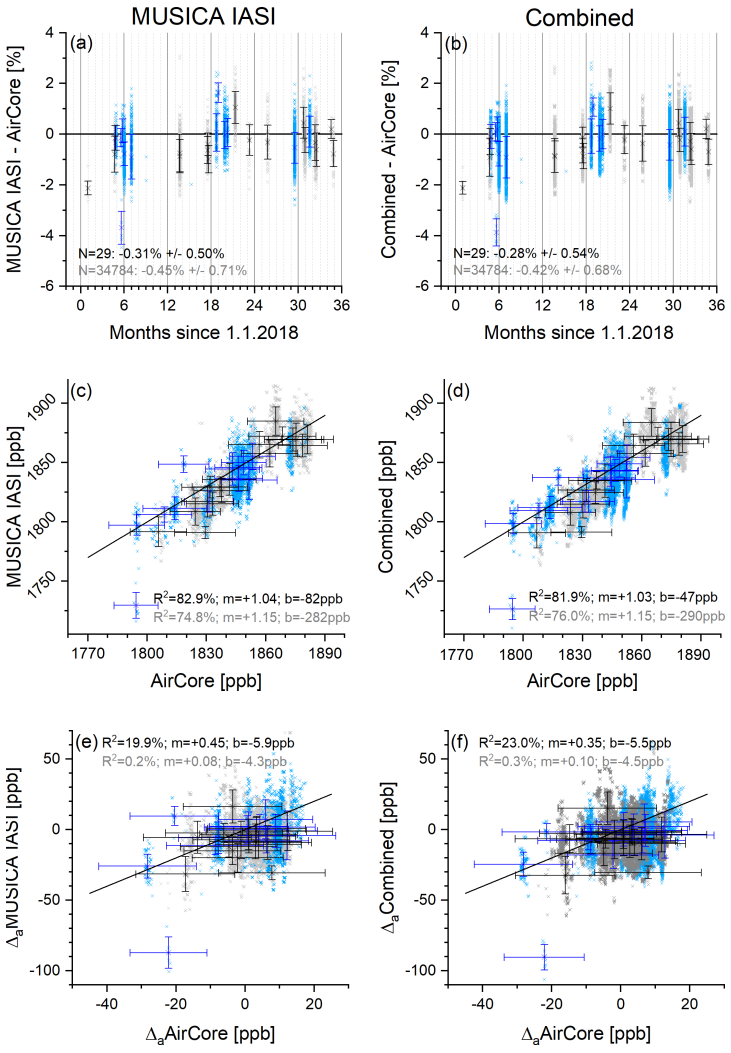

Figure 12. Same as Fig. 11, but for comparisons of UTLS partial column averaged CH_4 data.

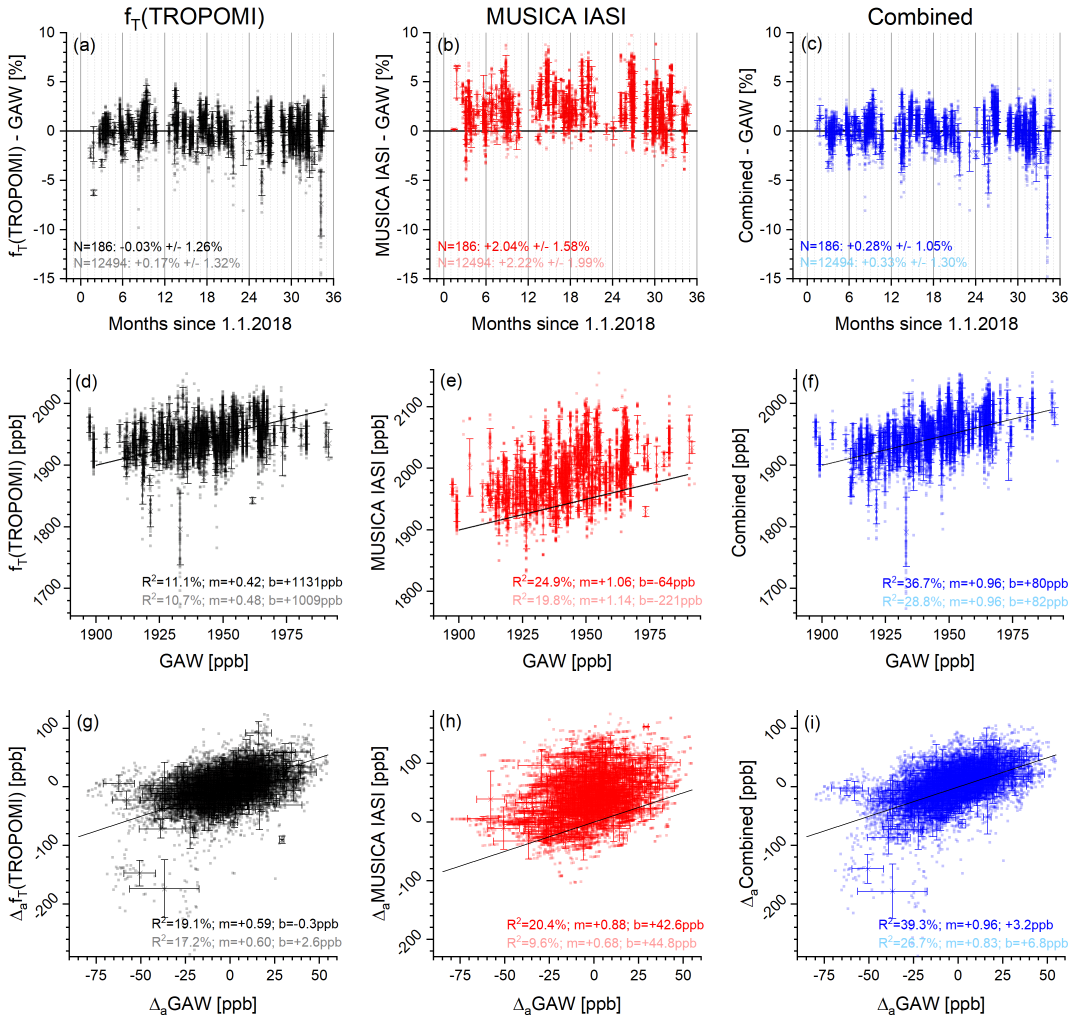

Figure 13. Comparison of GAW measurements made at Jungfraujoch and Schauinsland with the TROPOMI tropospheric CH_4 proxy product according to Eq. 8 and the IASI and the combined tropospheric CH_4 products. Data for all individual coincidences are shown in the background as squares and daily averages are depicted as crosses with error bars representing the daily 1σ standard deviations (daily means are only calculated if there are at least 3 observations per day). (a)-(c) Time series of differences. (d)-(f) Correlation between GAW and satellite data (the black line is the one-to-one diagonal). (g)-(i) Correlations between the difference of GAW and a priori data ($\Delta_a\mathrm{GAW} = \mathrm{troXCH_4(GAW)} - \mathrm{troXCH_4(apriori)}$) and the a priori free satellite data ($\Delta_a\mathrm{Satellite} = \mathrm{troXCH_4(Satellite)} - \mathrm{troXCH_4(apriori)}$). The inserted text reports median and scatter (hIPR68.2, a-c) and the coefficients of determination, the slope, and the intercept of the robust linear regression model (R^2, m, and b, d-i). Dark and pale coloured fonts represent the values for the daily mean data and for data from all individual collocations, respectively.

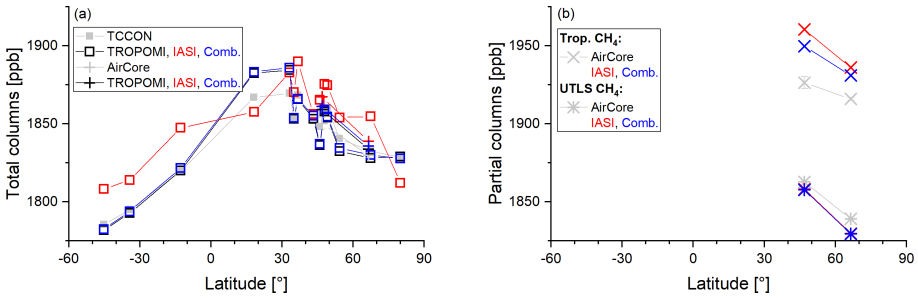

Figure 14. Latitudinal dependency of the overall mean values obtained at the ~~six~~ 14 TCCON and two AirCore observation sites. Grey colour represents the TCCON and AirCore reference data and black, red and blue colours the TROPOMI, MUSICA IASI, and combined satellite data, respectively: (a) for total columns (XCH_4) and (b) for tropospheric and UTLS partial columns. The error bars on the AirCore data describe the variability range due to the AirCore data treatment – according to Eq. (7) – with the different averaging kernels of the TROPOMI, MUSICA IASI and combined data product.

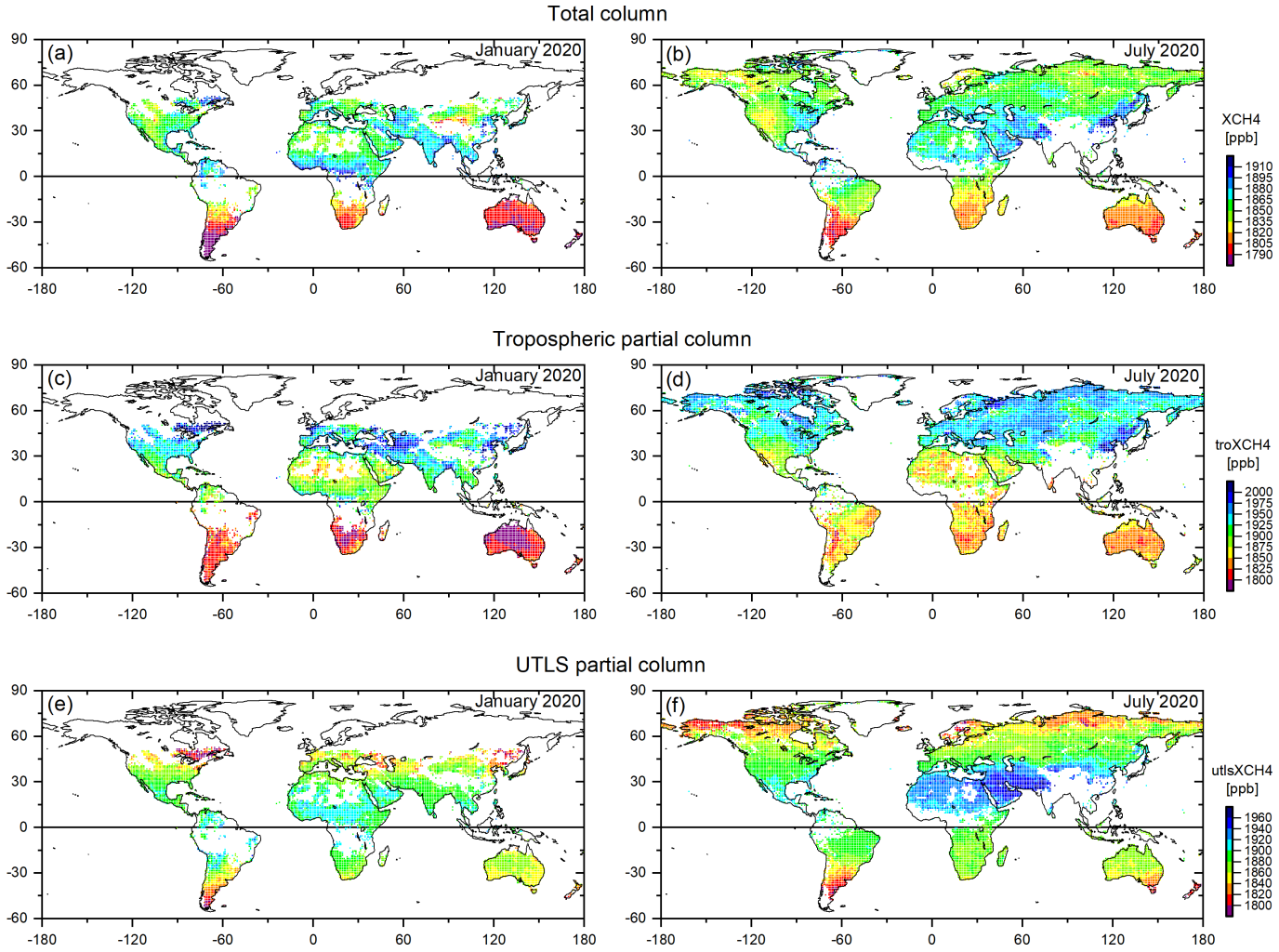

Figure 15. Global maps with 1° × 1° (longitude × latitude) resolution of monthly mean data for January and July 2020. (a)+(b) XCH_4 as observed by TROPOMI. (c)+(d) Tropospheric partial columns of CH_4 as obtained by the combined product. (e)+(f) UTLS partial columns of CH_4 as obtained by the combined product.

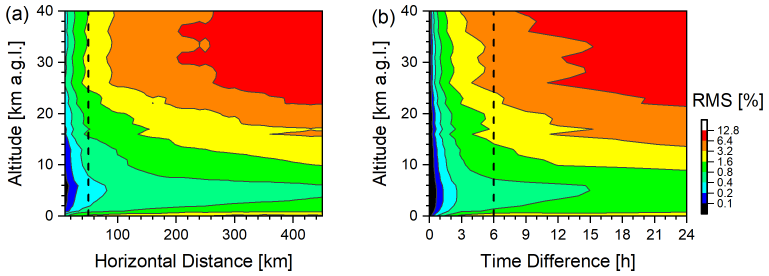

Figure E1. Square root values of the diagonal entries of different dislocation cavariance matrices ($\mathbf{S}^{\mathrm{l}}_{\Delta_{\mathrm{dl}}}$). These values are the root-mean-squares (RMS) of the difference between the reference methane profile (CAMS forecast for location 49.1°N and 8.4°E, corresponding to the location of Karlsruhe) and other forcasted profiles dislocated with respect to the reference: (a) horizontal dislocations; (b) temporal dislocations. The dashed black lines indicate the collocation threshold values used for valid combinations of IASI and TROPOMI.

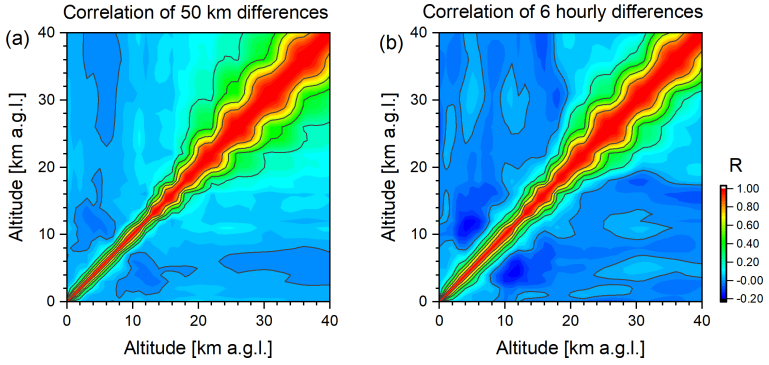

Figure E2. Characteristics of the vertical dependencies covered by the matrices $\mathbf{S}^{\mathrm{l}}_{\Delta_{\mathrm{dl}}}$. Shown are the vertical correlation matrices for the difference between the reference CH_4 profile (location 49.1°N and 8.4°E, corresponding to the location of Karlsruhe) and profiles dislocated with respect to the reference: (a) horizontal dislocation of 50 km; (b) temporal dislocation of 6 hours.

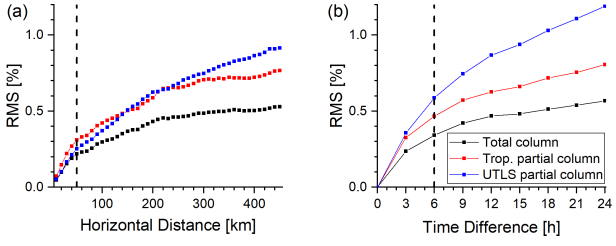

Figure E3. Same as Fig. E1, but for column averaged data: total column, tropospheric partial column, and UTLS partial column.

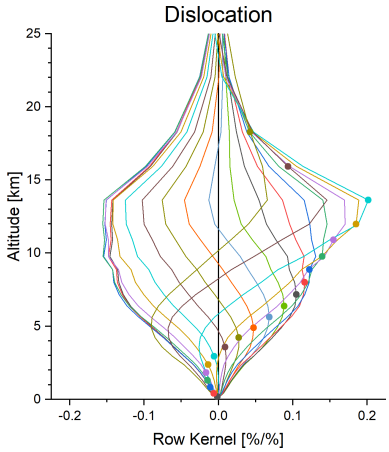

Figure E4. Example of dislocation kernel $\mathbf{A}^{1}_{\mathrm{C,dl}}$ – calculated according to Eq. (E3) – for the same late summer observation as used in the context of Figs. 1 to 3.

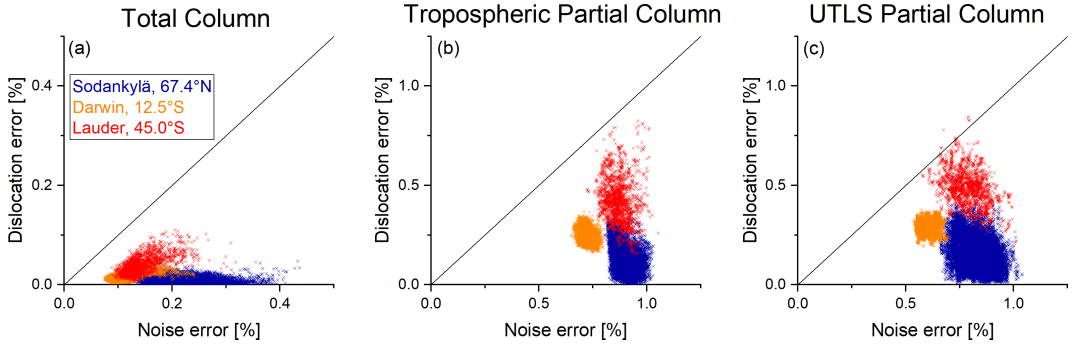

Figure E5. Comparison of the dislocation error (due to the CH_4 dislocation uncertainty) and the noise error (an example of the typical temporal dependencies of the noise error is shown in Fig. 6). The comparison is depicted for a northern high latitude location (Sodankylä, violet crosses), a tropical location (Darwin, organge crosses), and a southern middle latitudinal location (Lauder, red crosses). (a) Total column product; (b) Tropospheric partial column product; (c) UTLS partial column product.

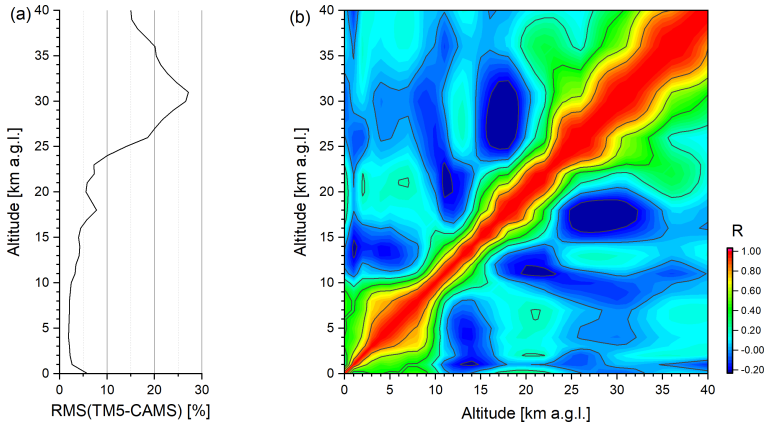

Figure F1. Comparison of the CH_4 state obtained from the TROPOMI a priori model TM5 ($\boldsymbol{x}_{\mathbf{TM5}}$) and the collocated CAMS high resolution forecasts ($\boldsymbol{x}_{\mathbf{CAMS}}$). (a) RMS of the relative differences; (b) Matrix showing the correlations of TM5-CAMS differences at different altitudes.

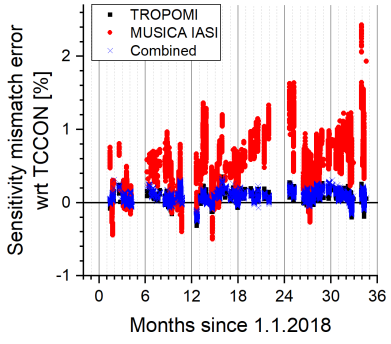

Figure F2. Error in the comparison of TCCON and satellite products due to the a priori model error and the different column sensitivities of the TCCON product and the satellite products. These values are calculated as $(\boldsymbol{a}^{*T} - \boldsymbol{a}^{*T}_{\mathbf{TC}})(\boldsymbol{x}_{\mathbf{TM5}} - \boldsymbol{x}_{\mathbf{CAMS}})$ and are represented in Eq. (F1) by the square root value of the term $(\boldsymbol{a}^{*T} - \boldsymbol{a}^{*T}_{\mathbf{TC}})\mathbf{S}_{\mathbf{\Delta a}}(\boldsymbol{a}^{*T} - \boldsymbol{a}^{*T}_{\mathbf{TC}})^T$.

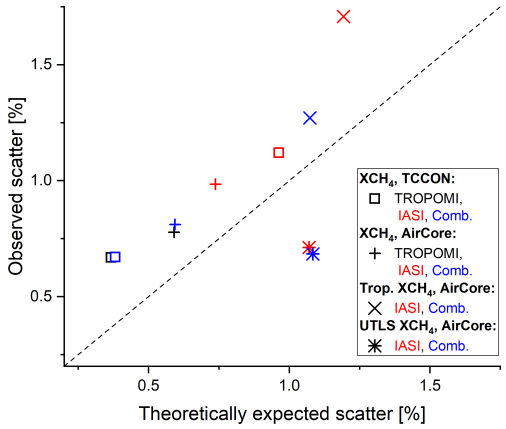

Figure F3. Theoretically predicted and observed 1σ scatter for the comparison of single pixel satellite data with individual TCCON and AirCore reference data. Black, red and blue colours represent TROPOMI, MUSICA IASI, and combined satellite data, respectively. The squares and vertical crosses are for XCH_4 comparisons with TCCON and AirCore references, respectively. The diagonal crosses and stars are for tropospheric and UTLS partial column comparisons, respectively, with AirCore references.